Mechanisms of Military Coatings Degradation
Final Technical Report
SERDP PP-1133

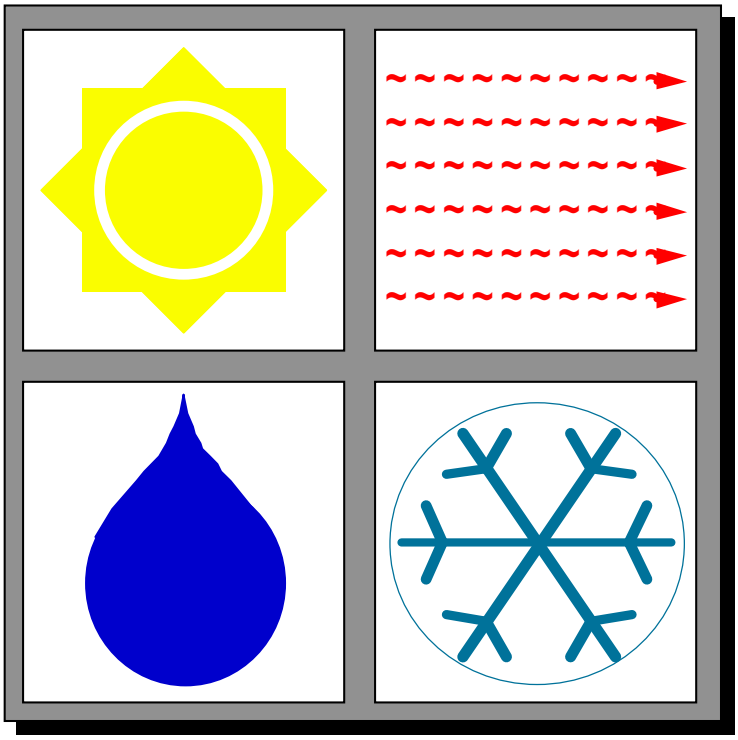

August 2003

Lead Agency: Weapons and Materials Directorate
Army Research Laboratory (ARL), APG, MD
PI: Ms. Wendy E. Kosik <wkosik@arl.army.mil>

Table of Contents

P 4 PERFORMING ORGANIZATIONS

P 5 EXECUTIVE SUMMARY

P 5 BACKGROUND
P 7 OBJECTIVE
P8 DESIGN OF EXPERIMENT
P9 RESULTS AND DISCUSSIONS
P10 CORRELATIONS
P14 PROJECT ACCOMPLISHMENTS
P15 CONCLUSIONS

P17 MECHANISMS OF MILITARY COATINGS DEGRADATION: ACCELERATED AND OUTDOOR EXPOSURE EVALUATIONS

P 35 ELECTROCHEMICAL IMPEDANCE SPECTROSCOPY

P 47 SPECTROSCOPIC CHARACTERIZATION OF SURFACE AND INTERFACIAL PROPERTIES OF TWO-COMPONENT MILITARY COATINGS

P 77 SURFACE CHARACTERIZATION VIA X-RAY PHOTOELECTRON SPECTROSCOPY

P 91 DYNAMIC MECHANICAL TESTING AND ANALYSIS OF MILITARY COATING SYSTEMS

P 93 APPENDIX A: CORRELATION DATA TABLES

Performing Organizations:

The Weapons and Materials Directorate of the Army Research Laboratory (ARL), Aberdeen Proving Ground, MD was the lead organization responsible for the overall management and coordination of this project. Technical specialization in the areas of coating formulation, color and gloss, Dynamic Mechanical analysis (DMA), profilometry, surface microscopy, corrosion, and transport theory

The Survivability, Structures, and Materials Directorate of the Naval Surface Warfare Center, Carderock Division (NSWCCD), Philadelphia, PA provided expertise in Dynamic Mechanical Thermal Analysis (DMTA) study of the military coatings. They also served as the organization representing the interest of the Marine Corps.

The Aerospace Materials Division of the Naval Air Systems Command (NAVAIR), Patuxent River, MD conducted the Electrochemical Impedance Spectroscopy (EIS) of military coatings. It also represents Navy's interests.

Benet Labs, ARDEC, Watervliet, NY performed laser scanning confocal microscopy for quantitative characterization of the military coatings as well as fracture toughness studies. They are a no-cost partner.

The Materials Science and Engineering Department of the State University of New York (SUNY), Stony Brook, NY conducted the characterization and analysis techniques such as chemical analysis, depth profiling, synchrotron spectroscopy and surface topography of the composite coating systems.

Executive Summary

Background:

When the Mechanisms of Military Coatings Degradation program was initiated four years ago, corrosion cost for the Department of Defense was estimated to be $10B/year. Therefore, logic followed that if a better understanding of coating degradation mechanism could be obtained then significant cost savings may be realized through enhanced coating systems and / or processes.

A review of current and relevant repainting practices indicated that military coating systems are repainted for the following reasons: loss of appearance (aesthetics, camouflage, cleanliness); chipping, peeling, debonding of the coating; and corrosion of the substrate. Such paint/depaint/repaint (PDR) operations are a significant source of DoD pollution. Frequency of the PDR increases pollution through increased consumption as well as through the economic and logistic burden associated with the maintenance waste stream. A 30% decrease in frequency of paint/depaint/repaint operations would save the Army $25-$40M in topcoat materials and approximately $40M annually for Air Force painting operations. Military coating system degradation impacts: 1) Environment 2) Economics 3) Force Survivability and 4) Force Readiness.

The importance of maintaining force readiness and survivability can clearly be seen through the Army's 3-axis transformation strategy; i) Legacy Force, ii) Interim Force and iii) Objective Force. Today, 75% of the Army's major combat platforms exceed their service half-life. The Army Transformation requires maintaining essential legacy war fighting readiness to execute the national military strategy. Improved coating performance in corrosion protection, camouflage appearance retention and chemical agent protection as part of a "drop-in" technology is not only vital for the Legacy Force, but also for the Interim and Objective Force. Through extending the coating system lifecycle, paint/depaint/repaint (PDR) driven pollution will be reduced while maintaining if not enhancing military survivability and readiness.

Military coating formulators, the environmental community and DoD system Program Managers (PMs), have a longstanding, successful, symbiotic history. Mission drives formulators, formulation improvements advance mission capabilities, and environmental requirements guide both formulation and mission protocol.

The commercial coating industry, as well as academia, perform fundamental research on individual coating constituents such as pigments, binder systems, UV inhibitors, extenders and the like. Their primary customer base lies in the automotive, manufacturing and architectural coatings. The function, aesthetics and demands on these commercial types of coatings are extremely different than those of a military coating system. The work performed under the SERDP PP1133 Mechanism of Military Coating Degradation (MMCD), was to bring all of these resources together, leveraging common scientific factors while recognizing unique performance requirements of military coatings.

The cross-section shown in Figure 1 illustrates a typical military coating system, composed of a substrate with pretreat, primer and finally topcoat. There is a synergistic performance between topcoat/primer and pretreat combinations; therefore the coatings are studied as a system. There also exists synergistic effects between the individual coating constituents; ingredients themselves are relevant to the coating system degradation. Typical raw materials and their contribution to the coatings are resins (binder), solvents (flow), additives (flow or processing) and pigments and extenders (color, gloss or flatners).

Fig 1: Cross section of typical military coating system

This program used a highly leveraged approach to study the degradation mechanisms leading to PDR operations. We chose coatings of military importance for aircraft (Navy), combat ground vehicles (Army, Marines) and support equipment (Navy, Army and Marines). The coating systems used by all branches of military are based on similar chemistry, but are formulated to meet specific mission needs. Table 1 highlights the coating systems and their related chemistry, which were selected for our degradation study.

Table 1. Coating Systems Selected for Study

A=(46168), ARMY CONTROL SYSTEM
Top Coat: MIL-C-46168 TYPE IV *Solvent based* Polyurethane (Siliceous Extender)
Aliphatic isocyanates and polyester polyols
Primer: MIL-P- 53022 Solvent Based Epoxy
Surface Treatment: TT- C-490 Zinc Phosphate on a steel substrate

B=(64159), LOW VOC and Zero HAP ARMY SYSTEM (SERDP PP1056)
Top Coat: MIL-DTL-64159 Water Dispersible *CARC* Polyurethane (Polymeric Bead Extenders.)
Aliphatic PU dispersion and modified isocyanate
Primer: MIL-P- 53030 water Based Epoxy
Surface Treatment: TT- C-490 Zinc Phosphate on a steel substrate

C=(85285), NAVY CONTROL SYSTEM
Top Coat: MIL-C-85285 Solvent based Polyurethane Aliphatic isocyanates and polyester polyols
Primer: MIL-P- 23377Solvent Based Epoxy
Surface Treatment: MIL-C-5541 Chemical Conversion on Aluminum substrate

D=(ZERO VOC TC), NAVY FUTURE SYSTEM
Top Coat: MIL-C-85285 Type II ZVOC TC water based Polyurethane
Primer: MIL-P- 85582 water Based Epoxy
Surface Treatment: MIL-C-5541 Chemical Conversion on an Aluminum substrate

Objective:

The primary technical objective of this program is pollution prevention via extended coating durability. The research objective is to identify individual degradation mechanisms that lead to military coating system failures, initiating depaint/paint operations. Two overall deliverables of the proposed effort would be pollution prevention via intelligent reduction of the paint/repaint frequency and a scientific basis to develop new durable coating formulations. We will develop models of coating degradation and provide a scientific basis to develop new durable coating formulations that will help to achieve this goal. The research findings will be transitioned through appropriate vehicles to the Army, Navy, Air Force, and Marine Corps. Improved confidence in environmentally friendly coatings would increase acceptance of these new systems by reluctant military end-users

A fundamental understanding of the mechanisms of coating degradation is necessary for the development of regulatory compliant, long life, protective coatings systems for DoD weapon systems. The pay-off to the military would be reduced environmental pollution, cost savings, and improved readiness of the force.

Technical Approach

The four year project approach is illustrated in Figure 2 and may be summarized as follows: 1) Study military coatings as a synergistic system in order to identify relevant degradation mechanisms and their related failure modes. 2) Conduct aging and weathering studies using lab accelerated conditioning, and static field conditioning. 3) Develop characterization and analysis techniques for bulk coating properties, surface and interface analysis, and corrosion behavior. 4) Develop independent parameter models. 5) Transfer discoveries and insights in real time to coating formulators for immediate feedback as to their implications. 6) Perform matrix correlation of research results, performance parameters and aging/weathering conditions for the coating systems 7) Initiate intelligent optimization of coatings and development of next generation coating systems

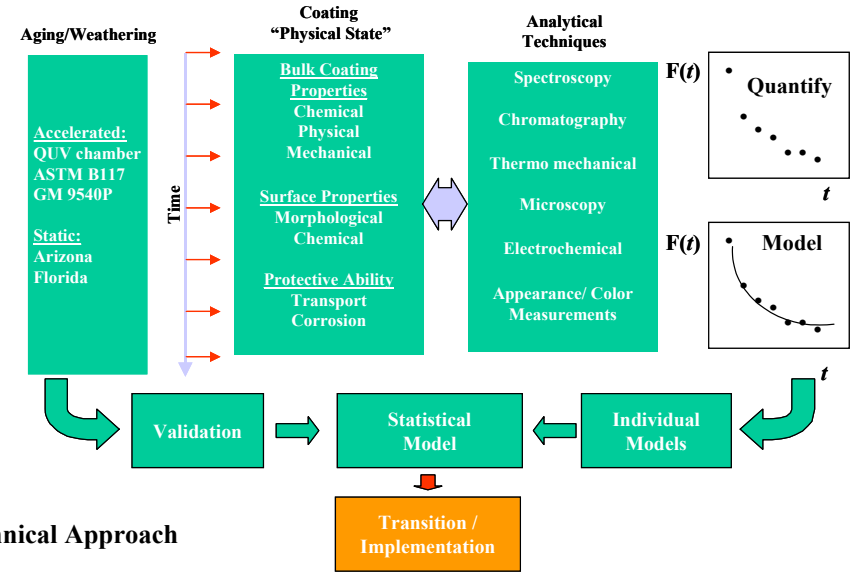

Fig 2: Technical Approach

Design of experiment:

Degradation modes vary with exposure/aging conditions. The goal was to quantify changes in physical, chemical and morphological properties as a function of static and accelerated aging. This required the development of a state-of-the-art characterization toolbox. With this toolbox, we could examine the degradation at both macroscopic and microscopic level. Figure 3 below illustrates the varied techniques developed for characterization and modeling of the coatings degradation.

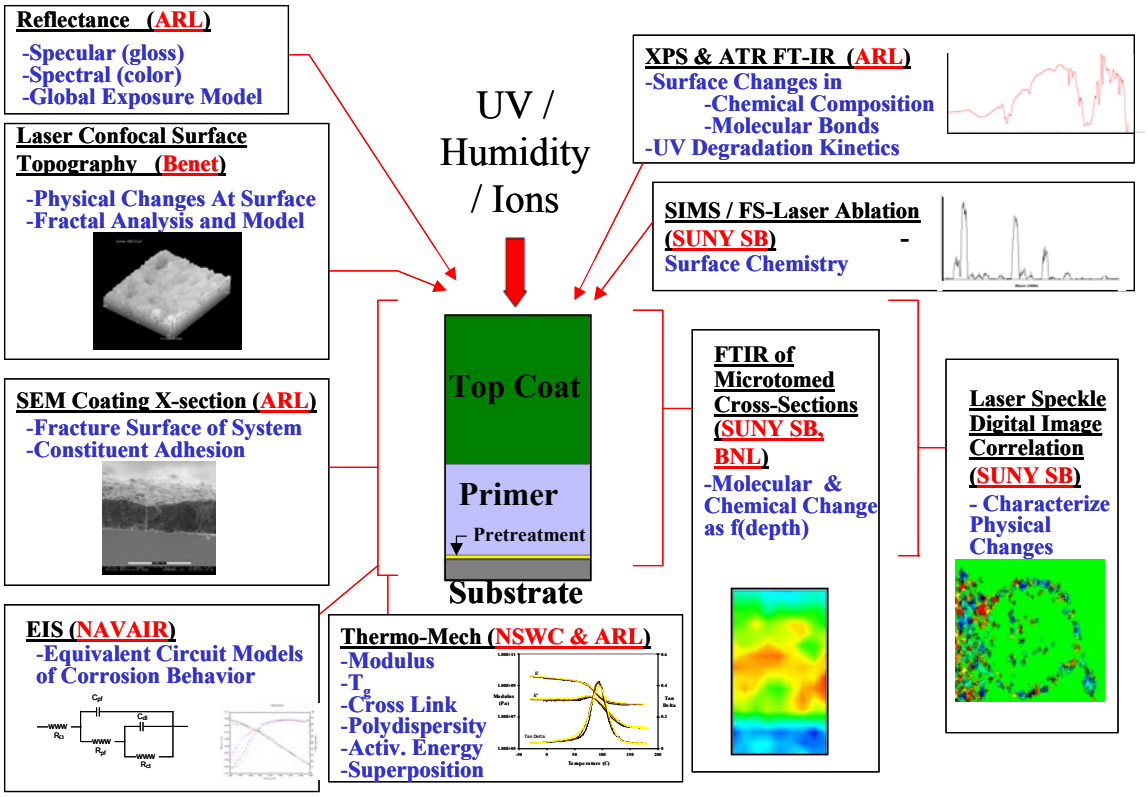

Fig 3: State-of-the-Art Toolbox for Macro- & Micro-Characterization

When a failure criteria for the coating system was met, 1) loss of appearance, 2) chipping, peeling debonding, or 3) corrosion of substrate, these techniques and analysis protocols aided in providing qualitative and quantitative information to be utilized in the statistical correlations.

Results and Discussions

These project highlights are provided to aid in interpretation of the correlation results. Detailed results may be found in either previous SERDP Annual Reports or are discussed in sections that follow.

Of the four coating systems evaluated, system A (solvent based polyurethane topcoat) showed the most pronounced signs of color degradation due to accelerated UV exposure. Coating system C (solvent based polyurethane topcoat) also eventually failed in color retention with continued irradiance. Coatings systems B and D (water dispersible topcoats) demonstrated the best UV color stability.

When the topcoat surfaces were examined using X-ray Photoelectron Spectroscopy (XPS) and Fourier Transform Infra Red spectroscopy (FTIR), a photo-oxidation mechanism was proposed and confirmed for the cases of color failure. The photo-oxidation and chain scission of the urethane linkage occurred in the binder. Through a series of reactions this results in carboxylic acid and urethane group as the end products of the degradation. Both the destruction of the urethane linkage and the increase of the bi-product were traceable in the case of color loss providing a first order approximation model of urethane linkage degradation kinetics as a function of irradiance.

Surface topography and fracture studies were used to further investigate the implications of this UV induced photo-oxidation of the coatings. Scanning Electron Microscopy (SEM) illustrated the resin-poor nature of coating system A and in conjunction with XPS, showed how the binder material was being ablated, exposing the siliceous extenders, pigments and inducing micro-cracking along their interfaces. These conditions were not observed for the water-dispersed systems. Coating system B showed great adhesion between the binder and the polyurethane bead extender. This was found to be very significant in the dynamic, mechanical and thermal properties of the coating.

The thermo-mechanical response of the coating systems prior to and after exposure was investigated by the Naval Surface Warfare Center, Carderock Division. This characterized the bulk response of the coating systems providing glass transition temperatures, crosslink polydispersity, activation energy and cure kinetics of the coatings. A significant observation was that even though there was confirmed chain scission of the surface binder, DMTA did not show significant decrease in crosslink densities of the coatings' bulk. The coating systems performance under various exposures was greatly influenced by the glass transition temperature of the coating in comparison to the degradation environment the systems were exposed to. Such results were crucial to the interpretation of the EIS correlation study.

MMCD efforts included advanced surface morphology and spectroscopy techniques for investigating highly pigmented coatings. Custom Laser Speckle Digital Image processing software was created and tested to detect the onset of microscopic morphological changes to coating systems due to weathering/aging. The sensitivity was verified through the detection of chemical surfactant migration due to simulated

weathering event. Laser Confocal Microscopy (LCM) was able to detect very small (<5 μm) changes in surface morphology of coating systems after UV/humidity exposures. Pitting was found on the Al 2024-T3 substrate beneath the coating using Confocal Large Area Mapping. LCM was also critical in the development of a fractal analysis and modeling technique enabling a mathematical quantification of the varied rough surfaces, correlating surface topography to exposure conditions. Femto-second Laser Ablation provided depth profiling of aged surfaces without disrupting the chemical composition information.

The integration of Electrochemical Impedance Spectroscopy (EIS) with coating characterization enabled quantitative corrosion assessment of the coatings. EIS enables study of the entire degradation process - from penetration of coating by electrolyte to metal/coating interfacial activity (including corrosion, and other electrochemical processes). Equivalent circuits were developed where each element relates to a physical parameter of the coating system. Changes in each element with varied exposures were quantified providing insight into moisture uptake, interface and bonding, corrosion kinetics and thermal impact of bulk.

Coating system D experienced some failure (blisters and adhesion loss) after GM9540 exposure. This was a result of improper mixing and/or curing of the primer that led to an incomplete curing reaction that, ultimately, created poor adhesion and film properties. SEM micrographs and small spot XPS mapping showed the presence of intermetallic phases within the host matrix alloy, AA2024-T3, which hindered chromate conversion coating protective properties and failed to passivate the corrosion reactions nucleating at these sites. The result was a complete loss of corrosion protection at certain locations of the substrate. The dynamics of this substrate/pretreatment interface will govern the anti-corrosive properties of the polymer coating/pretreatment system.

Correlations:

Statistical analysis was used to correlate EIS circuit parameter obtained after accelerated exposures to the performance of the Florida and Arizona outdoor exposures. Multiple linear regression using least squares was performed. The dependant variable, color change, was correlated to independent variables such as the ECM parameters determined after accelerated exposures. (Example of an independent variable would be $QC_{pf} = C_{pf}$ after exposure to QUV.) Linear models developed have the form:

$$Y = \beta_0 + \beta_1 X_1 + \beta_2 X_2 + \beta_3 X_3 + \ldots \beta_n X_n$$

Y is the chosen dependent variable (ΔE, ASTM rating), β the calculated coefficients, and x the parameter predictor(s) (ECM parameter(s)). Models were determined using the minimum number of variables to achieve confidence levels on the order of 95%. Best statistical practices were used to ensure models were valid. The NAVAIR section details this effort.

Coating System A:

Coating System A which is the solvent based polyurethane topcoat with siliceous extender, implementing aliphatic isocyanates and polyester polyols for the resin system.

The primer is solvent-based epoxy/polyamide material applied onto a pretreated phosphated steel substrate.

The linear model for color correlation of coating A for the Arizona exposure is:

$$\Delta E \sim \beta_0 - (\beta_1)\, QC_{pf} + (\beta_2)\, QR_{pf} + (\beta_3)\, QC_{dl}$$

where;

ΔE ⇨ Color Loss

β_0 ⇨ Constant

$\beta_1 QC_{pf}$ ⇨ Dielectric constant decrease due to UV-induced heat: No further ability for the chains to align in electric field; x-link formation and/or densification

$\beta_2 QR_{pf}$ ⇨ Increased Rpf with UV-induced heat: Supports theory of x-link formation and/or densification

$\beta_3 QC_{dl}$ ⇨ Increased interfacial (epoxy/substrate) capacitance with increased temperature. Possible increased adhesion of primer, effectively decreasing the "d" in the capacitance equation, $C = \varepsilon\varepsilon_0 A/d$

Coating A had significant color loss with AZ exposure. Color loss best correlated with QUV aging parameters. (QUV average temperature was 60 degrees Celsius, non-cyclic, no humidity). It is postulated that damage, as seen by color change, is caused by bond breakage at the thin resin layer at the surface. The subsequent ablation of the resin and exposure of the pigment is exacerbated by the decreasing free volume of the bulk polymer. Polymer development characterized by increasing Tg data supports densification and/or x-link formation theory of the bulk. The Dynamic Temperature Ramp (DTR) response of the QUV samples showed large consistent reduction in dampening which was thought to be due to non-chemical reaction related curing effects such as liberation of residual solvents, decrease in polymer free volume and bulk film compaction. Coating A is a less sterically and thermally stable biuret trimer of HDI in comparison to the HDI of coating system B. This correlation model for coating A with Arizona exposure has a 99% fit.

The linear model for color correlation of coating A for the Florida exposure is:

$$\Delta E \sim \beta_0 - (\beta_1)\, QC_{pf} + (\beta_2)\, QR_{pf} + (\beta_3)\, BC_{pf}$$

where;

ΔE ⇨ Color Loss

β_0 ⇨ Constant

$\beta_1 QC_{pf}$ ⇨ Dielectric constant decrease due to UV-induced heat: No further ability for the chains to align in electric field; x-link formation and/or densification

$\beta_2 QR_{pf}$ ⇨ Increased Rpf with UV-induced heat: Supports theory of x-link formation and/or densification

$\beta_3 BC_{pf}$ ⇨ Dielectric constant increase due to moisture and/or ions: Indicates water randomly diffusing into bulk coating. No conductive pathways forming since no significant Rpf change

Coating A had significant color loss with FL exposure. Color loss was best correlated with QUV and B117 aging parameters indicating significant role of heat and moisture. (QUV average temperature was 60 degrees Celsius, non-cyclic, no humidity. B117 average temperature was 35 degrees Celsius, non-cyclic, 100% humidity). It is postulated that damage, as seen by color change, is caused by bond breakage at the thin resin layer at the surface. The subsequent ablation of the resin and exposure of the pigment is similar to that observed in the AZ exposure with the following caveat: When only moisture is present, densification of the polymer is not as severe as in its absence. Densification in the FL exposure may be retarded by the moisture contribution (plasticization); therefore, the resin is not pulling away from the extender and pigments as drastically as it does in AZ. This correlation model has a 97% fit.

Coating System B:

Coating System B is the water dispersible CARC polyurethane topcoat with polymeric bead extenders. The primer is a water-based epoxy applied on a steel substrate pretreated with zinc phosphate.

The linear model for color correlation of coating B for the Arizona and Florida exposure is:

$$\Delta E \sim \beta_0 + (\beta_1)\, QC_{pf} - (\beta_2)\, GC_{pf}$$

where;

ΔE ⇨ Color Loss

β_0 ⇨ Constant

$\beta_1 QC_{pf}$ ⇨ Dielectric constant increase due to UV-induced bond breakage: Smaller chain segments at the surface and increased long-range polymer mobility in the bulk allow for easier alignment in electric field

$\beta_2 GC_{pf}$ ⇨ Decreased Cpf with cycles of temperature and varying moisture content

Coating system B maintained color stability (minimal change) throughout the weathering trials. The minimal color loss measured under both Arizona and Florida weathering best correlated with QUV and GM9540P accelerated aging parameters. (QUV average temperature was 60 degrees Celsius, non-cyclic, no humidity. GM 9540P range of temperatures 25C to 60C, cyclic in heat, humidity and salt mist, drying.)

The steric stability provided by the isocyanurate ring trimer of hexamethylene diisocyanate (HDI) for this polymer may play a role in the thermal and mechanical stability. Spectroscopic and fracture studies showed no evidence as to UV-induced photo-oxidation, neither photo-oxidative ablation of the resin nor exposure of the pigment/extender particles. The higher Tg of Coating B's binder restricts conformational changes when exposed to temperature and humidity extremes. Lower but stable values of AZ-Rpf and FL-Rpf (from non-correlation EIS study) indicate that the water-dispersible coating system B is more porous than the coating system A. For coating system B, the contribution of the parameters $(\beta_1)\, QC_{pf} - (\beta_2)\, GC_{pf}$ to any color change is important to show influence of cyclic temperature and moisture change , but is insignificant in the coatings overall color retention. This correlation model has a 88-96% fit

Coating System C:

Coating System C is a solvent-based polyurethane. The primer is a solvent-based epoxy applied on an aluminum substrate with a chromate chemical conversion coating .

The linear model for color correlation of coating C for the Arizona exposure is:

$$\Delta E \sim \beta_0 + (\beta_1)\, QC_{pf} + (\beta_2)\, QR_{pf}$$

where;

ΔE	⇨ Color Loss
β_0	⇨ Constant
$\beta_1 QC_{pf}$	⇨Dielectric constant increase due to UV-induced bond breakage in top 25micron: Smaller chain segments at the surface and increased long-range polymer mobility in the bulk allow for easier alignment in electric field
$\beta_2 QR_{pf}$	⇨Increased Rpf with UV-induced heat hence becomes a better barrier. This supports densification/ free volume decrease of the bulk. Densification is present, but not to same extent as Coating A

Coating C had significant color loss with AZ exposure. Color loss was best correlated with QUV aging parameters. (QUV average temperature was 60 degrees Celsius, non-cyclic, no humidity). Damage, as seen by color change, is supported by spectroscopic studies that indicate UV-induced photo-oxidation and photo-oxidative ablation of the resin. Coating system C is more resin rich than coating system A. Coating C experiences a decrease of free volume and exposure of pigments, however it is to a lesser degree than that which was observed in coating A. This correlation model has a 95% fit

The linear model for color correlation of coating C for the Florida exposure is:

$$\Delta E \sim \beta_0 + (\beta_1)\, QC_{pf} + (\beta_2)\, QR_{pf} + (\beta_3)\, BC_{pf}$$

where;

ΔE	⇨ Color Loss
β_0	⇨ Constant
$\beta_1 QC_{pf}$	⇨ Dielectric constant increase due to UV-induced bond breakage: Smaller chain segments at the surface and increased long-range polymer mobility in the bulk allow for easier alignment in electric field
$\beta_2 QR_{pf}$	⇨ Increased Rpf with UV-induced heat: Supports theory of x-link formation and/or densification, but not to same extent as Coating A
$\beta_3 BC_{pf}$	⇨ Dielectric constant increase due to moisture and/or ions: Indicates water randomly diffusing into bulk coating. No conductive pathways forming since no significant Rpf change

Coating C experienced color loss with FL exposure. Color loss was best correlated with QUV and B117 aging parameters indicating significant role of heat and moisture. (QUV average temperature was 60 degrees Celsius, non-cyclic, no humidity. B117 average temperature was 35 degrees Celsius, non-cyclic, 100% humidity). Damage, as seen by color change, is a result of UV-induced photo-oxidation. Coating C is more resin rich than Coating A and it appears that there is less of a free volume decrease occurring

in Coating C. When enough of the surface layer is oxidized, the extender and pigments are exposed and the visual damage is observed. As with Coating A, when moisture is present, any densification is retarded (plasticization) and color change is not as prominent.
This correlation model has a 98% fit

Coating System D:

Coating System D is a NAVY Zero VOC water based polyurethane topcoat. The primer is water-based epoxy applied on aluminum substrate with a chromated chemical conversion coating.

The linear model for color correlation of coating D for the Arizona and Florida exposure is:

$$\Delta E \sim \beta_0 + (\beta_1)\, QC_{pf} - (\beta_2)\, GC_{pf}$$

where;

ΔE	⇨ Color Loss
β_0	⇨ Constant
$\beta_1 QC_{pf}$	⇨ Dielectric constant increase due to UV-induced bond breakage: Smaller chain segments at the surface and increased long-range polymer mobility in the bulk allow for easier alignment in electric field
$\beta_2 GC_{pf}$	⇨ Decreased Cpf with cycles of temperature and varying moisture content:

Coating system D maintained color stability (minimal change) throughout weathering trials. The minimal color loss measured under both Arizona and Florida weathering best correlate with QUV and GM9540P accelerated aging parameters. (QUV average temperature was 60 degrees Celsius, non-cyclic, no humidity. GM 9540P range of temperatures 25C to 60C, cyclic in heat, humidity and salt mist, drying.)
It is postulated that damage, as seen by color change, is caused by UV-induced photo-oxidation. The lower Tg of Coating D's binder allows for long-range conformational changes when exposed to temperature and humidity extremes. The contribution of the parameters $(\beta_1)\, QC_{pf} - (\beta_2)\, GC_{pf}$ to any color change is important to show influence of cyclic temperature and moisture change , but is insignificant in the coatings overall color retention. This correlation model has a 70-88% fit

Project Accomplishments and Deliverables

This program characterized on the order of 20 coating performance parameters. We established models of parameter/coating system performance, providing insight into coatings degradation through mathematical polymer kinetics, equivalent circuit models, establishing digital pass/fail criteria. Observations, models and values were incorporated into a statistical matrix system, which has and will continue to improved formulations, performance, predictability and survivability of military coating systems. Increased confidence in technology transition as well as financial benefits will be realized. Specific deliverables achieved are as follows.

Identified Degradation Modes & Mechanisms
•Change of color was primary appearance failure
•UV oxidation of polyurethane binder driving mechanism

Prioritized Degradation Factors
•UV exposure was a factor in all the EIS correlations
•Solvent borne systems had moisture as a correlation factor (B117) only for the FL exposures
•Both the Low- and Zero-VOC coatings had QUV and GM EIS correlations in both their FL and AZ weathering
•Enhanced degree of conversion is expected to be critical to the degradation stability of these coatings
•Intermetallic phases within the host matrix alloy, AA2024-T3, hindered chromate conversion coating protective properties and failed to passivate corrosive reactions nucleating at these sites (primer/pretreat interface critical performance factor)

Provided Formulation Recommendations
•Binders: Waterborne PU over solvent system (improved CARC color retention upwards of 4 times that of current fielded Solvent Borne CARC)
•Extenders: implementation of polymeric bead (MIL-DTL-64159) incorporated into all topcoat CARC systems over inorganic extenders
•HALS and UV inhibitors did not seem to provide any significant enhancements to C & D. Rather Pigment/Binder plays a greater determining rule in these type coatings

Established Models
•Cure Kinetics Model (activation energy & Time-Temperature Superposition) Via DMTA
•Moisture Transport kinetics of urethane system
•Topcoat urethane chain scission kinetics, first order approximation
•Surface roughness correlation to exposure conditions
•Electrochemical models of coating systems that approximate the system's behavior in certain environments
•Dynamics of substrate pretreatment interface will govern the anti-corrosive properties of the polymer coating/pretreatment system

Achieved Durability Database
•Baseline chemical and structural properties & tech base for coating durability evaluation
•EIS statistical correlation to Color as performance parameter
•Unique implication of predicting color via EIS, normally used for corrosion predictions
•Confidence levels of factors influencing coating performance

Summary/Conclusion

The information discovered combined with the correlations made will aid in achieving pollution prevention via extended coating durability. Statistically important degradation mechanisms that result in military coating system failures have been identified.

Independent assessment of potential degradation mechanisms and their correlation to a failure mode have been achieved. These efforts have provided a scientific base to prioritize the mechanisms for specific military coating system formulations and direct future durable coating formulation efforts. Recommendations for improved performance of current and future topcoat and primer systems as well as substrate protection have been favorably received. Many research findings have been transitioned through to the Army, Navy, Air Force, and Marine Corps and have been inserted into military protocols. Current environmentally friendly military coating systems are used with confidence in their ability to exceed previous levels of performance. The pay-off to the DoD as well as Homeland Defense Office will be reduced environmental pollution, cost savings, and improved readiness of the force. Reduced frequency of paint/depaint operations will lead to cost savings, reduced environmental pollution and better maintenance planning

Mechanisms of Military Coatings Degradation: Accelerated and Outdoor Exposure Evaluations

John A. Escarsega, William Lum, and Philip Patterson, Amirh Whitt
Army Research Laboratory, Aberdeen MD 21005-5069 USA

Abstract

The Weapons and Materials Directorate of the U. S. Army Research Laboratory (ARL) has completed a four-year research investigation on identifying and quantifying key degradation mechanisms of legacy and newly developed coatings systems used by the Army, Marine Corps and Air Force. This study has incorporated numerous analytical tools and methods in an effort to better understand the fundamental principles of environmental degradation that lead to coating failures. These environmentally related failures are broadly characterized in two different ways -- one as minor, such as appearance changes (color loss/fade) and the other as catastrophic, such as film protection changes (substrate corrosion). This report will summarize the coatings' appearance performance when exposed to enhanced ultraviolet radiation and to outdoor static weathering. Specifically discussed are the results obtained on the coatings change in color and specular gloss. These evaluations will serve as a performance baseline providing the knowledge required to formulate more durable military coatings. Additionally, when correlated with results obtained from other techniques, a failure analysis model can be established predicting a coating's actual field service life.

Acknowledgement

This coating research was supported in part, by the United States Department of Defense though the Strategic Research Development Program (SERDP) under the task area of pollution prevention (PP-1133). The authors gratefully acknowledge the principal investigator, Ms. Wendy Kosik of ARL, for her efforts in coordinating and managing the many facets of the program.

Introduction

The U.S. Army, Marine Corps and Air Force utilize polyurethane coatings as camouflage "topcoats" and epoxy coatings as "primers" on all tactical vehicles and aircraft. Pretreatments for the substrates vary depending upon the composition of the vehicle or aircraft and whether it is a refurbished item or a piece of Original Equipment from the Manufacturer (OEM). In either case it is typically a chromated wash primer for refurbished equipment and an alodine based conversion coating for aluminum or Zinc Phosphate based material for ferrous substrates for OEMs. This "Coating System" not only serves to provide camouflage for vehicles and aircraft but also provides protection against chemical warfare agents for the Army and Marine Corps with their Chemical Agent Resistant Coatings (CARC). A visual schematic of the system is shown in Figure 1. The coatings must retain their physical properties over a broad temperature range in widely varying climatic environments. The "Coating System" is the first line of defense in preventing corrosion, thereby extending the life cycle of a military vehicle or aircraft.

In an effort to specifically minimize overall vehicle corrosion and reduce costly refurbishment and maintenance expenditures an ongoing Tri-service research effort has been established to examine the mechanism and relationships involving coatings' degradation. Four polyurethane topcoat and epoxy primer coating systems representing the Army, Marine Corps and Air Force were selected. Standard specification, as well as, and newly developed, "greener" materials were evaluated. This report will present data on gloss, color, and general appearance changes occurring in samples exposed in Arizona and Florida, as well as, in an accelerated ultraviolet light (QUV) chamber. The weathering effects on topcoat degradation and "coating system" interaction will be discussed.

Figure 1. A typical camouflage "Coating System" is shown below:

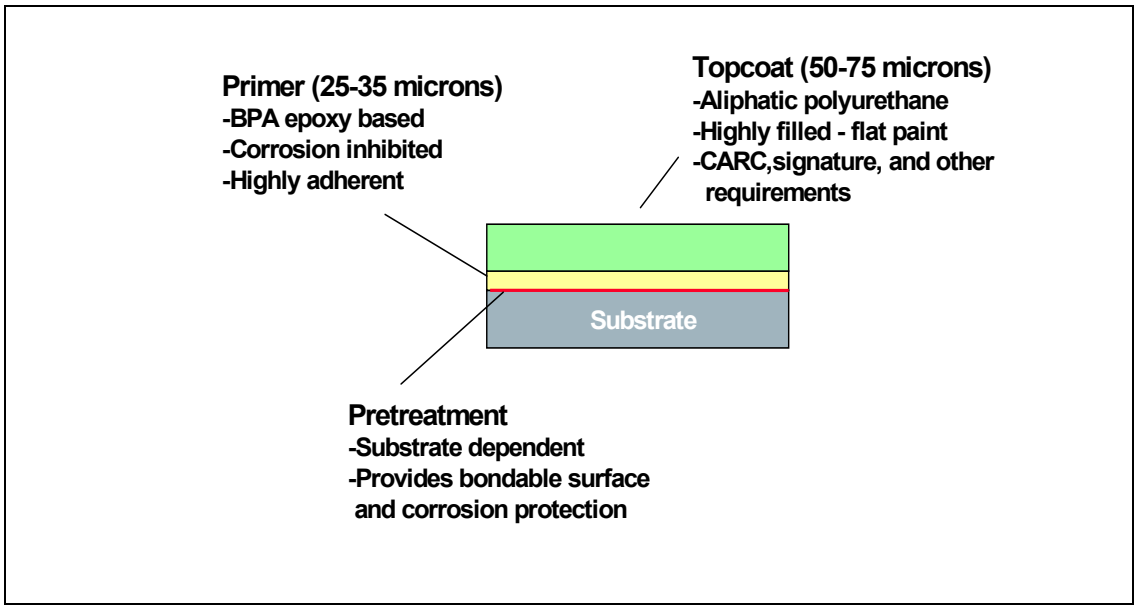

Experimental:

The coatings were sprayed onto two different metal substrates, cold rolled steel (SAE 1008) panels pretreated with zinc phosphate (Bondrite® 37) and a chromate sealer (Parcoolene® 60) conforming to TT-C-490 and 2024 T3 Aluminum Alloy panels pretreated with a chemical conversion Iridite 14-2 conforming to Mil-C-5541. Free films were also prepared with only the topcoats sprayed onto a low surface tension Tedlar polyvinyl fluoride (DuPont Inc., Buffalo, NY) release film. Additionally a primer and topcoat system were also prepared onto a stainless steel mesh substrate for additional thermal analysis conducted by the Marine Corps. Only color data from the QUV exposures were obtained for these samples, due to their irregular surface. The panels and free films were sprayed to a dry film thickness of 50-65µm for the topcoats and 25-37µm for the epoxy primers (applied to the metal panels only). Film thickness for the stain steel mesh required additional primer and topcoat to adequately eliminate any surface defects and resulted in film thickness of 155 µm. The topcoat formulations reported in this paper were pigmented to conform with Army Color number 34094 *(Green 383) as stated in*

MIL-C-46168D (1), the military's specification for two-component, chemical agent resistant, polyurethane coatings and Air Force color number 36375 (Medium Gray) as referenced in MIL-C-85285 (2), the military's specification for high-solids polyurethane coatings.

The water-dispersible formulations are identified as Systems "B" and "D". The solvent-based formulations are designated as "A" and "C". The Army's water-dispersible topcoat (Part of System "B") is formulated with a water-dispersible hydroxy-functional polyurethane (PUR) and a water-dispersible polyisocyanate. The coating's pigment package includes prime pigments used to make the Army's camouflage color number 34094 (Green 383), as well as, polymeric-type extenders for flattening purposes. While the water-dispersible topcoat of System "D" uses no polymeric flattening agents and is pigmented to Air Force Color number 36375 (Medium Gray). The solvent based topcoats also use non-polymeric flattening agents and incorporate their respective prime pigments for the Army Color number 34094 (Green 383), System "A", and the Air Force Color number 36375 (Medium Gray), System "C".

Summary of Coating Systems

A=(MIL-C-46168), **ARMY CONTROL SYSTEM**
Top Coat: MIL-C-46168 TYPE IV *Solvent based* Polyurethane (Siliceous Extender)
Primer: MIL-P- 53022 Solvent Based Epoxy
Surface Treatment: TT- C-490 Zinc Phosphate on a steel substrate

B=MIL-DTL-64159 TYPE II, **ZERO HAPs Polymeric flattening agents (3,4)**
Top Coat: Water Dispersible *CARC* Polyurethane (Polymeric Bead Extenders)
Primer: MIL-P- 53030 Water Based Epoxy
Surface Treatment: TT- C-490 Zinc Phosphate on a steel substrate

C=MIL-PRF-85285, NAVY CONTROL SYSTEM
Top Coat: MIL-PRF-85285 Solvent based Polyurethane
Primer: MIL-PRF-23377 Solvent Based Epoxy
Surface Treatment: MIL-C-5541 Chemical Conversion on Aluminum substrate

D=MIL-PRF-85285 TYPE III (ZERO VOC TOP COAT)
Top Coat: Zero VOC Top Coat Water based Polyurethane
Primer: MIL-PRF-85582 Water Based Epoxy
Surface Treatment: MIL-C-5541 Chemical Conversion on an Aluminum substrate

Conditions and Evaluations

Three types of exposures were conducted, two at separate outdoor weathering locations (Florida and Arizona) and one in an accelerated UV weathering (QUV) chamber. The test procedures established for the Arizona and South Florida exposures conform to ASTM G-7 and ASTM G-147. The exposure testing was performed in Miami, Florida (26º N) and New River, Arizona (34º N) in accordance with ASTM Governing Standards at a tilt angle of 5º from the horizontal facing south. The exposure intervals ranged from 7 to 97 weeks. The accelerated UV testing was conducted using a weathering chamber operated under the requirements established by ASTM G-53. Cycling involved total UV light exposure with no condensation or water spray. A series of UVA 340 lamps were used as the light source set to emit a spectral irradiance of 0.77 W/m^2. An automatic sensor controller kept this irradiance level, measured at 340nm, stable throughout the testing and was calibrated after every 400 hours of lamp operation. An exposure temperature of 60 ºC was maintained inside the weathering chambers. The study was conducted following an elapsed time schedule, with the samples exposed to continuous UV over the intervals of 3 to 48 weeks. With each timed interval, the solar UV energy dosage was recorded as well.

After each exposure interval, the samples were rinsed with de-ionized water and allowed to dry before color and gloss measurements were made. During the performance testing, all specimens were carefully handled to avoid marring and the operators wore lint free gloves in order to keep coating surfaces clean.

For the outdoor exposures, color measurements were performed on a Hunterlab Ultrascan Colorimeter with a 6-inch integrating sphere. Color measurements for the QUV exposures were made using a Data Color Chroma Sensor Spectrophotometer equipped with an 8-inch integrating sphere. In both cases, the spheres were set up to include the specular component of the sample's reflectance. All of the color readings were made in accordance to ASTM D-2244 and ASTM E-308 using a 2º observer under illuminant C.

Gloss measurements were made in accordance with ASTM D-523 using a BYK Gardner GB4606 Haze-Gloss Reflectometer. The measurements were taken at 60 and 85-degrees. The instrument was calibrated using the manufacturer's Reflectometer standard gloss tile. A BYK-Gardner Micro-Tri-Gloss portable glossmeter was used for the outdoor exposures.

Results and Discussions: Appearance Characterization

The results from all of color measurements made on the samples' QUV, Florida, and Arizona exposures are provided in Tables 1-3, respectfully. Tables 4-6 are averaged measurements provided to simplify the data. It should be noted that listed in the last 8 columns of Table 1 is color data obtained from specifically prepared samples. These coatings were prepared as either free films (T designation) or having a screen mesh (B designation) as its substrate.

From reviewing Table 4, it is apparent that of the four coating systems evaluated, System "A", using the MIL-C-46168 - *Solvent based Polyurethane Topcoat*, shows the most pronounced signs of appearance degradation due to accelerated UV exposure. Severe color fade/degradation (3.23 color-difference units) occurs after just 6 weeks/149.1 MJ/m^2 (UV dosage) of exposure. The change is primarily due to an increase in the brightness of the coating's color. It is interesting to note that this degradation trend continues throughout the remaining exposure intervals. Conversely, the UV color stability is best for the topcoats used in the water-based systems ("B" and "D"). This weathering characteristic is most certainly related to the coatings' extender pigment content for the topcoats (5). A comparison of the pigment to binder (resin) ratio is greatest for the System "A" topcoat (2 to 1 pigment/binder ratio) and the least is System "B" with "C" and "D" falling in between.

The test results from Florida and Arizona outdoor weathering, provide insight to the effects of humidity and moisture on the exposed coatings. Because the Arizona environment has very little humidity or moisture (i.e. rain), degradation effects are primarily the result of UV radiation. However, the Florida environment has a significant amount of humidity and moisture in conjunction with UV radiation that often accelerates the degradation of organic coatings.

As Table 5 shows, the System "B" topcoat, MIL-PRF-64159, *Water Dispersible Polyurethane*, exhibited the least change in color for all the coatings exposed in South Florida. This subtropical environment was most detrimental (loss of color retention) to the System "A" coating, which displayed a color-difference value of 7.42 units at the final weathering interval. Also at this interval, the topcoats from both System "C and "D" showed significant color degradation (approx. 3 units). The color retention for the System "D" topcoat was actually compromised at the previous exposure interval, 49 weeks/270.6 MJ/m^2 (UV dosage), whereas with System "C", the color remained stable. It should be noted this behavior for coating "D" did not manifest itself under the Arizona or the QUV exposures. This is an example of how humidity and moisture combined with UV radiation synergistically increase the degradation of a specific coating.

As summarized in Table 6, the color retention is good for all of the coating systems through the first 13 weeks of weathering in Arizona. It is not until 25 weeks /203.4 MJ/m^2 (UV dosage) of exposure that the degradation trends begin to appear. As with the QUV exposures, the topcoat of System "A" is the first to show a visually significant color change (3.26 units). System "C", using the MIL-PRF-85285, *Solvent*

based Polyurethane Topcoat, was the second most susceptible coating to color degradation, with a major color change (3.84 units) occurring after 97 weeks/603.5 MJ/m^2 (UV dosage) of exposure. Overall, the degradation trend and performance ranking for these coatings are in line with the results obtained from the QUV exposures.

The coatings' gloss values for both 60 and 85-degrees are summarized in Tables 7 through 9. The data was taken from the final evaluation interval (97 weeks) for the outdoor exposures and 27 weeks for the QUV exposure. This QUV interval was chosen to match, as closely as possible, the total UV energy dosage to that of the outdoor exposures. The gloss changes for the low matte samples, Systems "A" and "B" is minimal. Even the change in the 85-degree gloss reading (1.2 unit increase) for the "System "B" topcoat, under the Florida exposure, is an acceptable difference. For the higher gloss coatings, Systems "C" and "D", all of the weathering results show a similar gloss change trend. That is, a decrease in 60-degree gloss and an increase in the 85-degree gloss. The one exception to this trend was the loss of 85-degree gloss for System "D" in Florida. Although in its previous exposure interval, 49 weeks, the 85-degree reading did indeed rise. No explanation for this data reversal is readily apparent. These gloss degradation trends are best explained by the way in which formulators generally use larger particle sized pigments to lower the 85-degree gloss reading. As the coating film weathers and the binder degrades, these pigments are lost and a new surface topography develops that is generally smoother. Thus giving rise to the 85-degree reading and a lowering the 60-degree reading.

Conclusions and Observations:

- The protective film properties of all of the "Coating Systems" remained intact. No catastrophic failures (i.e. cracking, checking, blistering, delaminating) occurred under any of the exposure conditions.
- The water dispersible coatings "B" and "D" provided much better resistance to color changes than their solvent based counterparts, "A" and "C", when weathered under the QUV conditions (Figure 2). The Arizona results parallelled these findings, an indication that the coatings' degradation pathways (i.e. photolysis) are similar.
- For the Florida exposures, as with the other two exposure conditions, coating "B" outperformed coating "A" for color retention. However, for the Air Force systems, coating "D" reversed its excellent color retention behavior, as seen in the Arizona/QUV exposures. This system was actually the first of all the coatings to show significant color deterioration. This reversal indicates that for this coating, the subtropical environment created or enhanced a degradation mechanism that adversely impacted color durability greater than that of the arid exposures.
- The topcoat formulation with the lowest pigment to binder ratio (System "B") provided the best overall appearance stability. The performance of this camouflage coating was not enhanced by the addition of UV inhibitors or Hindered Amine Light Stabilizers (HALS), but rather through the selection of durable and effective flattening agents (extender pigments) that kept the gloss down while maintaining the low pigment to binder ratio.
- Overall, the weathering exposures had little significant impact on the gloss behavior of the coating systems. The gloss changes that did occur, in most instances, were within the tolerances as set forth in the coating's respective specification.
- Systems "A" and "B" (383 Green pigmentation) have lower reflectance values than "C "and "D" (Air Force Medium Gray color number 36375). It is generally acknowledged that higher reflectance properties result in lower ambient operating temperatures. Therefore by formulating a topcoat "B" binder system with medium gray pigmentation and polymeric flattening agents color retention would improve due higher pigment reflectance properties and to superior polymer durability.

The changes in surface appearance properties affected by environmental exposures are but one way of evaluating a coating's durability. Changes can occur on the surface that may or may not impact the bulk of the material. This research included additional degradational analysis that measured some of the coatings' intrinsic properties. The details of the instrumental analysis characterizing the functional changes involving the coatings' chemical and mechanical properties will be discussed in a future technical report.

Figure 2. Photographs Displaying Coating Systems after 48 Weeks of UV Exposure

Table 1: QUV Exposure Data: NBS Color Change from Initial Color

Sample Code	AA	BA	CA	DA	AN	BN	CN	DN	AM	BM	CM	DM	AMT	AMB	BMT	BMB	CMT	CMB	DMT	DMB
Exposure Time, Radiant UV Energy																				
3 Weeks, 74.57 MJ/m2	0.45	0.44	0.33	0.46	0.57	0.67	0.27	0.45	0.38	0.55	0.32	0.39	0.34	0.70	0.62	0.72	0.31	0.46	0.40	0.34
6 Weeks, 149.14 MJ/m2	3.50	0.54	0.26	0.56	3.40	0.53	0.28	0.54	2.8	0.63	0.4	0.47	3.30	2.50	0.74	0.76	0.37	1.80	0.35	0.32
12 Weeks, 298.28 MJ/m2	5.30	0.67	0.28	0.69	6.30	0.72	0.47	0.71	5.9	0.87	1.40	0.65	7.90	7.70	0.8	0.98	1.70	6.40	0.41	0.44
18 Weeks, 447.42 MJ/m2	8.60	0.82	0.26	0.78	7.75	0.98	1.38	0.77	7.85	0.89	2.09	0.75	8.59	8.49	0.86	0.91	8.20	3.02	0.52	0.51
27 Weeks, 671.13 MJ/m2	10.37	0.82	No Data	No Data	10.68	0.93	3.36	1.01	11.35	0.95	No Data	No Data								
36 Weeks, 894.84 MJ/m2	12.10	0.93	No Data	No Data	12.59	1.16	4.96	1.01	12.00	1.03	No Data	No Data								
48 Weeks, 1193.12 MJ/m2	12.86	1.04	5.47	0.74	13.30	1.34	5.99	1.15	13.35	1.30	6.13	0.68								

T = Samples tested as a free film. **B** = Sample films applied and tested on grid substrate.

Table 2: Florida Exposure Data: Color Change (Delta E) from Initial Color

Sample Code	AA	BA	CA	DA	AN	BN	CN	DN	AM	BM	CM	DM
Exposure Time, Radiant UV Energy												
7 Weeks, 75.03 MJ/m^2	0.11	0.90	0.39	0.96	0.13	0.95	0.35	0.99	0.20	0.78	0.39	0.86
13 Weeks, 91.15 MJ/m^2	0.54	1.12	0.34	1.31	0.42	1.1	0.44	1.32	0.42	1.15	0.18	1.28
25 Weeks, 151.41 MJ/m2	2.60	1.12	0.59	1.34	2.31	1.22	0.42	1.43	2.73	1.26	0.42	1.34
49 Weeks, 270.65 MJ/m2	4.90	1.32	0.79	3.33	4.67	1.32	0.87	2.73	5.14	1.22	0.92	3.91
97 Weeks, 501.37 MJ/m2	7.70	1.53	2.74	2.70	7.31	1.57	2.61	3.25	7.26	1.59	2.52	2.83

Table 3: Arizona Exposure Data: Color Change (Delta E) from Initial Color

Sample Code	AA	BA	CA	DA	AN	BN	CN	DN	AM	BM	CM	DM
Exposure Time, Radiant UV Energy												
7 Weeks, 65.29 MJ/m^2	0.33	0.59	0.14	0.23	0.51	0.76	0.165	0.21	0.65	0.71	0.16	0.21
13 Weeks, 120.08 MJ/m^2	0.59	0.81	0.27	0.61	0.54	0.91	0.18	0.64	0.55	0.91	0.28	0.63
25 Weeks, 203.40 MJ/m^2	3.02	1.23	0.46	0.95	3.46	1.24	0.52	0.95	3.29	1.30	0.48	0.87
49 Weeks, 305.37 MJ/m2	4.89	1.28	1.75	0.40	4.60	1.27	1.28	0.51	4.81	1.33	1.65	0.48
97 Weeks, 603.52 MJ/m2	9.03	1.30	4.12	1.98	9.39	1.30	3.80	1.45	9.31	1.32	3.59	1.75

Table 4: Summary QUV Exposure Data (Averaged): Color Change from Initial Color

Sample Code	A	B	C	D
Exposure Time, Radiant UV Energy				
3 Weeks, 74.57 MJ/m2	0.47	0.55	0.31	0.43
6 Weeks, 149.14 MJ/m2	3.23	0.57	0.31	0.52
12 Weeks, 298.28 MJ/m2	5.83	0.75	0.72	0.68
18 Weeks, 447.42 MJ/m2	8.07	0.90	1.24	0.77
27 Weeks, 671.13 MJ/m2	10.80	0.90	3.36	1.01
36 Weeks, 894.84 MJ/m2	12.23	1.04	4.96	1.01
48 Weeks, 1193.12 MJ/m2	13.17	1.23	5.86	0.86

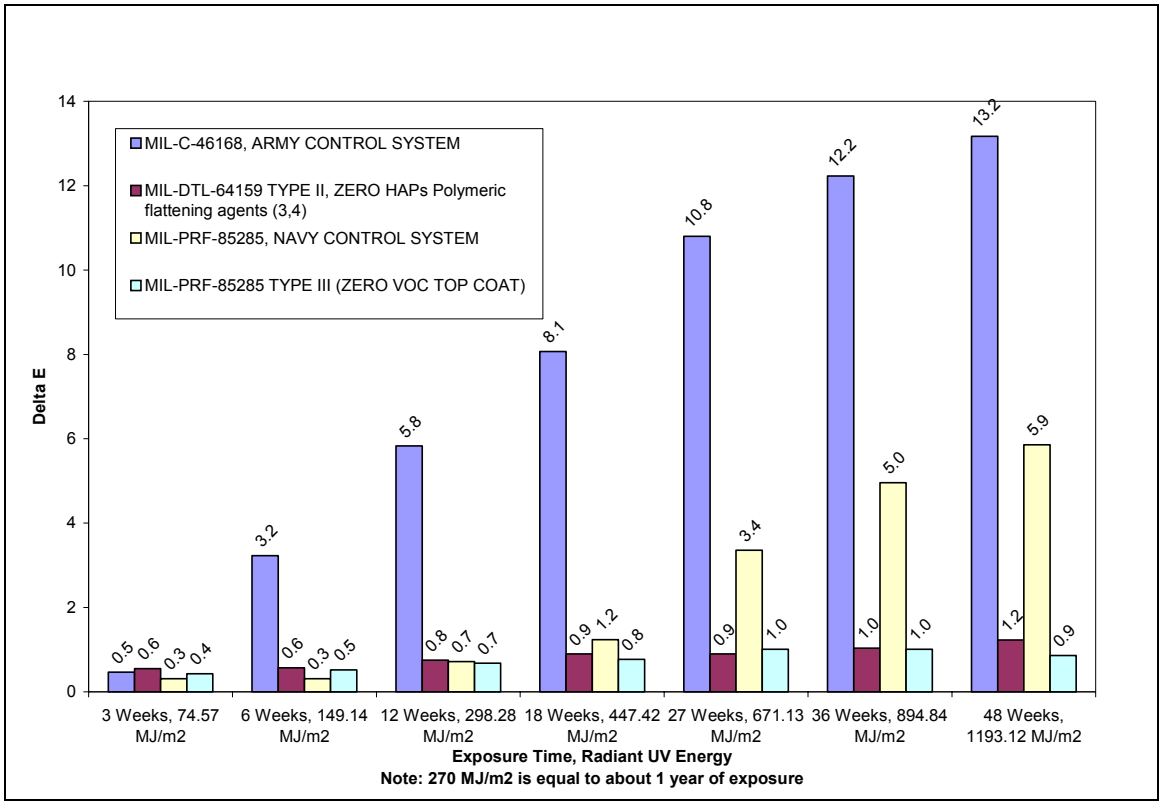

Table 5: Summary of Florida Exposure Data (Averaged): Color Change from Initial Color

Sample Code	A	B	C	D
Exposure Time, Radiant UV Energy				
7 Weeks, 75.03 MJ/m2	0.15	0.88	0.38	0.94
13 Weeks, 91.15 MJ/m2	0.46	1.12	0.32	1.30
25 Weeks, 151.41 MJ/m2	2.55	1.2	0.48	1.37
49 Weeks, 270.65 MJ/m2	4.92	1.29	0.86	3.32
97 Weeks, 501.37 MJ/m2	7.42	1.56	2.62	2.93

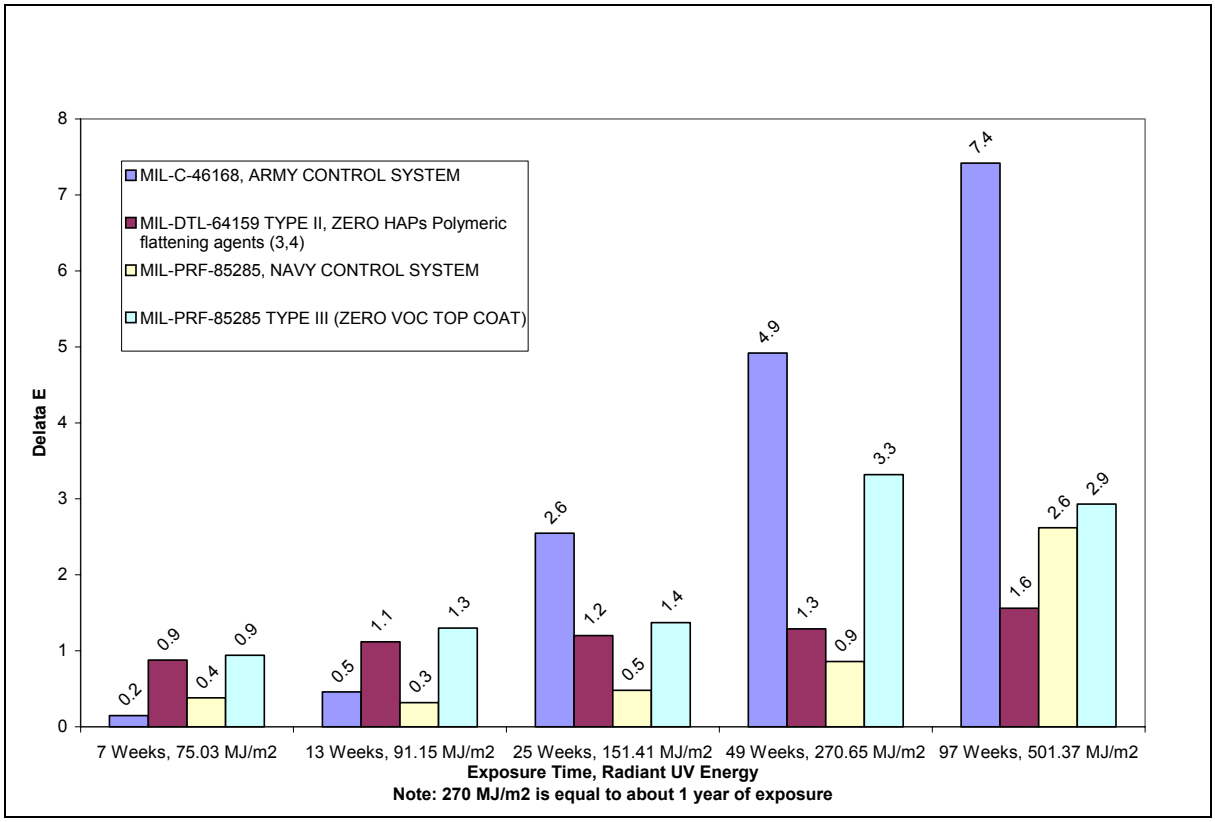

Table 6: Summary of Arizona Exposure Data (Averaged): Color

Change from Initial Color

Sample Code	A	B	C	D
Exposure Time, Radiant UV Energy				
7 Weeks, 65.29 MJ/m^2	0.50	0.69	0.16	0.22
13 Weeks, 120.08 MJ/m^2	0.56	0.88	0.24	0.63
25 Weeks, 203.4 MJ/m2	3.26	1.26	0.49	0.92
49 Weeks, 305.37 MJ/m2	4.77	1.29	1.56	0.46
97 Weeks, 603.52 MJ/m2	9.24	1.31	3.84	1.73

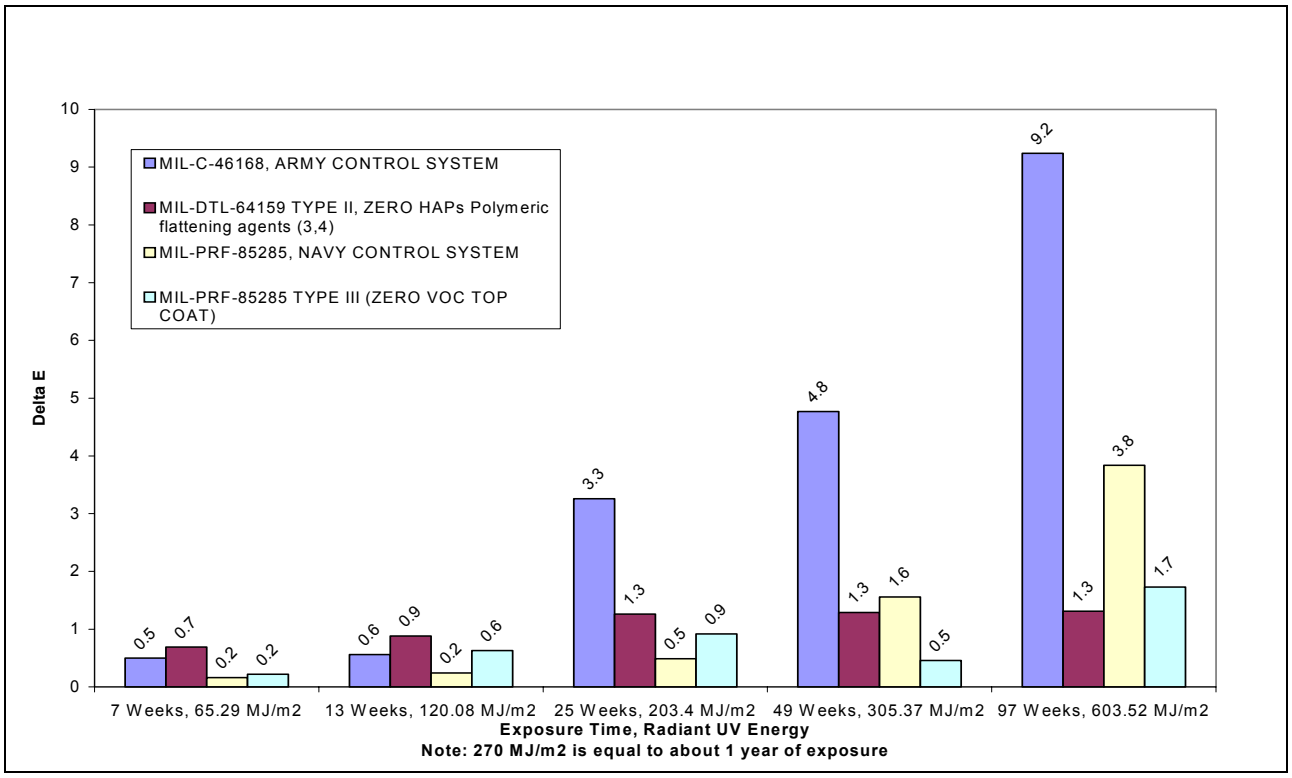

Table 7: Summary of Gloss values for QUV After 27 Weeks,

Radiant Energy UV: 671.13 MJ/m^2

QUV	Initial	Final	Initial	Final
Sample	*Gloss 60°*	*Gloss 60°*	*Gloss 85°*	*Gloss 85°*
A	0.6	0.7	2.9	2.5
B	0.7	0.8	1.6	2.2
C	2.3	1.6	3.6	3.8
D	2.1	1.4	4.4	4.3

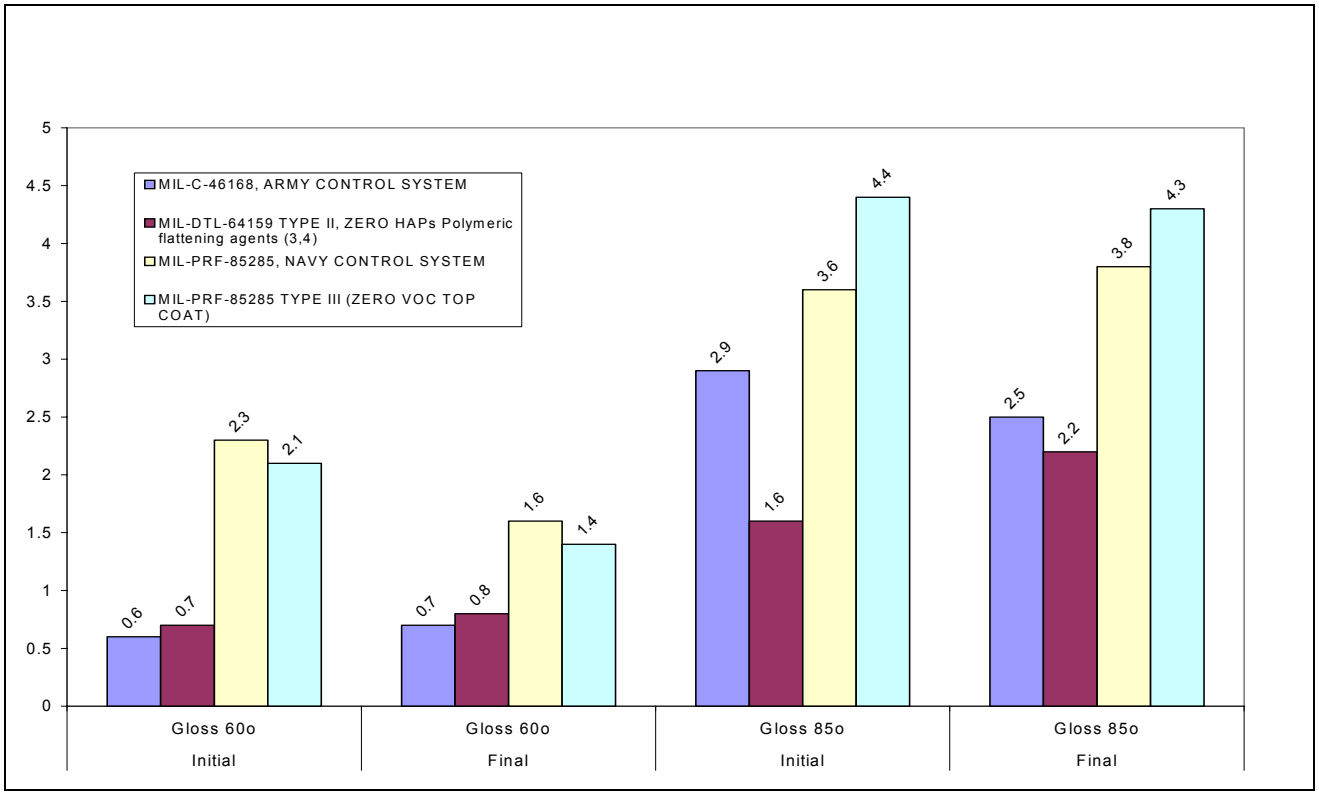

Table 8: Summary of Gloss values for Arizona After 97 Weeks,

Radiant Energy UV: 603.52 MJ/m^2

Arizona	Initial	Final	Initial	Final
Sample	*Gloss 60°*	*Gloss 60°*	*Gloss 85°*	*Gloss 85°*
A	0.6	0.6	3.6	3.4
B	0.6	0.6	2.2	2.5
C	2.1	1.4	4.1	8.7
D	2.0	1.3	5.4	6.6

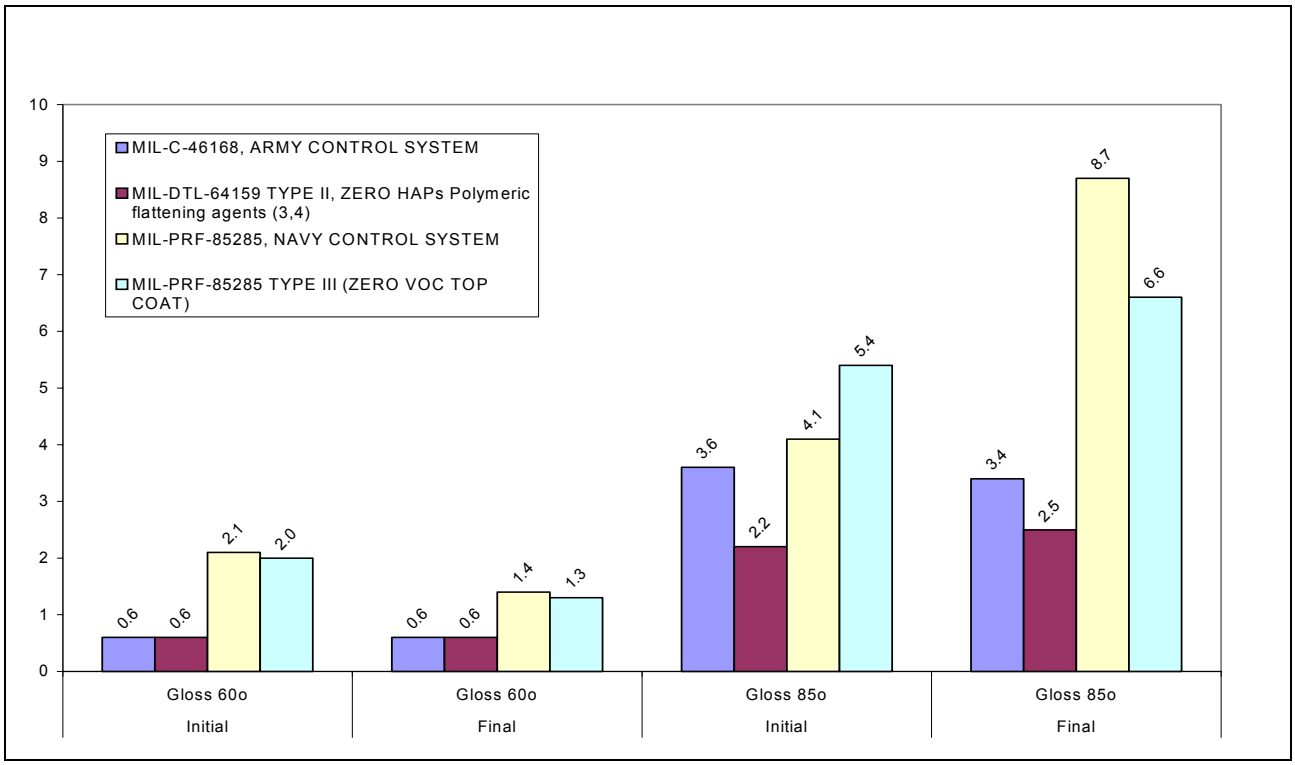

Table 9: Summary of Gloss values for Florida After 97 Weeks, Radiant Energy UV: 501.37 MJ/m^2

Florida	Initial	Final	Initial	Final
Sample	*Gloss 60°*	*Gloss 60°*	*Gloss 85°*	*Gloss 85°*
A	0.6	0.5	3.2	4.4
B	0.7	0.6	2.2	2.8
C	2.2	1.6	4.5	6.4
D	1.9	1.0	5.3	3.7

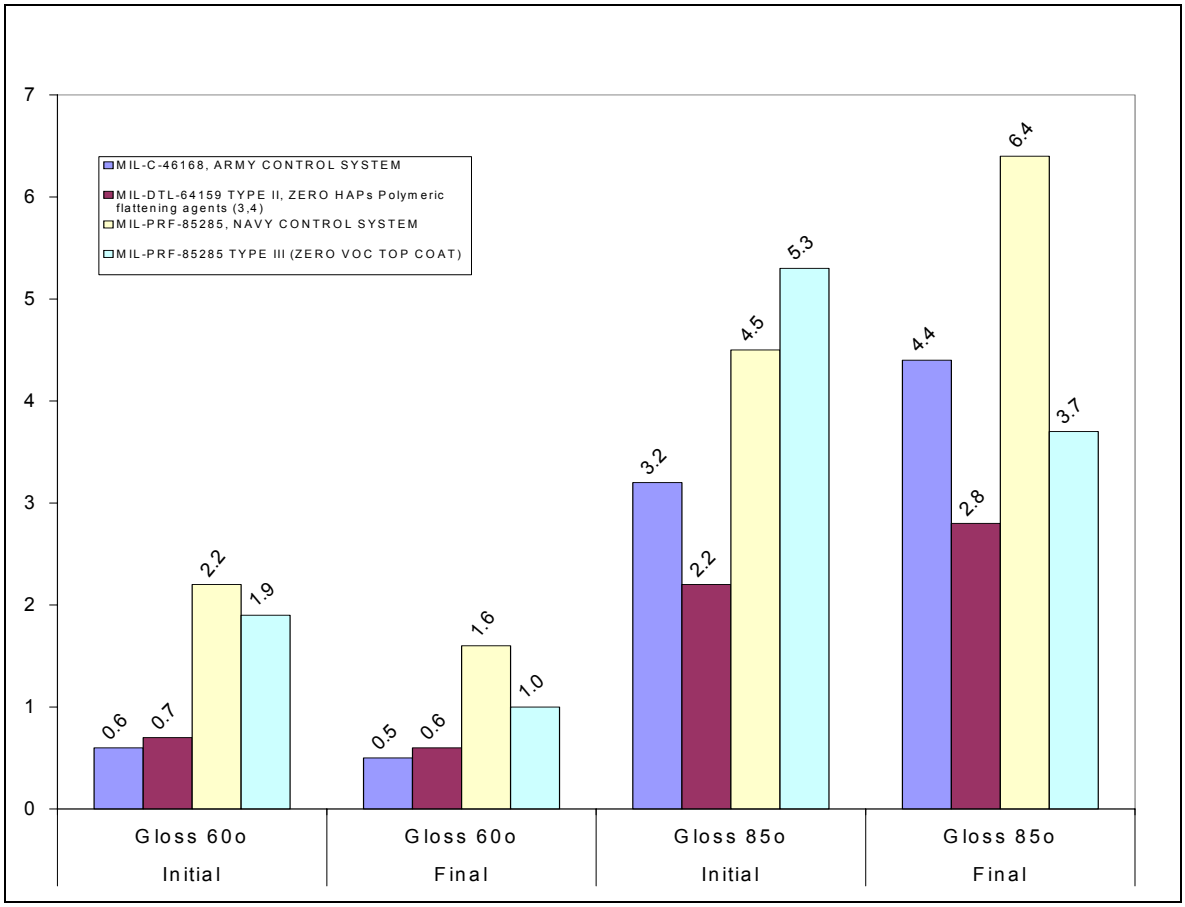

References:

1. U.S. Department of the Army, “Coating, Aliphatic Polyurethane, Chemical Agent Resistant”, Military Specification MIL-C-46168, Revision D, May 1987

2. U.S. Department of the Navy, “Coating: Polyurethane, Aircraft and support equipment” Military Specification MIL-PRF-85185, Revision D, June 2002

3. Crawford, D. et al. Analysis and performance of water-dispersible camouflage coatings International Waterborne, High-Solids, and Powder Coatings Symposium February 6-8, 2002 New Orleans, LA, USA

4. Escarsega, J.A. Crawford, D.M., Duncan, J.L., and Chesonis, K.G. “Water-Reducible PUR Coatings for Military Applications,” Modern Paint and Coatings, 1997

5. Patton, T.C. “Paint flow and Pigment Dispersions, 2nd Ed.,” John Wiley Interscience, New York, 1979

Project Title: Mechanisms of Military Coatings Degradation (PP-1133)
Electrochemical Impedance Spectroscopy Subtask

Performing Organization: Naval Air Warfare Center Aircraft Division, Patuxent River, MD
Kevin J. Kovaleski, NAVAIR Principal Investigator,
Edward W. Lipnickas, NAVMAR Applied Sciences
Bldg. 2188
Aerospace Materials Division
NAWCAD
48066 Shaw Road Unit 5
Patuxent River, MD 20670-1908
Phone: (301) 342-8049
E-mail: kovaleskikj@navair.navy.mil
lipnickasew@navair.navy.mil

Project Background: Due to environmental restrictions, coatings research has focused on the development of systems with less organic solvents and toxic corrosion inhibitors. This fact has caused concerns in the user communities that the new coating systems will not provide the same level of protection as their non-environmentally compliant counterparts under the harsh operating conditions experienced by the military. A better understanding of how coatings degrade needs to be developed to insure that new systems will be designed that meet or exceed the performance of the older systems while reducing volatile organic compounds (VOCs) and toxic corrosion inhibitors.

Objective: This project was initiated to identify, model, and predict degradation mechanisms that lead to military coating system failures and force depaint/paint operations to occur. Efforts focused on primer/topcoat systems that are being fielded to comply with environmental legislation and regulations. Two important failure modes that lead to repainting were examined. First, degradation of topcoat appearance and protective ability due to exposure to ultraviolet radiation and moisture was quantified and modeled. Also, the effect of topcoat degradation on corrosion resistance and primer-substrate adhesion was analyzed quantitatively and related to service life. Accelerated testing methodologies were developed and implemented to facilitate a more rapid fielding of future environmentally compliant coating systems with greater confidence and understanding.

During FY 2002, characterization of the coating system behavior utilizing electrochemical impedance spectroscopy (EIS) for both standard and environmentally friendly coating systems was completed. A statistical analysis of the collected EIS data was performed and predictive models developed.

Technical Approach: EIS data were obtained in accordance with the Aerospace Materials Division's Quality Manual using a standardized procedure. The EIS system consisted of an EG&G Princeton Applied Research Model 283 potentiostat/galvanostat interfaced to a computer-controlled EG&G Princeton Applied Research Model 1025

frequency response analyzer. The impedance spectra were determined from 1 MHz to 0.01 Hz using AC amplitude of 20 mV at open circuit DC potential. A schematic diagram of the apparatus is shown in Figure 1.

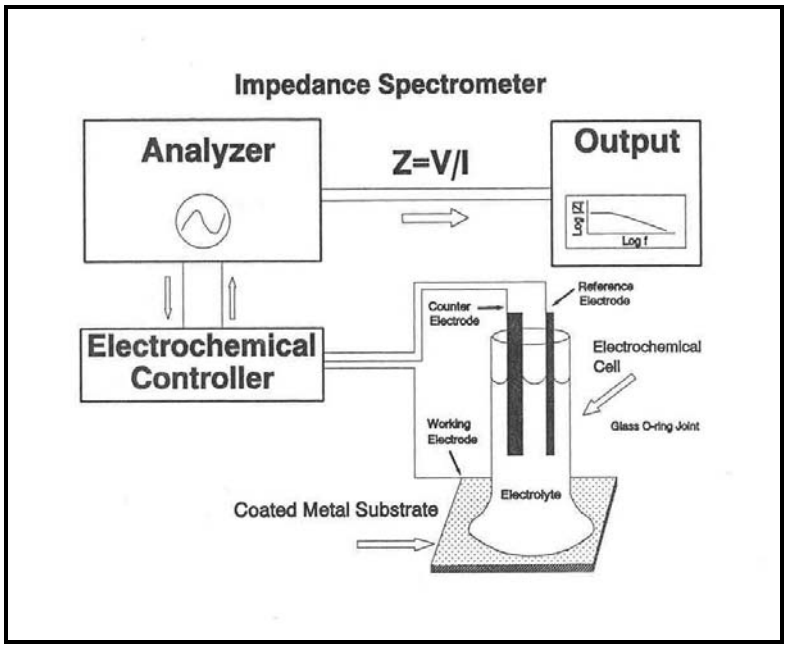

FIGURE 1. Schematic diagram of the EIS experimental set-up.

The cell was a glass cylinder clamped and O-ring sealed to the sample surface, as shown in Figure 1 above. The seal exposed 7.75 cm^2 of sample surface area to the test solution medium. The reference electrode was saturated calomel and a platinum wire/disk assembly served as the counter electrode.

Baseline samples were conditioned by continuous immersion using the assembly above in either 3.5% NaCl solution or a solution of 1% NaCl and 0.1% $CaCl_2$ (GM9540P). Measurements were made after 1, 4, and 7 days, then after 2, 4, 8, 12, and 16 weeks.

EIS was performed on panels that were exposed to either laboratory or static field aging. Different sets of laboratory-aged panels were exposed to neutral salt spray/fog (ASTM B 117), accelerated artificial weathering (QUV-A), and cyclic corrosion (GM9540P). Different sets of static field-aged panels were exposed at sites in Arizona (AZ) and Florida (FL). The laboratory and static field-aged samples were conditioned by immersion using the assembly above for one hour in 3.5% NaCl solution before the EIS measurements were made.

Four EIS spectra were obtained for each coating system for each baseline interval and each laboratory/static field exposure test to ensure reproducibility of the data. Due to time constraints and good reproducibility, it was determined during the testing that only two spectra would suffice for the purposes stated above. For simplicity, one

representative EIS spectrum per coating system was fitted for each exposure condition for tests conducted after laboratory/field aging and for each time interval for both solutions for specimens under immersed conditions.

Wet tape adhesion tests were performed on laboratory/field-aged panels following the EIS tests. The tests were performed in the center of the panel, between the areas where the electrochemical cell was attached. These tests were conducted in accordance with the Aerospace Materials Division's Quality Manual using a standardized procedure. The panels were immersed in distilled water at 120°F for four days and inspected for peel away and blistering. Peel away was evaluated as per ASTM D 3359, Method A and blistering was evaluated as per ASTM D 714.

Coating systems are summarized in Table 1. Exposure was quantified in time for samples subjected to neutral salt spray and cyclic corrosion tests. For QUV-A and field aging the exposure was quantified in UV irradiance.

TABLE 1. Summary of coatings evaluated in program.

Coating System	**Primer**	**Topcoat**	**Substrate**	**Description**
A	MIL-P-53022	MIL-C-46168, Type IV	Steel	Army Control
B	MIL-P-53030	MIL-C-64159	Steel	Army Future
C	MIL-PRF-23377, Type II, Class C	MIL-PRF-85285, Type I	Aluminum	Navy/AF Control
*D	MIL-PRF-85582, Type II, Class N	Deft Zero-VOC Topcoat	Aluminum	Navy Future

*Coating D was found to have poor performance and the IR signature of properly formulated coating D versus the questionable sample was investigated. A strong signature for epoxy component A (polymer of diglycidyl ether of bisphenol-A) was found, which normally disappears when properly mixed with component B for the primer portion. Hence, it was concluded that improper mixing of the 2 components caused poor primer adhesion resulting from insufficient cure.

The EIS data for waterborne coatings B, D was initially fit to a 7-element circuit [1]. It is desirable to have as few elements as possible while maintaining a minimal systematic deviation between measured and fitted result[2]. After further investigation it was decided to refit the data to a 5-element circuit (Fig. 2) for the following reasons: EIS published in literature generally use 100 kHz as the high frequency limit; this is because most EIS systems are only capable of handling data up to this frequency. The system consists of a frequency response analyzer interfaced to a potentiostat to make the impedance measurements over a frequency range. The potentiostats used cannot make reliable measurements at frequencies above 100 kHz and thus the data in the 100 kHz to 1 MHz range was questionable. Fitting the program in this area resulted in an additional time constant in the100 kHz to 1 MHz interval, necessitating a 7-element circuit. By eliminating the frequencies in the 100 kHz to 1 MHz range, the data was successfully fitted (including coating D) to the circuit in Figure 2.

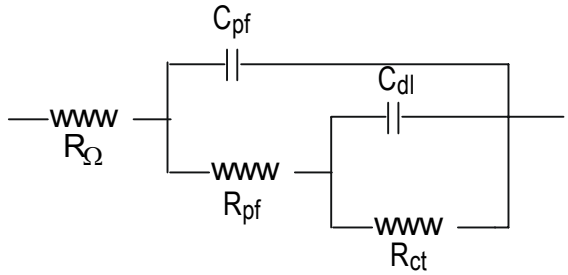

Figure 2. 5-Element Equivalent Circuit model

The equivalent circuit model (ECM) was utilized to determine resistive and capacitive parameters and their logarithmic values plotted vs. time/UV exposure. Capacitances were fit using constant phase elements (CPE's), a circuit element that more accurately describes the behavior of the "real world " systems. These systems are generally inhomogeneous (porous) and the true "capacitance" is a distribution of values. A factor *n,* is associated with the CPE value; it ranges from 0 to 1 and indicates the degree of inhomogeneity. A perfect capacitor would have a value of 1.0

Statistical Approach

A table of Pearson's correlation coefficients was generated and coefficients with low values (near zero) were eliminated as potential linear correlations. Pearson's correlation coefficients are an indicator of interrelatedness and is the covariance of the two data sets divided by the product of their standard deviations. Multiple linear regression using "least squares" was then performed on the chosen dependent variable (ASTM D 2244) with the independent variables being the parameters (R_{pf}, R_{ct}, C_{pf}, C_{dl}) from the Equivalent Circuit Model (ECM), obtained from accelerated weathering tests (ASTM B117, GM9540P, QUV-A). The linear model has the form:

$$Y = \beta_0 + \beta_1 x_1 + \ldots \beta_m x_m$$

Y is the chosen dependent variable (ASTM rating), β the calculated coefficients, and x the parameter predictor(s) (ECM parameter(s)).
The independent variables were chosen until a Fisher statistic (F-stat) greater than the critical F- distributions is obtained for the corresponding degrees of freedom. Probability values (p-values) were generally < 0.05 (the accepted publishable limit), which corresponds to the 95% confidence level. The t-stats were determined to be above their critical values. In addition, care was taken not to have closely correlated independent variables to avoid the problem of multicollinearity. The best models were determined to have the least amount of variables and still meet the listed criteria.

The Coefficient of Determination (R^2) is the fraction of the variation of the dependent variable that can be explained by the independent variables, and the "Adjusted R^2" is the R^2 value adjusted for the degrees of freedom. The Fisher statistic is an overall test of the model's fit, which is a ratio of the mean square errors. P-values provide a sense of the strength of the evidence against the "null hypothesis", the lower the p-value the stronger the evidence.. In hypothesis testing one wishes to show real effects of an experiment. By showing that the experimental results were unlikely, given that there were no effects, one may decide that the effects are, in fact, real. The hypothesis that there were no effects is called the "null hypothesis". The t-stat for correlation tests the significance and reliability of the correlation coefficient, the larger the absolute value of the t-stat, the more significant the estimated correlation.

Results

Color change

A color change (dE, ASTM D 2244) in the AZ exposure of coating A can be predicted from the QUV–A exposure with the paint film resistance and capacitance parameters (QR_{pf}, QC_{pf}) and the capacitance of the double layer (QC_{dl}). The adjusted R^2 value indicates that the model explains >95% of the variation in the color of the coating. The Fisher distribution (F-distribution) value (>2000) is in excess of the tabled critical value (19.16) for the corresponding degrees of freedom (3,2) at the 95% confidence level. The t-stats (>7) of the variable coefficients are greater than the critical value of 2.015 at the 95% confidence level; the model therefore has statistical significance.

A color change (dE) in the AZ exposure of coating C can be predicted with the paint film resistance and capacitance (QR_{pf}, QC_{pf}) from the QUV-A exposure. The adjusted R^2 value indicates that the model explains >95% of the variation in the color of the coating. The F-distribution value (>55) is in excess of the tabled critical value (9.55) for the corresponding degrees of freedom (2,3) at the 95% confidence level. The t-stats (>3.6) are greater than the critical value of 2.015 at the 95% confidence level; the model therefore has statistical significance.

The color change (dE) in the FL exposure of coating A was modeled with a combination of the ECM parameters from the QUV-A (QC_{pf}, QR_{pf}) and B117 (BC_{pf}) accelerated tests. The adjusted R^2 value indicates that the model explains >97% of the variation in the color in the coating. The F-distribution value (>58) is in excess of the tabulated critical value (19.16) for the corresponding degrees of freedom (3,2) at the 95% confidence level. The t-stats (>3.8) are greater than the critical value of 2.015 at the 95% confidence level; the model therefore has statistical significance.

The color change (dE) in the FL exposure of coating C was modeled with a combination of the ECM parameters from the QUV-A (QC_{pf}, QR_{pf}) and B117 (BC_{pf}) accelerated tests.

The adjusted R^2 value indicates that the model explains >98% of the variation in the color in the coating. The F-distribution value (>104) is in excess of the tabulated critical value (19.16) for the corresponding degrees of freedom (3,2) at the 95% confidence level. The t-stats (>3.2) are greater than the critical value of 2.015 at the 95% confidence level; the model therefore has statistical significance.
A color change of coating B in the AZ exposure was modeled with the paint film capacitance parameter (QC_{pf}) from the QUV-A exposure and the paint film capacitance from the GM9540P test (GC_{pf}). The adjusted R^2 value indicates that the model explains >87% of the variation in the color of the coating. The F-distribution value (>18) is in excess of the tabulated critical value (9.55) for the corresponding degrees of freedom (2,3) at the 95% confidence level. The t-stats (>4.7) are greater than the critical value of 2.015 at the 95% confidence level; the model therefore has statistical significance.

A color change of coating D in the AZ exposure was modeled with the paint film capacitance (QC_{pf}) parameter from the QUV-A exposure and the paint film capacitance from the GM9540P test (GC_{pf}). The adjusted R^2 value indicates that the model explains >88% of the variation in the color of the coating. The F-distribution value (>20) is in excess of the tabulated critical value (9.55) for the corresponding degrees of freedom (2,3) at the 95% confidence level. The t-stats (>3.7) are greater than the critical value of 2.015 at the 95% confidence level; the model therefore has statistical significance.

A color change of coating B in the FL exposure was modeled with the paint film capacitance parameters from the QUV-A (QC_{pf}) and the GM9540P tests (GC_{pf}). The adjusted R^2 value indicates that the model explains >96% of the variation in the color of the coating. The F-distribution value (>66) is in excess of the tabulated critical value (9.55) for the corresponding degrees of freedom (2,3) at the 95% confidence level. The t-stats (>9.7) are greater than the critical value of 2.015 at the 95% confidence level; the model therefore has statistical significance.

A color change of coating D in the FL exposure was modeled with the paint film capacitance parameters from the QUV-A (QC_{pf}) and the GM9540P tests (GCpf). The adjusted R^2 value indicates that the model explains >69% of the variation in the color of the coating. The F-distribution value (>6.8) is less than the tabulated critical value (9.55) for the corresponding degrees of freedom (2,3) at the 95% confidence level. The t-stats (>2.66) are greater than the critical value of 2.015 at the 95% confidence level.

Adhesion

The adhesion of coating A in the AZ exposure was modeled with the double layer capacitance of the QUV-A exposure (QC_{dl}). The adjusted R^2 value indicates that the model explains >68% of the variation in the adhesion of the coating. The F-distribution values (>11) are in excess of the tabulated critical value (7.71) for the corresponding degrees of freedom (1,4) at the 95% confidence level. The t-stats (>3.4) are greater than the critical value of 2.015 at the 95% confidence level; the model therefore has statistical significance.

The adhesion of coating A in the FL exposure was modeled with the resistance to charge transfer of the QUV-A exposure (QR_{ct}) and the paint film capacitance of the B117 test (BC_{pf}). The adjusted R^2 value indicates that the model explains >91% of the variation in the adhesion of the coating. The F-distribution value (>28) is in excess of the tabulated critical value (9.55) for the corresponding degrees of freedom (2,3) at the 95% confidence level. The t-stats (>4.5) are greater than the critical value of 2.015 at the 95% confidence level; the model therefore has statistical significance.

The adhesion of coating C in both the AZ and FL exposures could not be modeled due to the poor adhesion from the onset of testing.

The adhesion testing of coating B in the AZ exposure correlated significantly to the GM9540P charge transfer resistance parameter (R_{ct}). The adjusted R^2 value indicates that the model explains >84% of the variation in the adhesion of the coating. The F-distribution value (>27) is in excess of the tabulated critical value (7.71) for the corresponding degrees of freedom (1,4) at the 95% confidence level. The t-stats (>5) are greater than the critical value of 2.015 at the 95% confidence level; the model therefore has statistical significance.

The adhesion testing of coating D in the AZ exposure correlated significantly to the B117 parameters (BR_{ct}, BR_{pf}, BC_{pf}). The adjusted R^2 value indicates that the model explains >87% of the variation in the adhesion of the coating. The F-distribution value (>13) is less than the tabulated critical value (19.16) for the corresponding degrees of freedom (3,2) at the 95% confidence level. The t-stats (>4.5) are greater than the critical value of 2.015 at the 95% confidence level.

The adhesion testing of coating B in the FL exposure was modeled with the GM9540P and the B117 double layer capacitances (GC_{dl}, BC_{dl}). The adjusted R^2 value indicates that the model explains >97% of the variation in the adhesion of the coating. The F-distribution value (>111) is in excess of the tabulated critical value (9.55) for the corresponding degrees of freedom (2,3) at the 95% confidence level. The t-stats (>11) are greater than the critical value of 2.015 at the 95% confidence level; the model therefore has statistical significance.

The adhesion testing of coating D in the FL exposure was modeled with the QUV-A paint film resistance (QR_{pf}) and the B117 parameters; BCpf and BRct. The adjusted R^2 value indicates that the model explains >99% of the variation in the adhesion of the coating. The F-distribution value (>1700) is in excess of the tabulated critical value (19.16) for the corresponding degrees of freedom (3,2) at the 95% confidence level. The t-stats (>49) are greater than the critical value of 2.015 at the 95% confidence level; the model therefore has statistical significance.

Discussion

The use of a single accelerated test (QUV-A) for the evaluation of color change (dE) in coatings A and C in the AZ environment is an indication that the primary degradation mechanism is UV irradiance. The R_{pf} of coating A in the AZ environment is at a maximum at ~200MJ/m^2 of UV exposure and coating C at ~300MJ/m^2; this is due to residual curing/cross linking. The sharp decrease of the R_{pf} in the 300-600MJ/m^2 exposures of both coating A and C indicates the formation of ionically conductive paths through the coating, which suggests that adhesion loss and corrosion are imminent.

The color change (dE) in the FL exposure of coatings A and C can be determined with combination of ECM parameters from the QUV-A (QR_{pf}, QC_{pf}) and B117 (BC_{pf}) accelerated tests. The UV irradiance and the exposure to the FL marine atmosphere and their synergistic effects necessitate the use of the two accelerated tests. The R_{pf} of the coating is at a maximum at ~100MJ/m^2 for coating A and at ~300 MJ/m^2 for coating C this is attributed to residual curing/cross linking and its decreasing porosity. The decrease in the R_{pf} of coating A at ~100-300MJ/m^2 exposure and the decrease in the R_{pf} of coating C at ~300-500MJ/m^2 exposure is due to the formation of ionically conductive paths through the coating, which suggests that adhesion loss and corrosion are imminent. Coating C has a longer cure time than coating A and better paint film resistance at longer exposure in the FL environment. The absence of an interfacial EIS parameter in coating A with comparison to the AZ exposure may be the consequence of humidity in the FL environment and the migration of inhibitors (i.e. chromates) to the substrate. Though coatings A and C are applied to different substrates (steel, aluminum) the performance of both solvent systems and their degradation mechanisms appear to be similar.

The color change of waterborne coatings B and D in the AZ and FL exposures can be predicted with the paint film capacitance parameter from the QUV-A exposure (QC_{pf}) and the C_{pf} from the GM9540P test (GC_{pf}). The statistical significance of the model for the color change of coating D in the FL exposure is questionable due to the small F-distribution value; additional testing is necessary to calibrate this model. The parameter from the QUV exposure correlates to the UV exposure and the significance of UV degradation. The GM9540P test simulates the temperature changes and subsequent thermal degradation in the AZ exposure and the humidity/ion penetration of the FL marine atmosphere. The fluctuations in the R_{pf} values of both coatings in the AZ and FL exposures are attributed to the migration of inhibitors within the coating and the competing cross linking and chain scission reactions. It is generally thought that color change is a surface phenomena, however; at increased exposures change is also occurring throughout the bulk of the coating, giving an indication of the reliable lifetime of the coating system. Hence; photo-oxidative degradation and the synergistic effects of humidity/ion penetration and thermal degradation can cause aesthetic and functional changes in organic coatings. Coatings B and D have similar degradation mechanisms as demonstrated with the use of the same electrochemical parameters to model their performance.

Adhesion

The adhesion of coating A in the AZ exposure can be predicted with the double layer capacitance from the QUV-A test (QC_{dl}); this parameter corresponds to the coating/substrate interface where adhesive failure occurs. The use of a single accelerated test (QUV-A) for the evaluation of coating A in the AZ environment is an indication that the primary degradation mechanism is UV irradiance.

The adhesion of coating A in the FL exposure can be predicted with the R_{ct} of the QUV-A accelerated test and the C_{pf} of the B117 test. The QR_{ct} parameter corresponds to the interfacial region where adhesion loss would be observed and the BC_{pf} to the increasing porosity of the coating, which would increase interfacial corrosion activity. The introduction of the B117 parameter (BC_{pf}) is necessary to simulate the marine atmosphere and the synergistic effects of UV irradiance and humidity/ion penetration in the FL exposure.

Adhesion data for coating C was inconclusive due to the suspected contaminants on the substrate prior to application of the coating; hence, poor adhesion from the onset of testing.

The adhesion testing of coating B in the AZ exposure can be predicted with the GM9540P resistance to charge transfer parameter (GR_{ct}), which relates to the coating-substrate interface. The thermal cycle of the GM9540P test simulates the temperature changes in the AZ exposure and indicates that thermal degradation is significant.

The adhesion testing of coating D in the AZ exposure can be predicted with the B117 parameters (BR_{ct}, BR_{pf}, BC_{pf}) that relate to interfacial activity and the porosity of the coating. Though the statistical significance of the model for the color change of coating D in the FL exposure is questionable due to the small F-distribution value, additional testing is necessary to calibrate this model.

The adhesion testing of coating B in the FL exposure can be predicted with the GM9540P and the B117 C_{dl} parameters. These parameters simulate the marine atmosphere of the FL environment and that the primary degradation mechanism for adhesion loss is due to the humidity/ion penetration of the coating.

The adhesion testing of coating D in the FL exposure can be predicted with the QUV-A (R_{pf}) and the B117 (R_{ct}, C_{pf}) parameters. These parameters are indicative of the marine atmosphere of the FL environment and exemplify the synergistic effects of UV irradiance and humidity/ion penetration. The use of B117 parameters C_{dl} and R_{ct} in coating B and D in the FL environment is indicative of the penetration of ionic species (Na^+, Cl^-) to the coating-substrate interface.

Blistering

There was no observed blistering of coatings A and B during the duration of the testing period; therefore it could not be modeled. The lack of an appropriate blistering grading system for comparison to EIS parameters prohibited the modeling of coatings C and D.

Though the correlations of the natural exposures to the accelerated tests are straightforward, the difficulty arises in determining the constant in the proposed equations for a predictive model. The constant is not the same when comparing the coatings systems or to the different exposures within the same system. A reasonable estimate can be achieved for the constant by fitting the model with the first few observed exposures (3-4), predictions then can be made for subsequent exposures. The number of necessary observed exposures varies with the number of independent variables, the greater the number of independent variables the more observations that are needed. Also, the more observations made, the greater the accuracy of the estimated constant. The constant is the dominating model component at the initial exposures but becomes less significant with prolonged exposure.

Future Work

Time comparisons of the natural exposure (0,7,13,25,49, and 97wks.) to that of the accelerated test (0,3,6,12,18,and 48wks.) parameters were implemented in the statistical analysis. An accelerated exposure for the QUV-A and B117 tests at 25 weeks will soon be completed and the models reanalyzed, this will be done to be consistent with the ~2:1 time ratio of natural to accelerated testing. This project coincides with a concurrent In-House Laboratory Independent Research (ILIR) project entitled, "The Role of Weathering Parameters on the Mechanisms of Naval Aircraft Coatings", which is examining EIS at elevated temperatures. Similar accelerated exposures are being used that will allow the integration of the hydrothermal electrochemical parameters into the MMCD test matrix.

It is apparent that changes in impedance parameters (i.e., QC_{pf}, BR_{pf}, etc.) statistically explain most of the degradation observed in the coating systems when exposed to the natural environment. Capacitance values are affected by changes in the dielectric properties of the coatings; polymer chain segment rearrangements, broken bonds, and ingress of water/ions are some of the phenomena that can change dielectric properties. Resistance values are affected by changes to the barrier properties of the films; increases/decreases of cross-link density and formation of conductive pathways through the film can influence the barrier properties of polymers. The last phase of this project is to explain the statistical model in terms of the physical, chemical, and spectroscopic data obtained by the other subgroups. This process will shed some light as to exactly which phenomena are affecting the performance of the coatings and then degradation mechanisms can be proposed. These mechanisms can then be used to develop greener, superior-performing coatings.

References

[1] K. Kovaleski, D. Dumsha, "Mechanisms of Military Coatings Degradation (PP-1133): Electrochemical Impedance Spectroscopy Part 1", Naval Air Warfare Center Report NAWCADPAX/TR-2001/55, Patuxent River, MD, June 2001.

[2] E.P.M. van Westing, G. M. Ferrari, Corr. Sci. 36, 8 (1994): p. 1323.

[3]M. Triola, Elementary Statistics 5th ed., Addison-Wesley Publishing Co. Inc., 1992.

[4]D. Stockburger, Introductory Statistics: Concepts, Model, and Applications, Southwest Missouri State University, Copyright 1996.

Spectroscopic Characterization of Surface and Interfacial Properties of Two-Component Military Coatings

Principal Investigators: C.R. Clayton and G.P. Halada (SUNY at Stony Brook)
Graduate Student: Lionel Keene

Project Background: Current environmental regulations require more benign coatings than are available with most contemporary formulations. These new formulations are not only expected to possess barrier properties that afford underlying vehicles the same (or better) level of corrosion protection, but are also expected to resist environmentally induced changes to their color signatures. They must also demonstrate the correct mechanical properties for their given applications. To achieve these superior formulations, the current families of coatings must under a comprehensive characterization process whereby their primary chemistry is well understood and cataloged. Changes to their fundamental chemical/mechanical properties can then be tracked and their sources pinpointed. Armed with this information, future military coatings formulators will be able to arrive at important conclusions by drawing upon subtle changes that have been comprehensively cataloged and investigated, ultimately leading to fundamentally more suitable coating systems.

Objective: The objective of this project was to precisely quantify and catalog the chemical nature and behavior of contemporary military coatings through a variety of spectroscopic means. These coatings include four families, namely coatings "A" (army green), "B" (army green), "C" (nav/air gray) and "D" (nav/air gray). These four coatings families represent VOC as well as Non (Waterborne)/Low-VOC formulations and comprise the bulk of coatings in use in the armed forces today. This effort involved not only advanced applications of current spectroscopic techniques but, due to the nature of the coatings themselves, also required innovative new approach to be applied. The analytical techniques that have been (or are currently being) recruited in this endeavor include Micro Fourier Transform Infrared (FTIR) spectroscopy, Scanning Electron Microscopy (SEM), Energy Dispersive Analysis of X-rays (EDAX), Micro-Raman Spectroscopy, Moiré interferometry, Confocal Laser Topography and Femtosecond Laser Ablation.

Technical Approach / Results

1. Scanning Electron Microscopy (SEM) & Energy Dispersive X-ray Analysis (EDAX) Spectroscopy

All four coating families included in this study have adopted a general binder chemistry formulation that is currently the mainstay of polyurethane coatings worldwide in both public as well as private sectors. This formulation is, generally, a two-part reaction between a polyfunctional hydroxide and a diisocyanate molecule to create block-polymerized polyurethane chains that are highly crosslinked. The two-package formulation is mixed just prior to application to prevent curing during storage. Ideally, the resulting polymer matrix (binder) permeates the free spaces residing between the pigments and additives and is itself free of porous defects while exhibiting the desired mechanical properties.

Samples were prepared via the cross-sectional microtome technique described in "Section 2 Micro Fourier Transform Infrared Spectroscopy". SEM images were captured as were general, spot and map EDAX spectra showing the bulk chemical composition and distribution. It serves as a general microscopic inspection tool showing additive distribution, degree of mixing and any obvious coating system flaws such as large voids due to improper pigment volume concentration (PVC) or accelerated weathering-induced cross-linking and subsequent free-volume reduction and topcoat embrittlement.

Given the general nature of the binder material (polymeric and hence electrically insulative) as well as the additives (insulative and semiconductive in nature), this poses a problem for SEM microscopy in terms of charge build-up effects. This problem has been overcome by pre-sputtering a 40-70 Angstrom layer of gold onto cross-sectioned samples to facilitate charge "bleeding". To further facilitate charge compensation samples were mounted on SEM vacuum-compatible copper tape.

Coating system A

Due to the large PVC ratio coating system A is substantially more brittle than coatings B, C and D and has proven extremely difficult to microtome. As a result SEM analysis results of this coating system are not yet available.

Coating system B

Coating system B is a two-part low-VOC water-dispersible polyurethane binder meant to replace coating A. Its primary innovation resides in its polymeric bead extender formulation, which replaces the more traditional diatomaceous earth silica extenders. Figures 1-5 shows the results of SEM/EDAX analysis of coating system B, baseline sample.

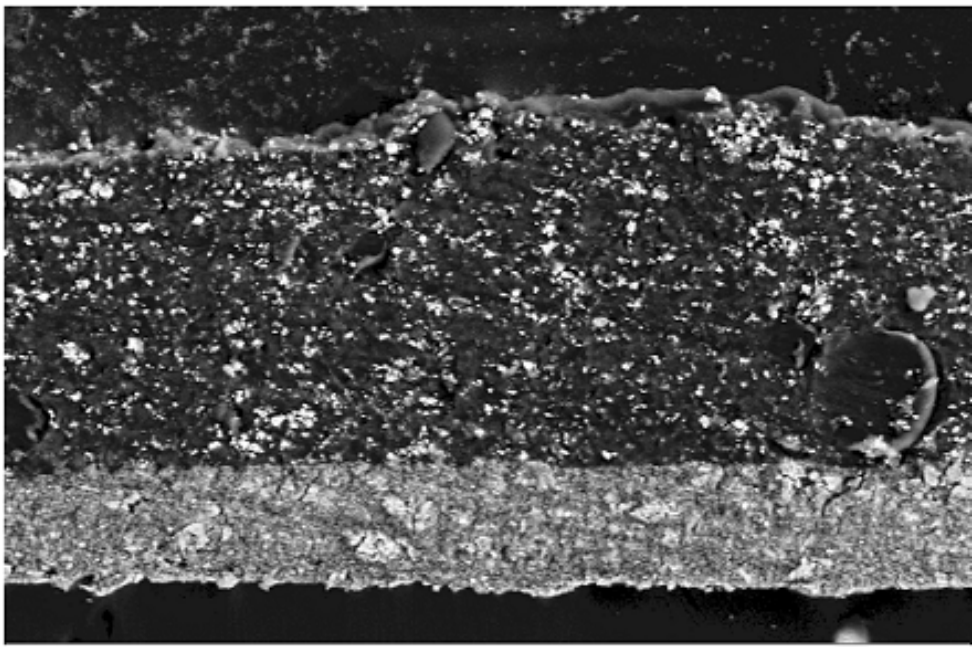

Figure 1. SEM image of coating system B microtomed cross-section showing both topcoat and primer.

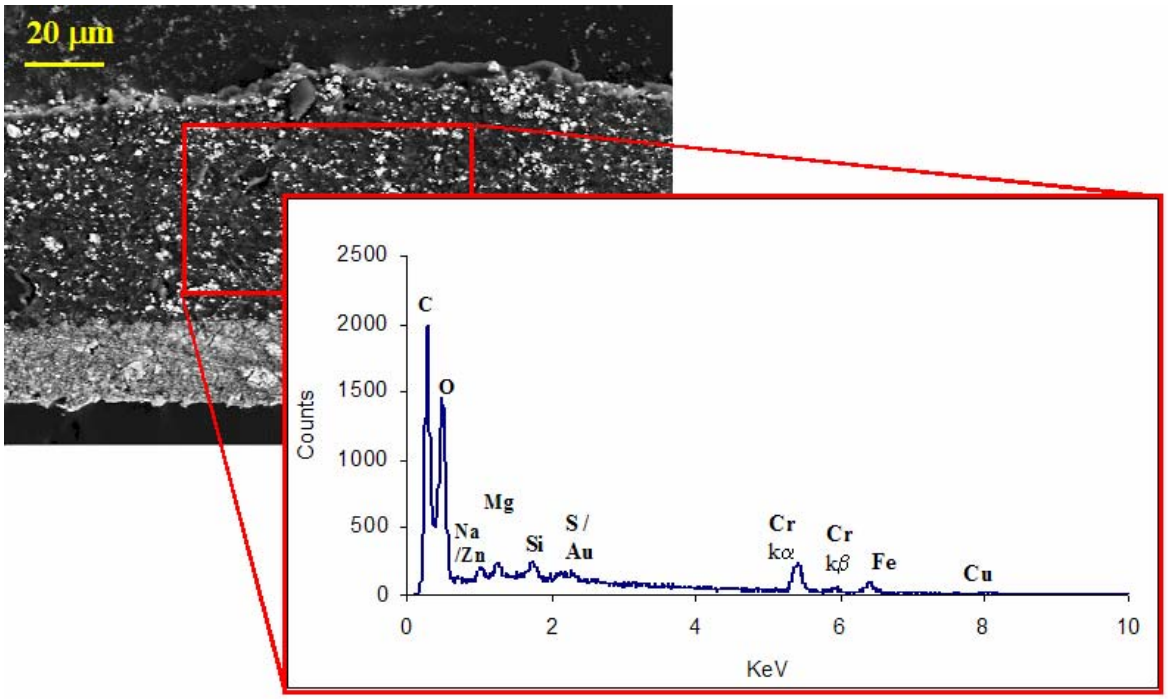

Figure 2. EDAX spectrum showing general elemental composition of topcoat layer for coating system B.

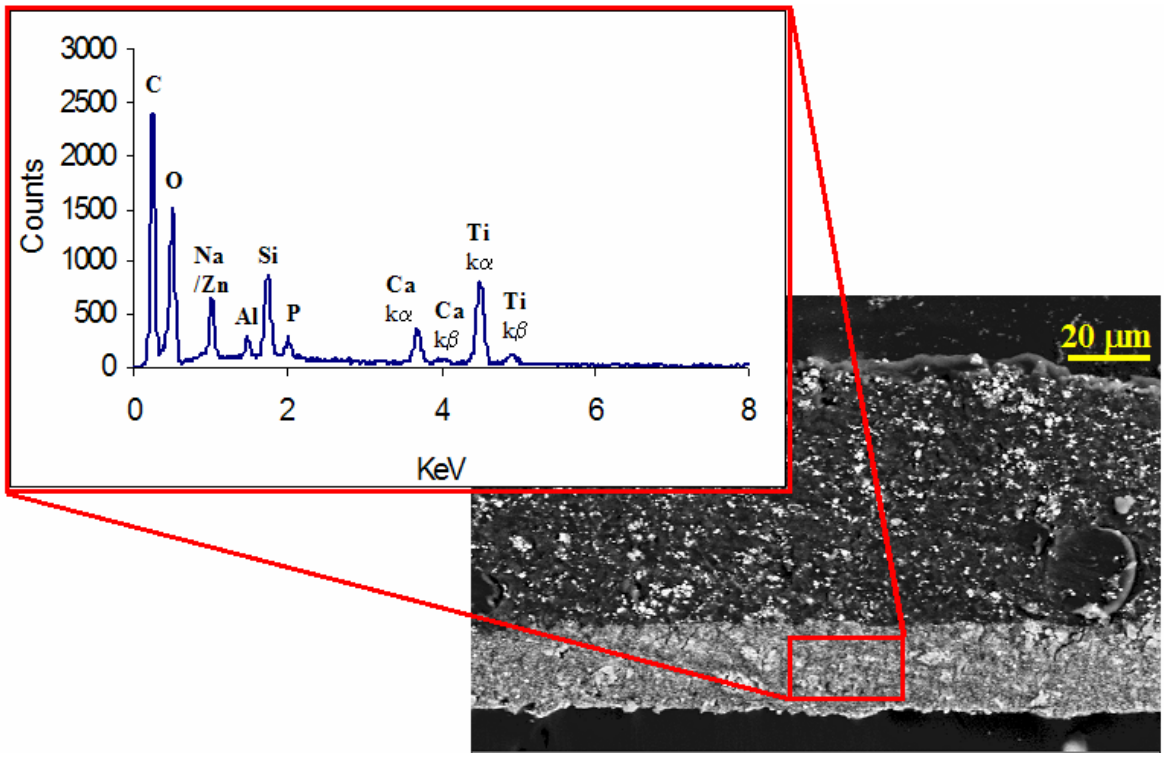

Figure 3. EDAX spectrum showing general elemental composition of primer layer for coating system B.

Figure 4. EDAX map of primer layer showing spatial distribution of primary elements in coating system B.

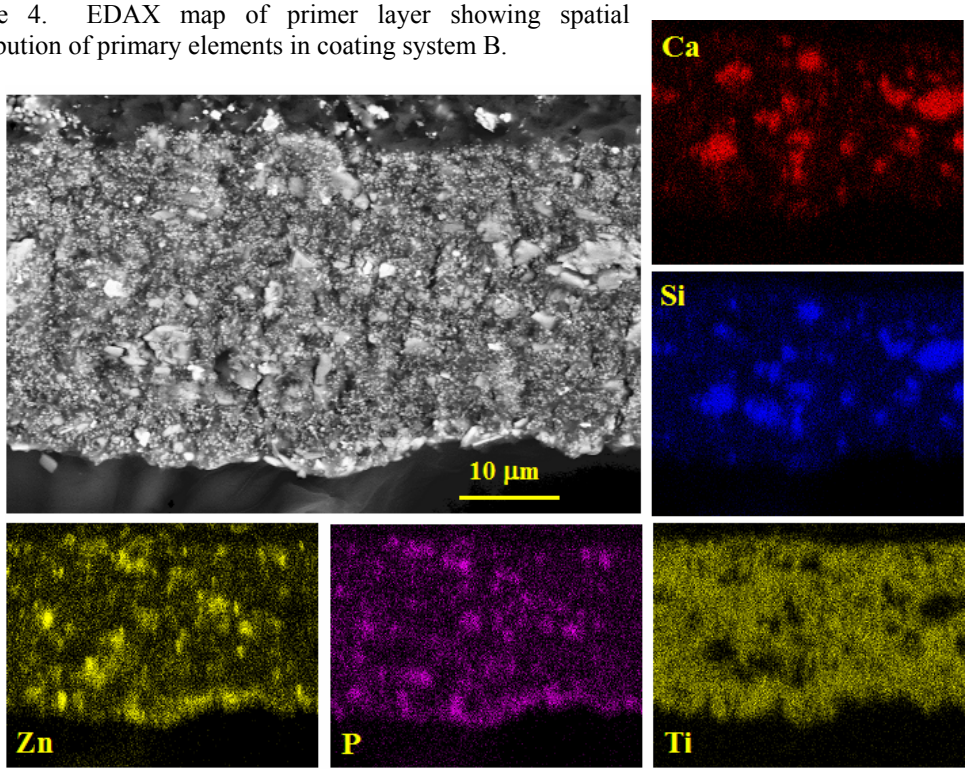

Figure 5. EDAX map of primer layer showing spatial distribution of primary elements in coating system B.

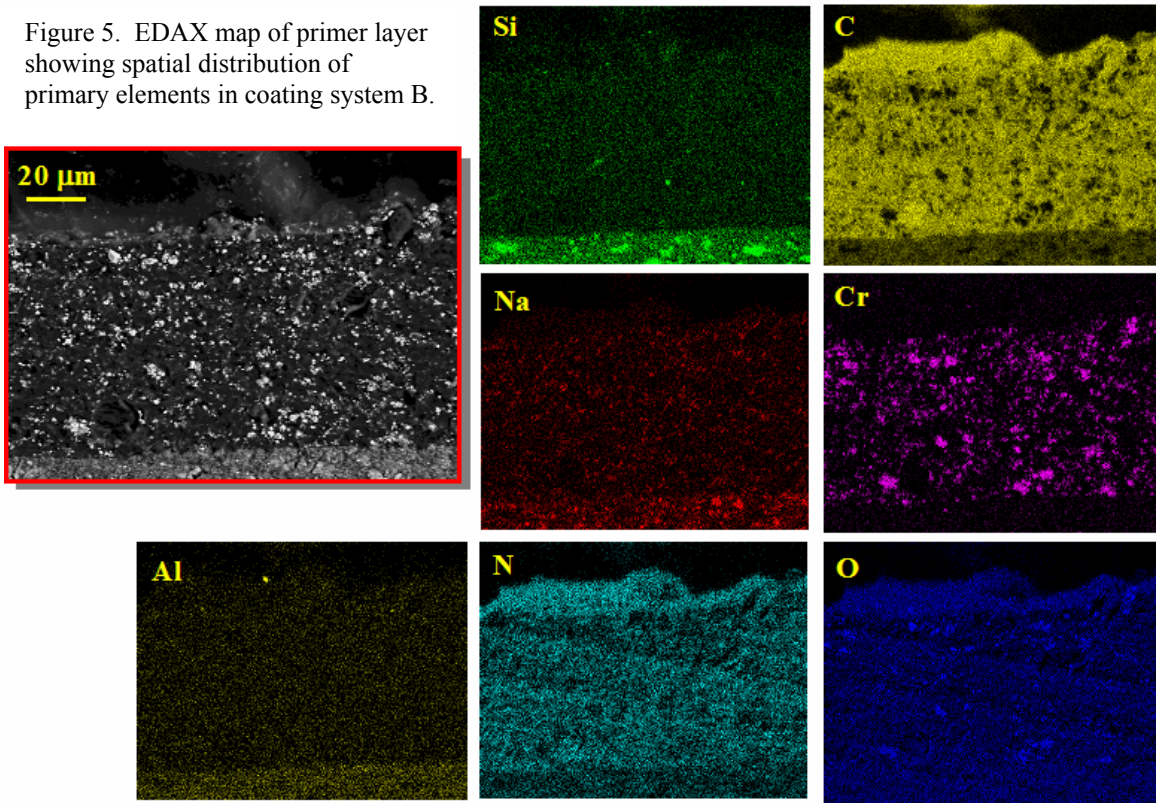

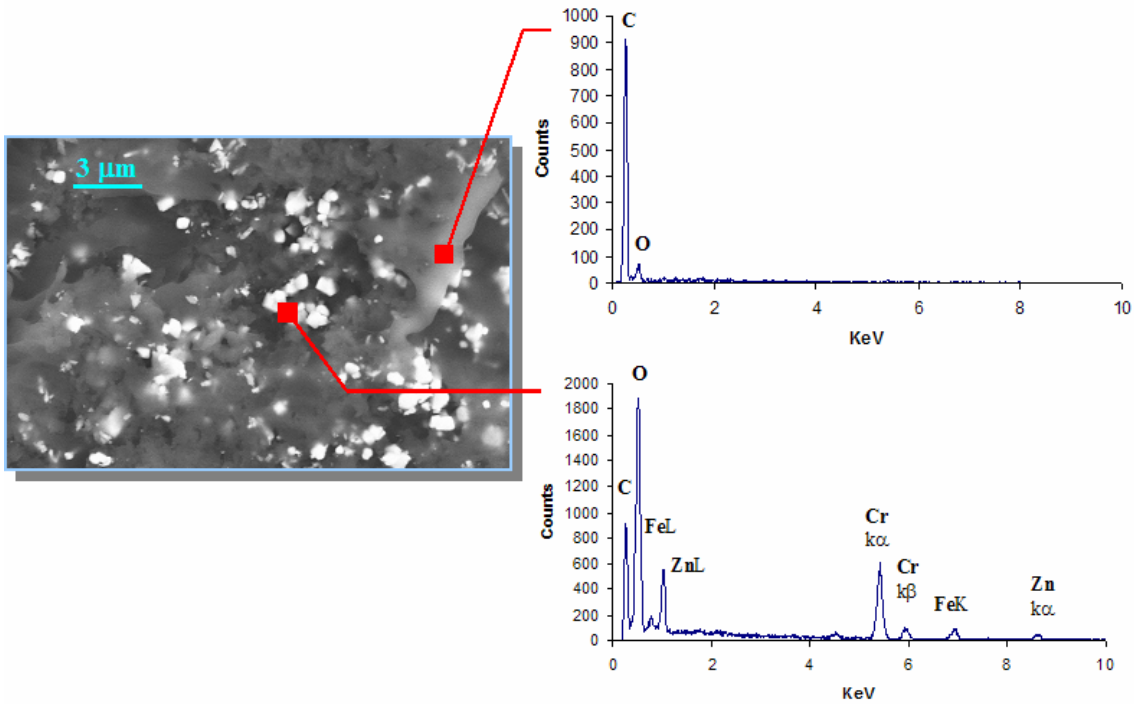

Figure 6. Topcoat detail / spot EDAX showing chemical composition of binder (upper spectrum) and pigment particle cluster (lower spectrum).

Coating System C

Coating system C is the naval control system consisting of a MIL-C-85285 solvent based polyurethane and MIL-P-23377 solvent based epoxy. Initial analysis has focused on samples subjected to 18 weeks QUV accelerated UV weathering protocol. This coating differs from coating system B primarily in the pigment and additive content (TiO_2 pigmentation and SiO_2 inert filler flattening agent). Figures 7 - 11 show the results of SEM/EDAX analysis of this coating system.

Figure 7. SEM image / EDAX maps of coating system C showing elemental distributions within topcoat and upper primer layers.

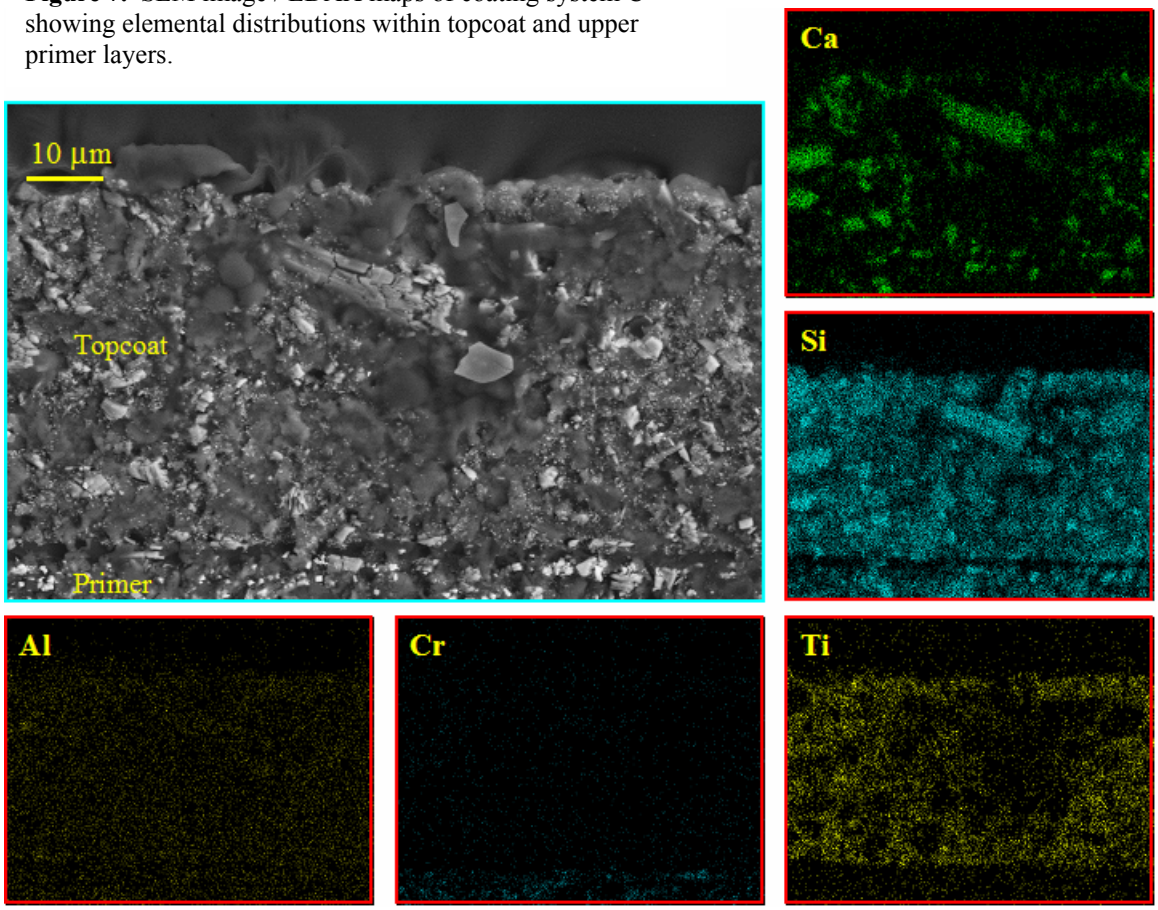

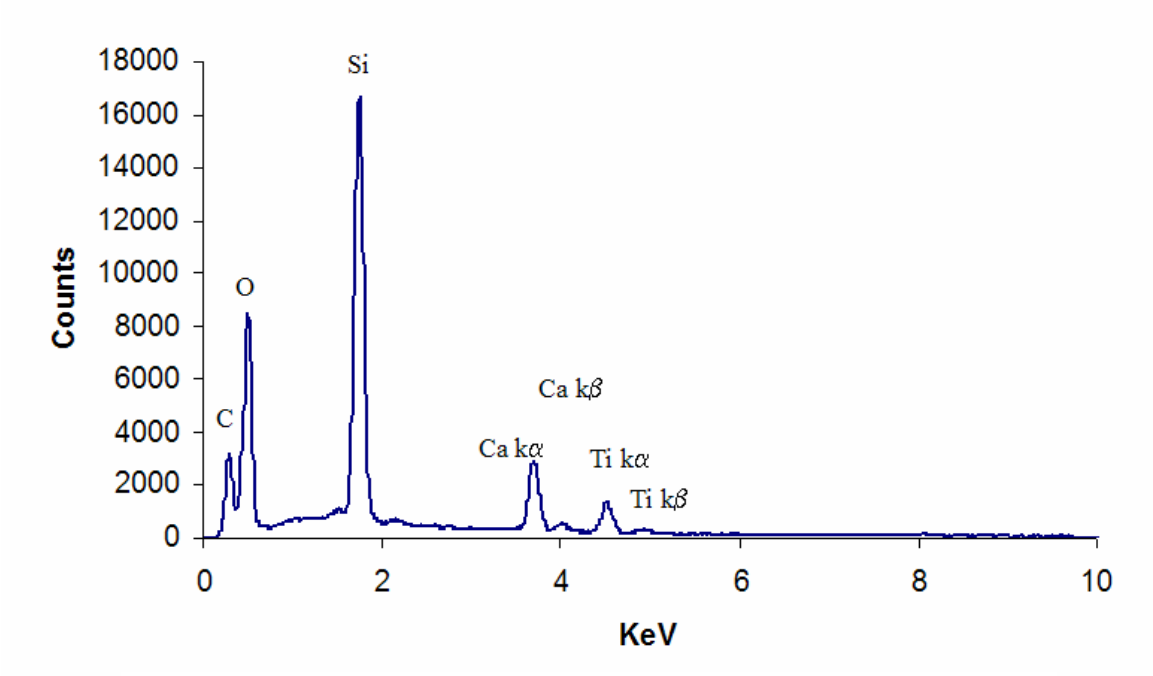

Figure 8. General topcoat EDAX spectrum for coating system C, 18 weeks QUV.

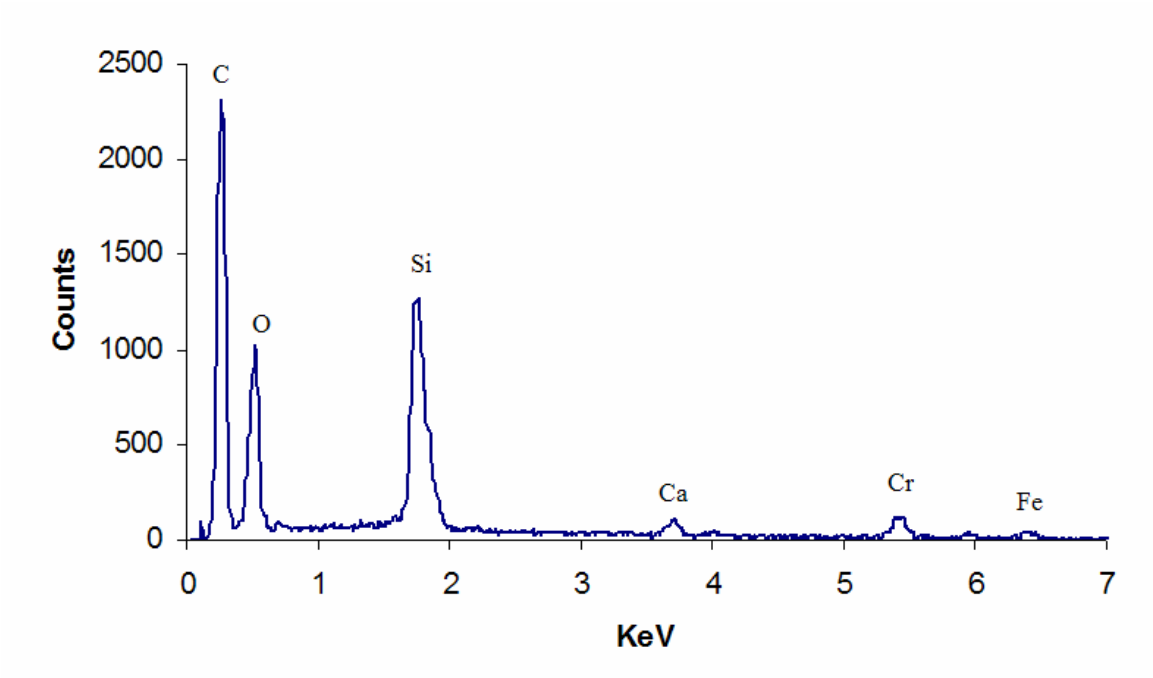

Figure 9. General primer EDAX spectrum for coating system C, 18 weeks QUV.

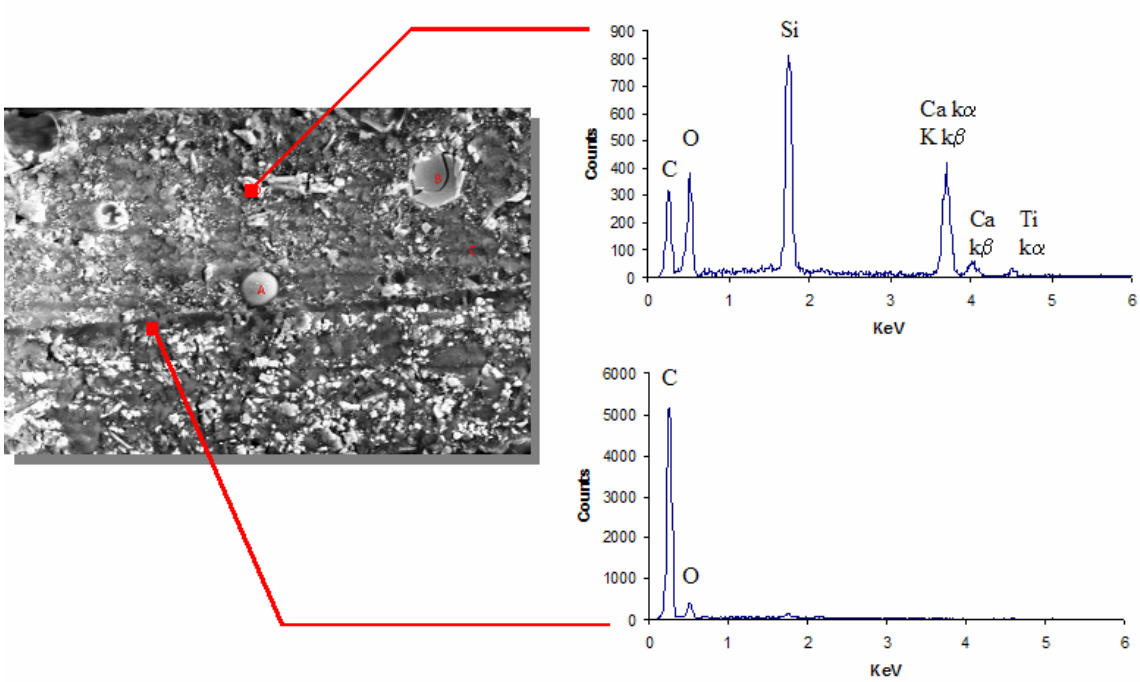

Figure 10. Spot EDAX spectra of coating system C, 18 weeks QUV showing chemical composition of pigment and additive-rich regions of topcoat layer (upper spectrum) as well as chemical composition of topcoat/primer interface zone (lower spectrum).

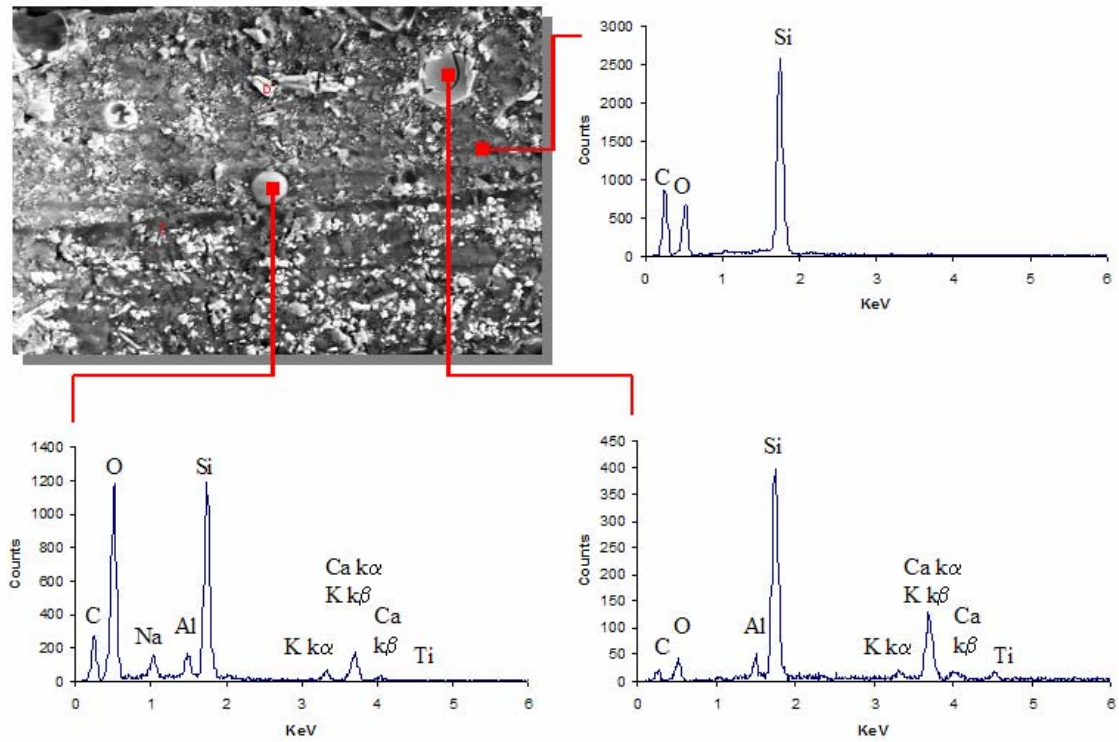

Figure 11. Spot EDAX Spectra showing general composition of binder/pigment matrix (upper spectrum) and inert flattening agents (lower two spectra).

Coating system D

Coating system D is the Navy future system based on a zero volatile organic compound (VOC) topcoat proprietary formulation consisting of a water based polyurethane binder applied on top of a MIL-P-85582 water based epoxy primer. The coating system is designed to be applied to aluminum substrates, which have been pretreated by a chromate conversion coating (CCC) to provide active passivation of the substrate surface. SEM/EDAX analysis has focused initially on samples that have been exposed to 18 weeks of QUV accelerated aging. Figures 12 – summarize the results of the analysis.

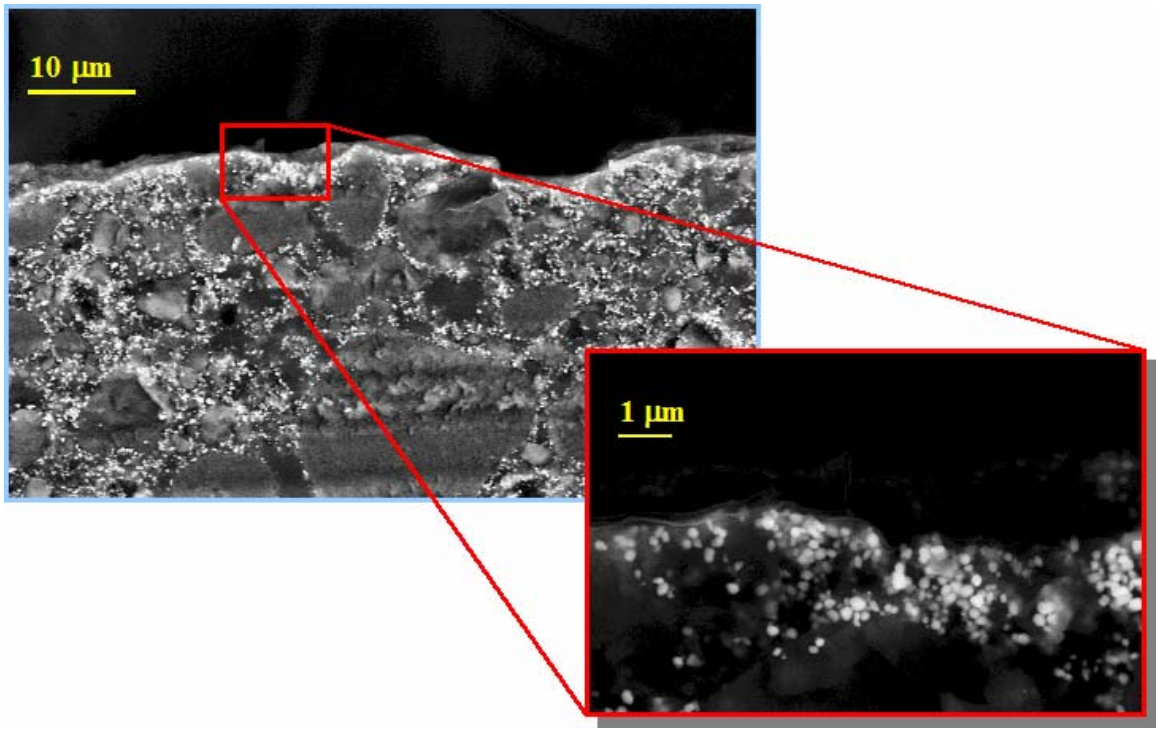

Figure 12. SEM micrographs of coating system D, 18 weeks QUV showing bulk of topcoat layer (upper image) and magnified detail of topcoat surface (lower image). TiO_2 pigmentation particles can be seen embedded in the polyurethane matrix and surrounding diatomaceous flattening agents. Scarcity of polymeric binder compared to additives/pigments is readily apparent.

Figure 13. Spot EDAX spectra showing chemical composition of coating system D, 18 weeks QUV collected from various regions of the topcoat and primer layers.

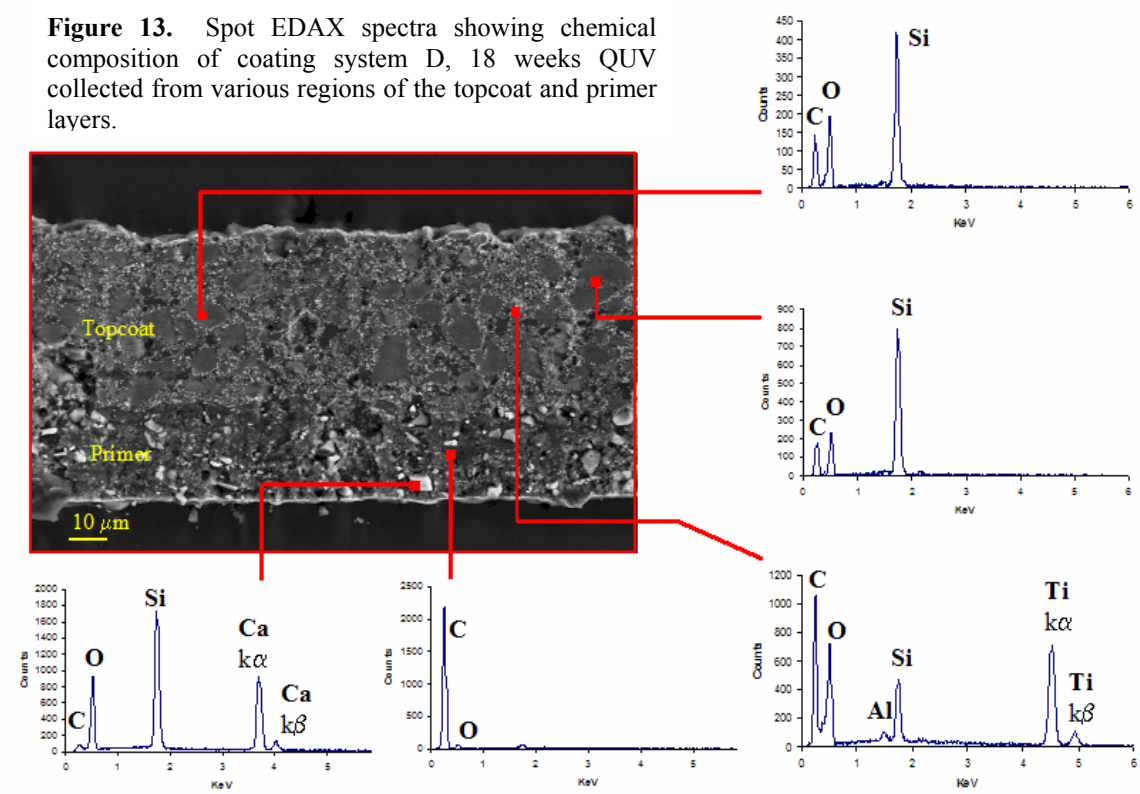

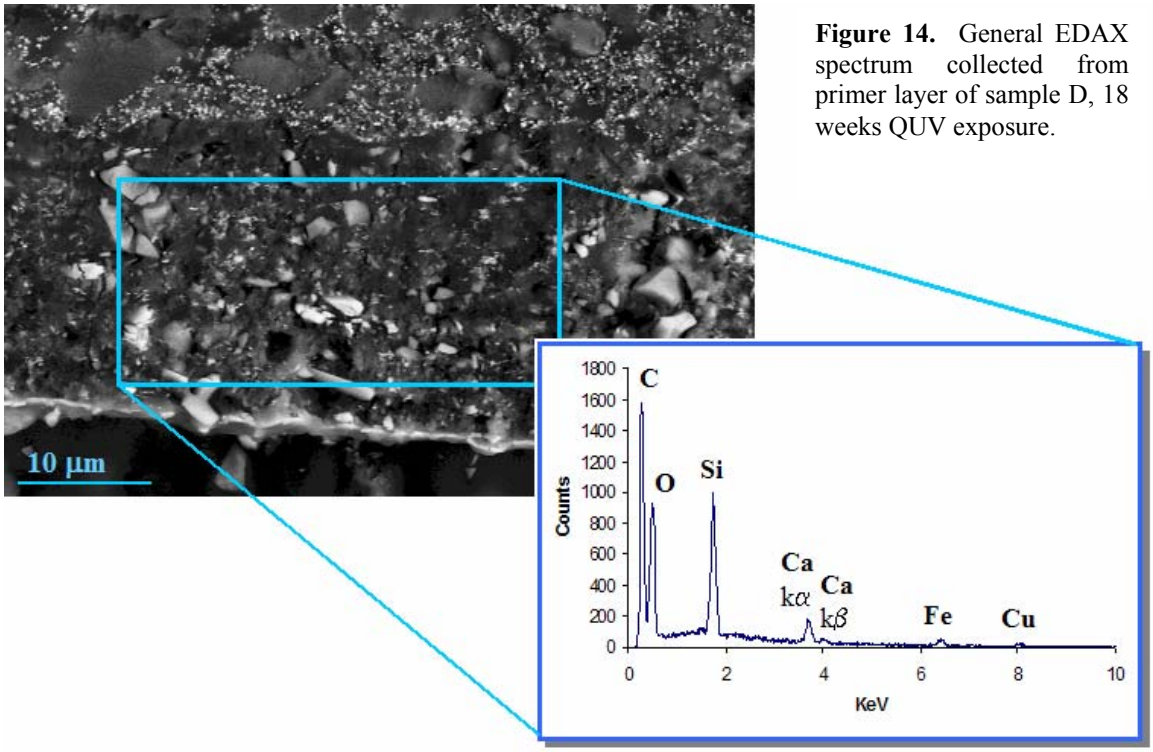

Figure 14. General EDAX spectrum collected from primer layer of sample D, 18 weeks QUV exposure.

Figure 15. EDAX maps of coating system D, 18 weeks QUV showing spatial distribution of elements within the topcoat. Large Si particles are indicative of diatomaceous silica fillers/flattening agents, Ti particles are indicative of TiO_2 pigmentation. Note scarcity of elemental carbon signal indicative of polymeric matrix.

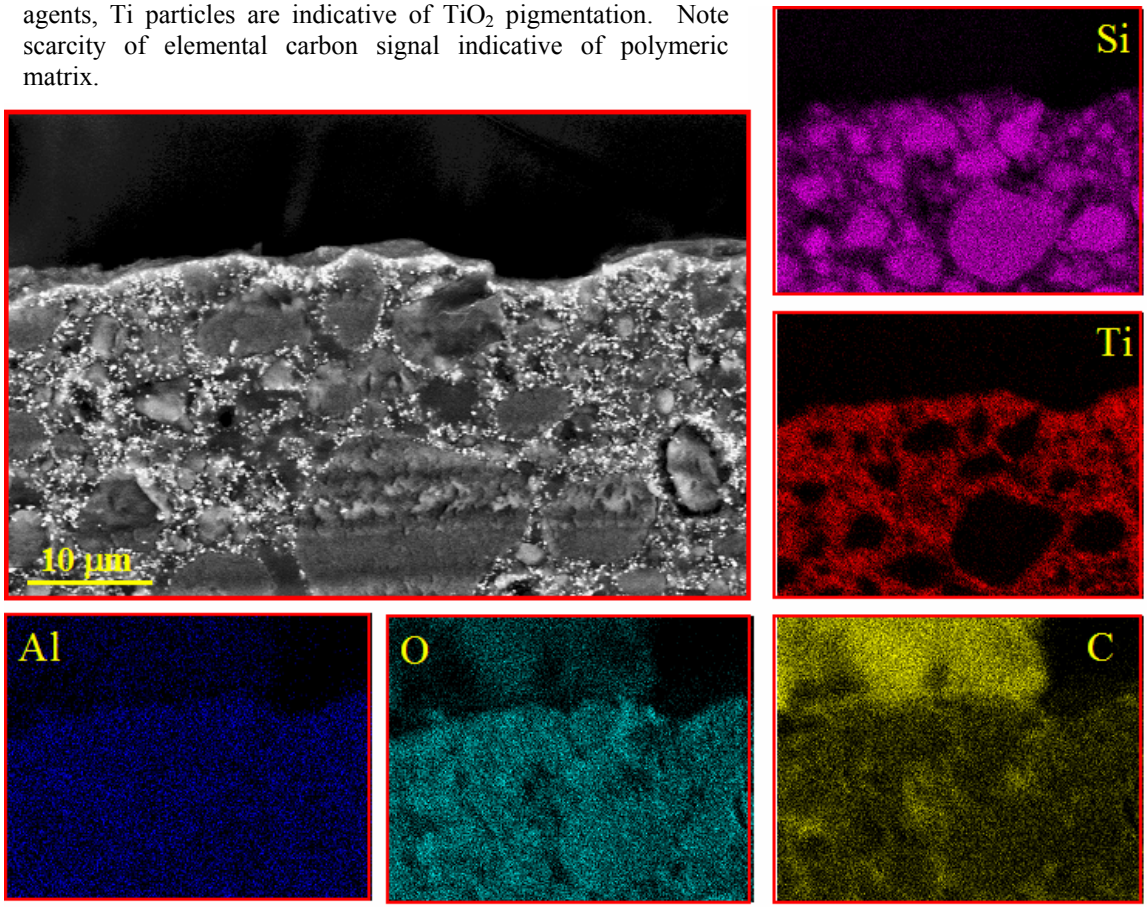

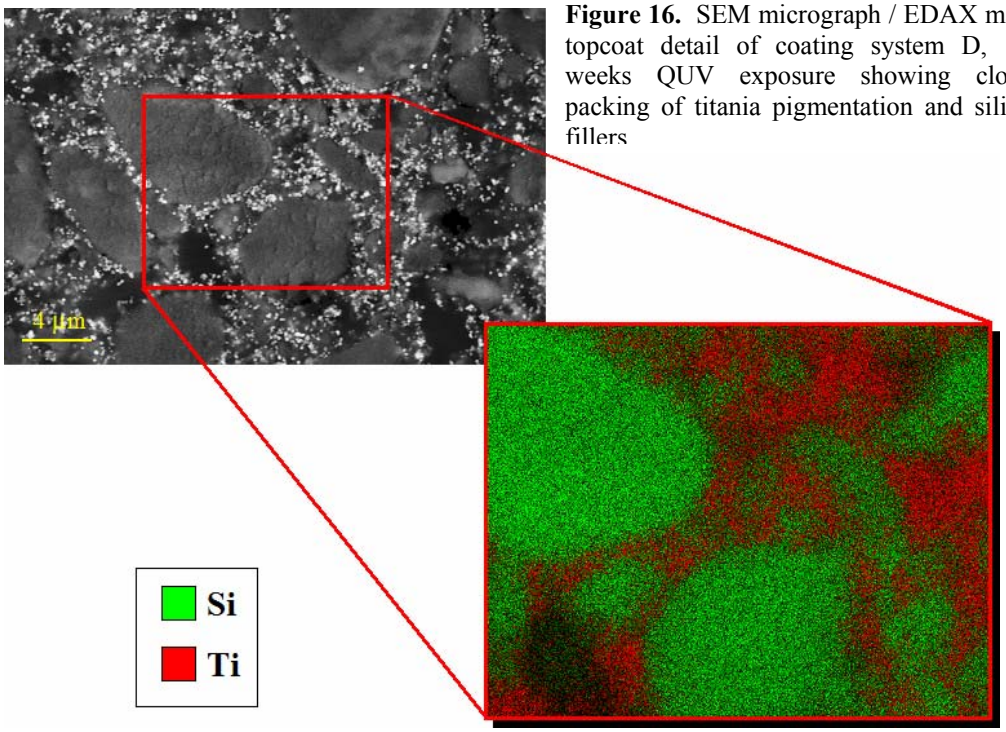

Figure 16. SEM micrograph / EDAX map topcoat detail of coating system D, 18 weeks QUV exposure showing close packing of titania pigmentation and silica fillers

Figure 17. SEM micrograph / EDAX maps of topcoat/primer interface for coating system D, 18 weeks QUV.

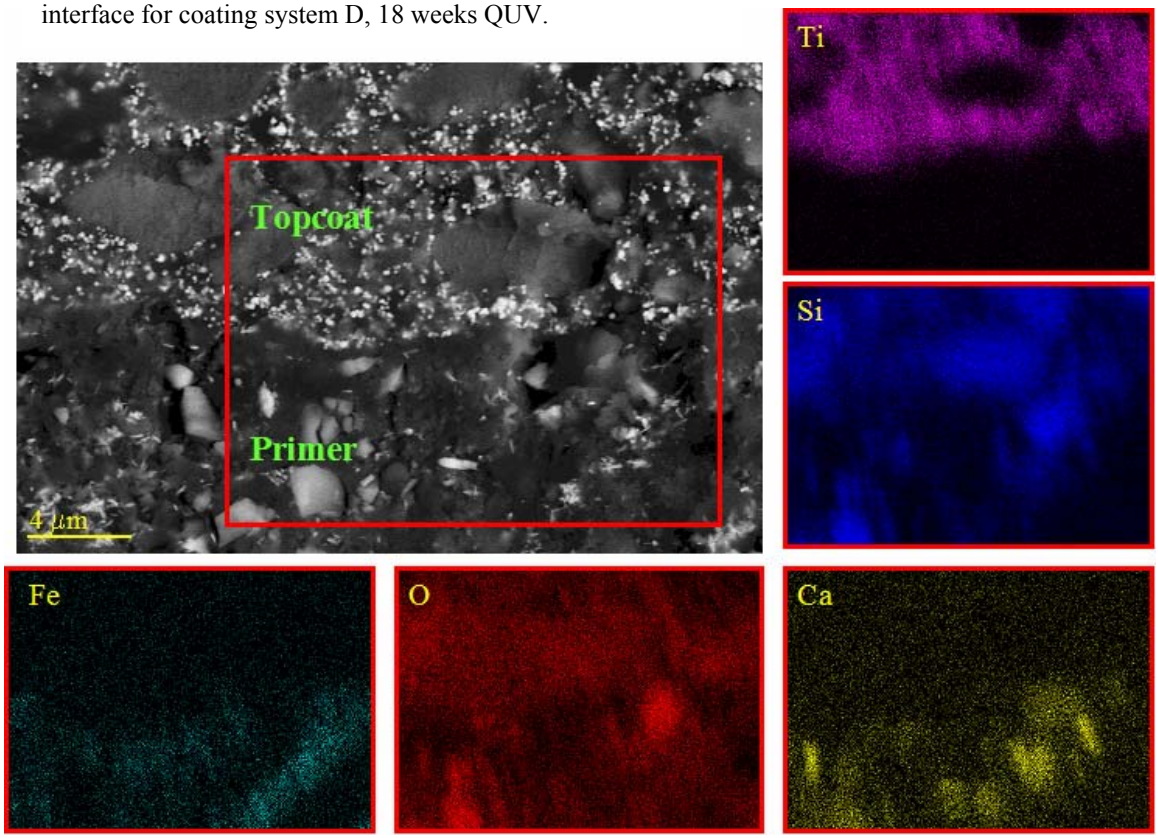

2. Micro Fourier Transform Infrared Spectroscopy

FTIR analysis has historically been one of the prime spectroscopic tools for the organic chemist. This is due to the preponderance of chemical bonds in organic compounds whose frequency of vibration fall within the infrared region of the electromagnetic spectrum. However, this same property is also responsible for the high opacity of most organics to infrared energy. This poses an interesting paradox for the spectroscopist who wishes to apply the technique to the analysis of thick organic coatings. Due to the thickness of the coatings under investigation in this study (50-75 micron thick topcoats) and their considerable opacity in the infrared band, samples in this study were in no way exempt from this paradox. Couple this optical absorbance effect with the desire to collect spectra at multi-level locations throughout the coating system, and it becomes obvious why most infrared analysis is conducted solely on the top surface of the coatings with spectral information extending only 1-2 microns below the surface of the topcoat.

The approach adopted herein has been to microtome the samples into 3-4 µm thick cross-sections and subject them to transmission-mode micro-FTIR analysis. This approach allows for the tracking of chemical changes in the infrared spectrum as a function of their spatial distribution throughout the coating system. As a side benefit, transmission mode

FTIT analysis is inherently less noisy than data collected via with the Attenuated Total Reflectance technique. Figure 18 below illustrates this analysis approach.

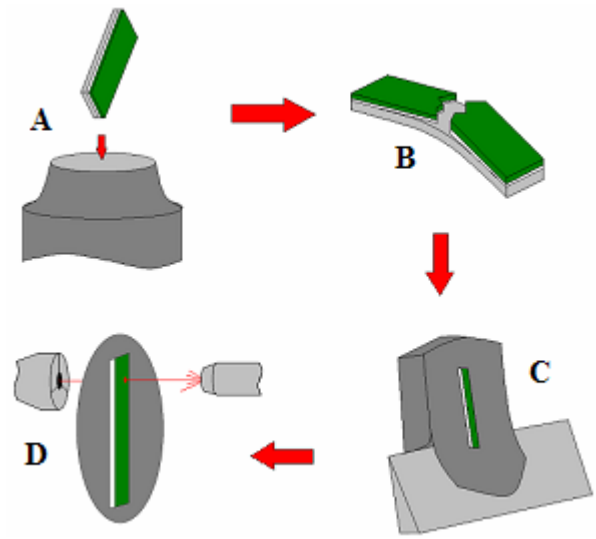

Figure 18. a) Sample (consisting of coating system and substrate) is immersed in liquid nitrogen. b) Thermal expansion mismatch between coating and subsequent induced shear stress causes disbondment between coating and substrate. c) Coating system sample is embedded in histological wax and microtomed to 3-micron cross-sections. d) Cross-sections are analyzed via transmission mode FTIR.

To ensure that data collected in this manner correctly indicates general trends within the sample the aspect ratio of the sampling beam is set to 10 μm x 70 μm (height x width). This has the dual effect of maximizing the vertical resolution while simultaneously generating a suitable averaging signal horizontally. Furthermore, the beam is rastered across the sample in a rectangular pattern, data being collected at 4 discreet locations at the same depth within the topcoat layer. Figure 19 illustrates how the spectra are collected with respect to the sample orientation.

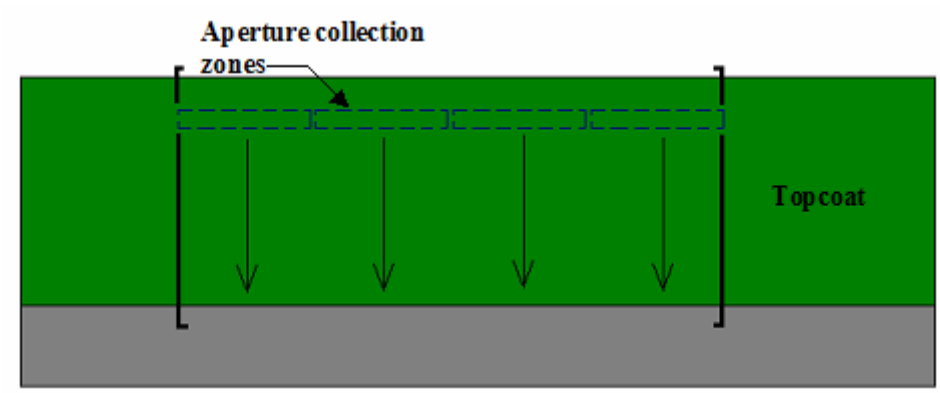

Figure 19. Cross-sectional transmission FTIR analysis geometry.

One goal of this project has been to create a comprehensive database consisting of 2-dimensional infrared characterization maps of the type previously described. This requires preparation and analysis of not only baseline type samples, but also those that have been exposed to the variety of accelerated weathering protocols included in this study (GM, QUV, B117, etc.). Since each 2-dimensional infrared map is comprised of close to 100 individual spectra, with each spectrum in turn containing information regarding the relationship between the coating system's chemical signatures as a function of their spatial location within the coating (which will change as the coating systems are subjected to accelerated weathering tests), this database represents a comprehensive collection of information regarding coating system chemistry in general and should serve military coating scientists well into the future. To date, data from the following sample types have been collected:

Coating system A:

1) *A-BL-0077-A2*
2) *A-G-0077-A8*
3) *A-Q-0077-A5*
4) *A-Q-0077-A8*

Coating system B:

1) *B-A-0075-A2*
2) *B-A-0075-A7*
3) *B-B-0075-A10*
4) *B-B-0075-A8*
5) *B-BL-0075-A2*
6) *B-BL-0077-A5*
7) *B-F-0075-A7*
8) *B-G-0075-A8*
9) *B-G-0075-A10*
10) *B-Q-0075-A5*
11) *B-Q-0075-A8*
12) *B-Q-0075-A10*
13) *B-Q-0156-AZ*

Coating system C:

1) *C-A-0069-AZ*
2) *C-B-0069-A5*
3) *C-BL-0069-A2*
4) *C-B-0069-A8*
5) *C-F-0069-A2*
6) *C-G-0069-A8*
7) *C-Q-0069-A5*
8) *C-Q-0069-A10*
9) *C-Q-0156-AZ*

Coating system D:

1) *D-A-0074-A2*
2) *D-B-0074-A8*
3) *D-BL-0074-A2*
4) *D-G-0074-A5*
5) *D-G-0074-A8*
6) *D-Q-0074-A5*
7) *D-Q-0074-A10*
8) *D-Q-0156-AZ*

Due to the large pigment volume concentration (PVC) of coating system A it has, for the most part, proven too brittle to be microtomed and therefore changes to the infrared spectrum cannot be depth profiled in the manner described above. We are currently in the testing/verification phase of a pioneering new technique to depth profile brittle high-solids coatings such as system A using the ultra-fast optical phenomenon of femto-second laser ablation. This will be discussed further on in this report.

FTIR Cross-Sectional Depth Profiling Results for Coating System C

Preliminary analysis has focused on Navy control coating system C, with the remainder of the coating systems (all branches) to follow. It is desirable to minimize experimental variables, that is, to begin analysis from the simplest of experimental cases wherein the coating phenomenon can be precisely quantified and move to progressively more complex weathering protocols. To this end, the QUV accelerated protocol was selected as the sample base with which to compare spectra to those provided by baseline samples. The QUV test involves continuous irradiation with UV radiation at ~340nm. The lack of both humidity as well as aggressive ionic ingress allow the researcher to attribute changes in the spectra to a combination of aging (additional curing) / UV irradiation / UV-induced heating effects.

It is crucial that precise peak identification is employed when interpreting the spectra in question. Peak assignments for coating system C (baseline) are given in the following table:

Peak Location (wavenumber)	***Band Assignment***
~ 3200-3500 cm^{-1}	*O-H Stretching*[6]
~ 2850-2950 cm^{-1}	*C-H Stretching*[6]
~ 1727 cm^{-1}	*C=O Ester Stretch*[7]
~ 1687 cm^{-1}	*C=O Amide Stretch*[7]
~ 1524 cm^{-1}	*Amide II*[4]
~ 1467 cm^{-1}	*CH2 Bend*[6]
~ 1376 cm^{-1}	*CH3 Bend*[6]
~ 1242 cm^{-1}	*C-O Ester Stretch*[6]
~ 1108 cm^{-1}	*Primarily Si-O-Si Stretch*[5]
~ 903 cm^{-1}	*Ti-O-Ti Stretch*[8]

Previous work has identified the Amide II band as being indicative of polymeric photo oxidation (an expected mode of failure given the nature of the polymeric binder and the QUV accelerated weathering protocol). This band is a complex vibrational composite of polymer backbone C-C stretching, C-N stretching of the urethane group and N-H wagging of the urethane group and is always present in polyurethane-based compounds[5]. Figure 20 shows a baseline transmission-mode IR spectrum vs. a transmission-mode spectrum collected from a coating system C sample subjected to 18 weeks QUV.

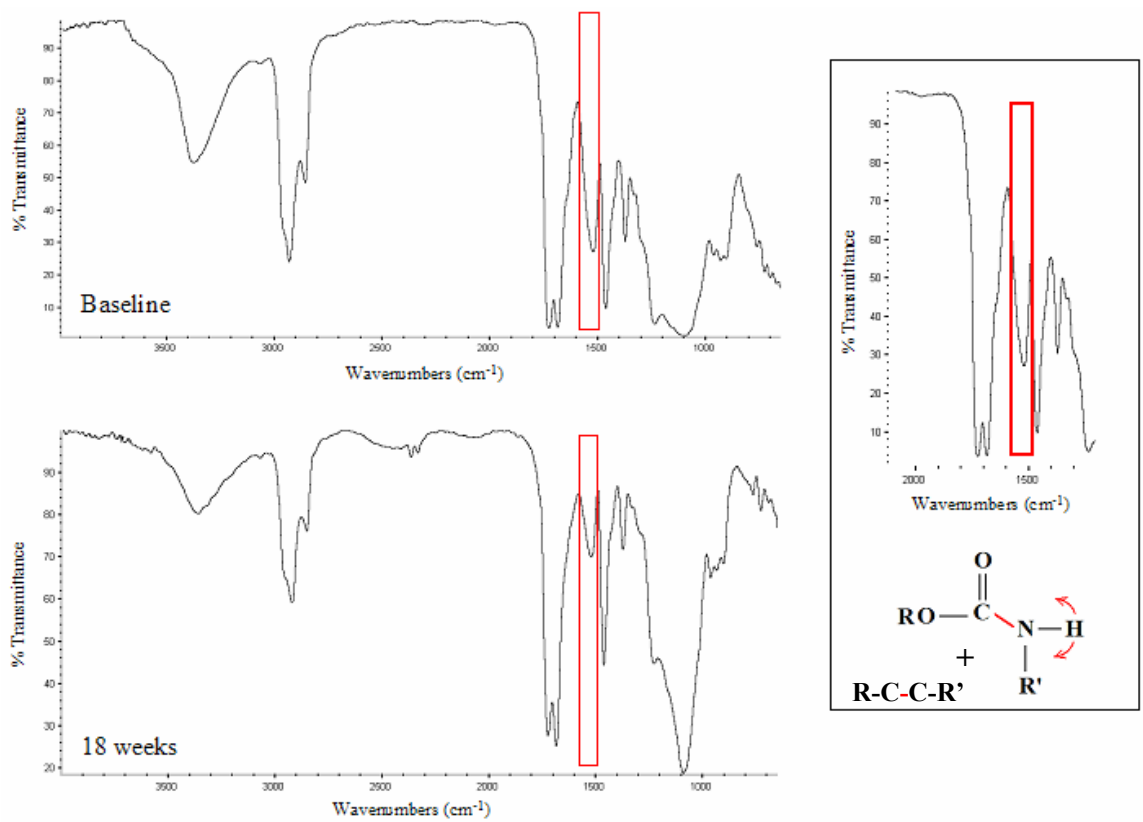

Figure 20. Baseline IR spectrum for coating system C (upper spectrum) vs. 18 weeks QUV IR spectrum (lower spectrum) showing apparent reduction Amide II band (highlighted).

While an apparent reduction in the signature strength of the Amide II band is readily apparent by comparison of the two spectra in figure 20, it remains a possibility that differences in sample thickness are the source of this discrepancy. In order to track true changes in peak intensity within each sample the Amide II band must be ratioed against a second peak within the same sample. This has the effect of normalizing changes in the individual spectra caused by fluctuations in sample thickness. Since CH_3 end groups are

not expected to participate in photooxidative reactions, the CH_3 bending band at 1376 cm^{-6} was chosen as the normalizing peak for the Amide II band. Figure 21 shows the intensity of the Amide II band ratioed with the CH_3 band as a function of its depth in the topcoat for both a baseline sample as well as 18 weeks QUV for coating system C.

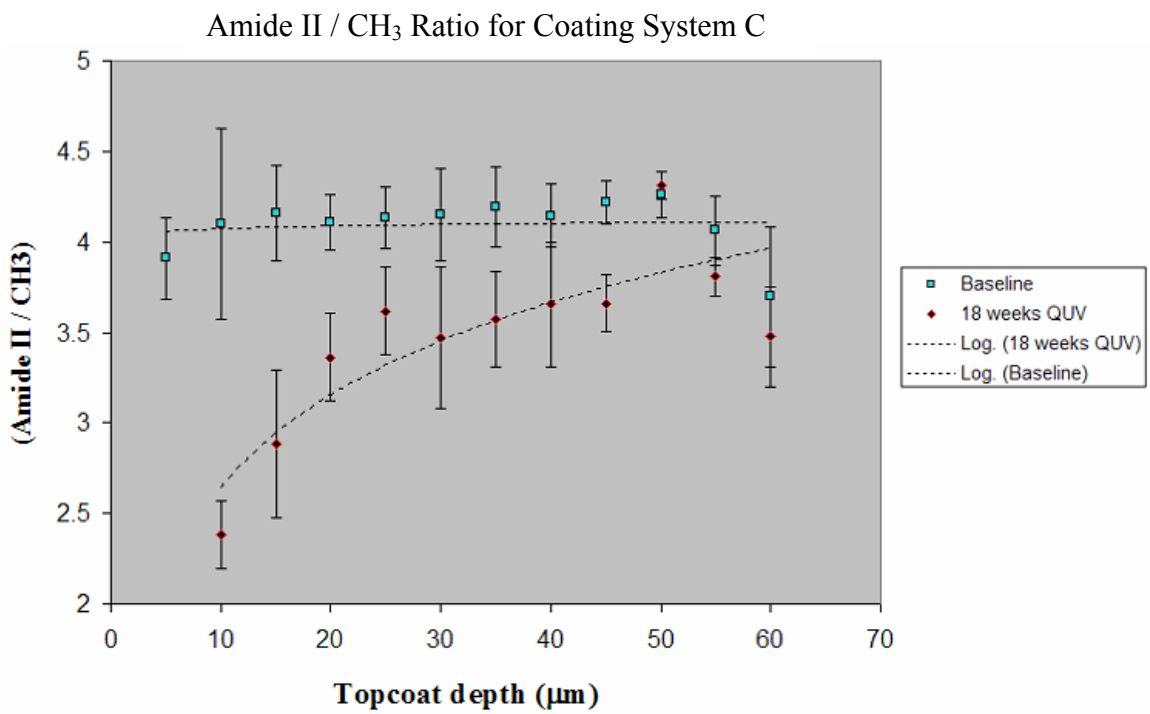

Figure 21. Amide II / CH3 ratio for coating system C for both baseline and 18 weeks QUV exposed samples. Data shows a reduction of Amide II activity extending approximately 30 µm into topcoat layer.

UV at the wavelengths used by the QUV protocol (340 nm) is sufficiently energetic that bond dissociation can readily occur. The reduction of the Amide II signature may indicate direct photoscission of the covalent backbone of the polymeric binder (C-C bonds), dissociation of the C-N or N-H bond, or some combination of these.

UV penetration depth was previously believed to be approx 5 µm. These results clearly indicate the penetration depth to be several times greater. A penetration to this depth is surprising given the opacity of the polyurethane binder present in these samples. It is hypothesized that the tight packing of the additives / pigments generate scattering paths throughout the coating and UV light infiltration.

The results shown in figure 21 are believed to be indicative of bond scission. One widely accepted model of polyurethane photooxidation[3] stipulates that the combination of incident energy (in the form of UV irradiation of the polymer) and atmospheric O_2 causes a condensation reaction wherein the $-CH_2-$ in the alpha position of the urethane group NH is converted to a carbonyl group through a reaction pathway involving the intermediate formation of peroxides. FTIR analysis is an unsuitable technique for the detection of the presence of peroxides (Raman spectroscopy is the technique of choice for this functional group) and therefore changes in the carbonyl group itself (C=O) were chosen for tracking in the same manner as the Amide II peak. Again, the band in question (carbonyl) has been ratioed against the CH_3 bending peak to eliminate misleading fluctuations in peak intensity due to sample thickness irregularities. Figure 22 gives the results of this ratioing for both baseline as well as 18 weeks QUV samples of coating system C.

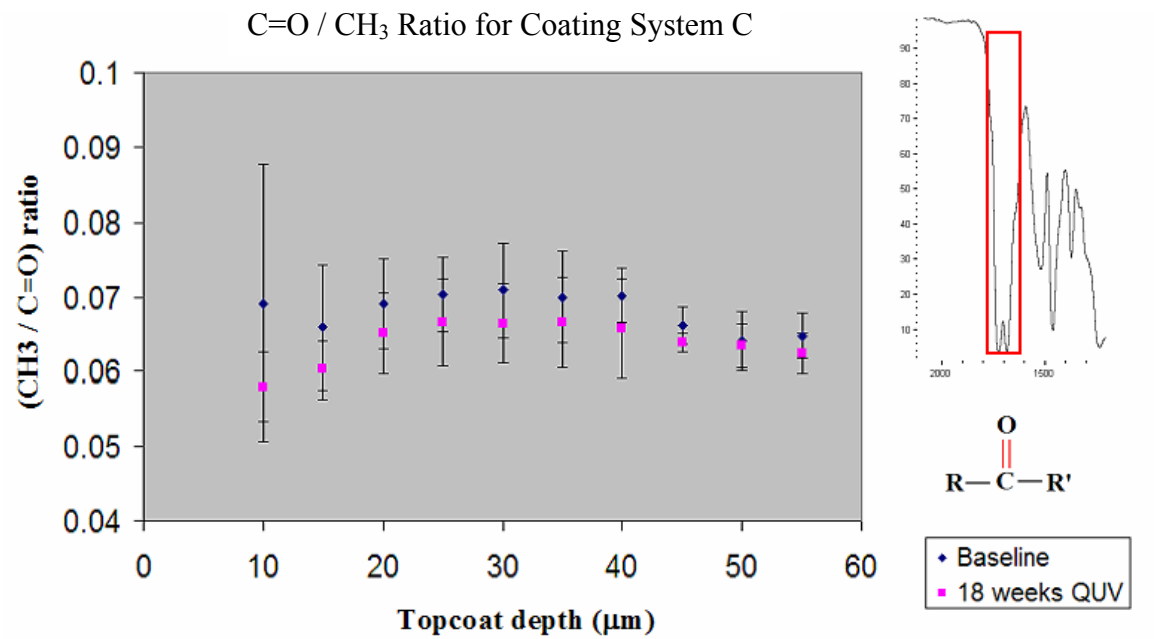

Figure 22. C=O/CH_3 ratio for coating system C for both baseline and 18 weeks QUV exposure. No reduction or increase trend between baseline and exposed sample is evident.

The lack of an increase in carbonyl signature between the baseline and exposed samples indicates that either the photooxidative mechanism occurs only on the surface due to the ready availability of O_2, or that this photooxidative mechanism is not being invoked.

The lack of any new bond formation as revealed by direct inspection of the IR spectra implies that direct photoscission of the urethane or carbon backbone bonds are the

primary mode of UV-induced failure for coating system C. This evidence compliments data gathered on coating system C by Kovaleski et. al. of Naval Air Warfare Center Aircraft Division, Patuxent River, displayed elsewhere in this document. That data has shown an increase in the coating capacitance as a function of UV irradiation, leading those researchers to hypothesize that chain scission was allowing reorientation of portions of the polymer binder within the induced field during EIS analysis and thus increasing coating capacitance.

Kovaleski et. al. have also noted a longer curing time for coating C as opposed to the other coating systems in this study. Transmission mode FTIR depth profiling shows an increase in hydroxide signature in the topcoat layer near the topcoat/primer layer of coating system C. Alcohol groups are abundant in these coatings since polyol-isocyanate reactions are used as precursors of the polyurethane matrix. Certain aspects of these coatings are proprietary (and therefore unknown to the researchers engaged in this project), such as the nature of the organic solvent used. It is strongly suspected, however, that the solvent for coating system C is composed primarily of either a) 2,4-Pentanediol, b) Methylamyl ketone, c) diisobutyl Ketone, or d) Methylethyl ketone, any of which may be the source of the hydroxide signature. Figure 23 shows the transmission-mode FTIR depth profile of OH ratioed against CH_3 for both baseline as well as 18 weeks QUV exposure for coating system C.

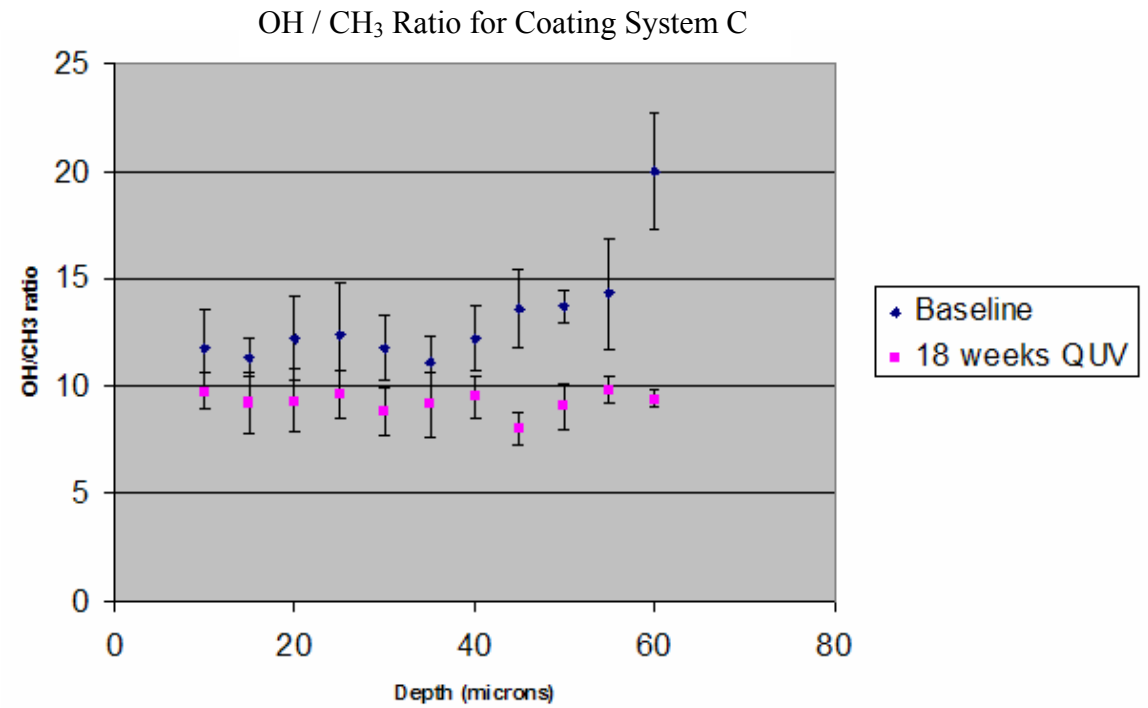

Figure 23. OH / CH_3 ratio for baseline and 18 weeks QUV exposure. Exposed sample shows reduction in hydroxide signature as topcoat/primer interface is approached.

Figure 23 shows the QUV exposure sample for coating system C exhibiting a flat hydroxide signature depth profile from the surface of the topcoat down to the topcoat / primer interface. The baseline however exhibits a marked increase in this signature as the topcoat / primer interface is approached. It is hypothesized that this signature is indicative of solvent entrapment within the topcoat layer (baseline profile). As the sample is exposed to the 18 weak QUV accelerated weathering protocol the additional heating and increase in free volume (caused by bond scission as evidenced from the two previous depth profiles) allows the entrapped solvent to diffuse out of the topcoat. The solvent entrapment occupies certain free volume spaces within the topcoat and prevents the polymer chains from approaching each other closely enough to achieve the desired cross-linking density and causing it to exhibit a slow curing rate.

FTIR Results for Coating System D

Coating system D is the Navy Future System consisting of a zero-VOC water-based polyurethane topcoat and a MIL-P-85582 water-based epoxy primer. The coating system is applied to aluminum substrates pretreated with CCC.

Early on in its testing coating system D exhibited poor performance in the GM cyclic salt spray accelerated weathering protocol. In addition, EIS spectra collected at the Naval Air Warfare Center Aircraft Division, Patuxent River, MD initially exhibited behavior best modeled by a controversial 7 element equivalent circuit.

The primer system used relies on a curing reaction between a prepolymer and a curing agent such as an amine. The prepolymer itself is the reaction product of Bisphenol A and Epichlorohydrin. Co-reaction with an amine agent during application causes the strained epoxy ring to open and form highly cross-linked chains that are very strong and chemically resistant (figure 24)[7].

FTIR analysis on failed samples has traced the cause of failure to poor mixing and/or curing of the primer components. It is believed this lack of proper cross-link formation compromised the integrity of the primer / substrate interface as well as, presumably, the cohesive strength of the coating itself allowing for the ingress and collection of corrosive ionic species at this location. The formation of ionic solutions at the interface, in turn, chemically attack the substrate at locations where the chemical conversion coating is thinnest.

To verify this hypothesis and confirm the failure analysis of coating system D diffuse reflectance-mode FTIR was performed on samples exhibiting failure and compared with FTIR spectra from samples showing the expected degree of protection. Failed samples were identified by the presence of osmotic blisters. A blister was chosen in the region wherein EIS data was collected to determine if the above-hypothesized mode of failure had contributed in any way to the EIS profiles collected at NAVAIR.

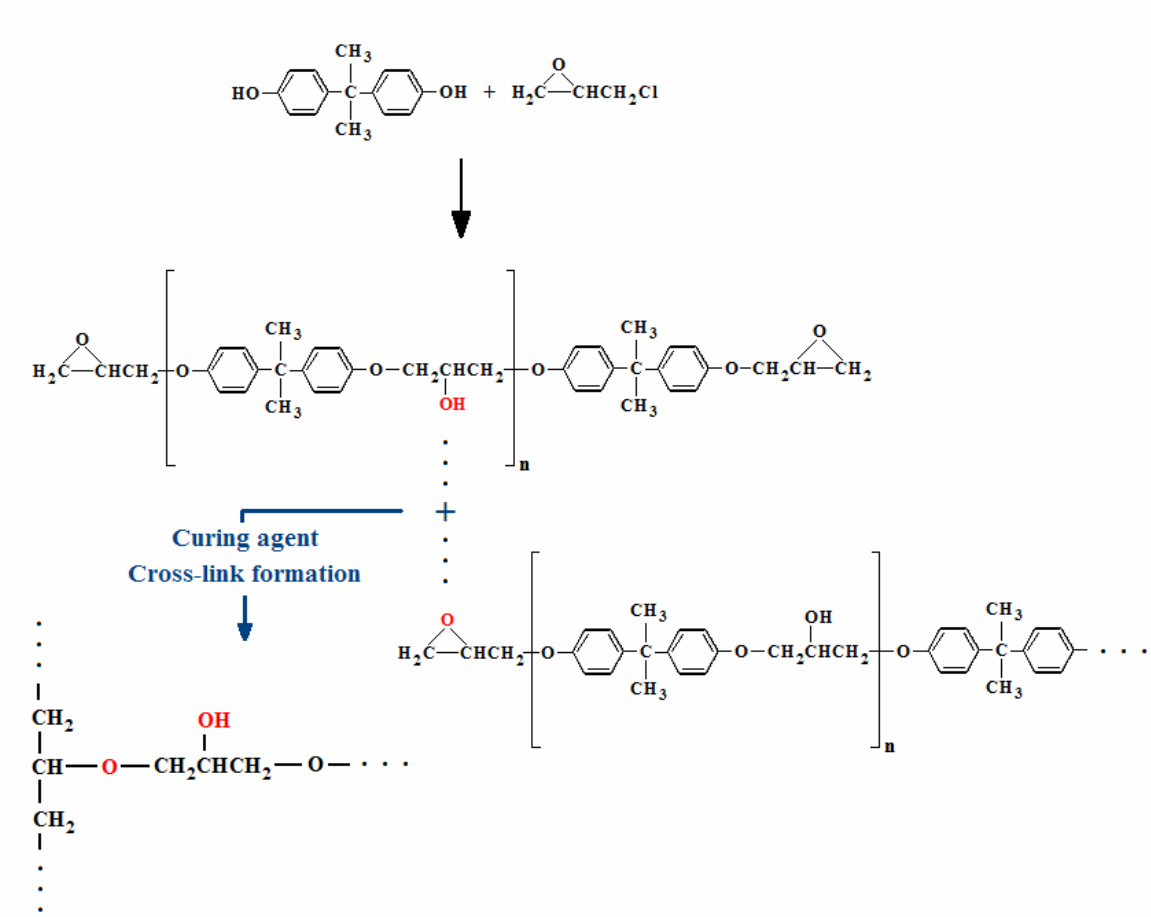

Figure 24. Epoxy ring-opening reaction causing cross-linking film formation from Epichlorohydrin / Bisphenol A precursors[7]. Proper cross-linking is expected to cause an alteration in C-O band IR signature.

The coating system from the blistered sample was removed from the substrate via liquid N_2 immersion. Both the primer as well as the underlying substrate were analyzed, the primer by diffuse reflectance mode FTIR and the substrate by a combination of optical microscopy, confocal laser profilometry (using a custom instrument assembled in our laboratory), SEM / EDAX analysis and small-spot XPS (performed at Army Research Laboratory, Aberdeen Proving Grounds, Aberdeen, MD).

Results of the FTIR analysis are shown in figure 25. For comparison, a spectrum of unreacted Poly(Bisphenol-A-CO-Epichlorohydrin) is shown alongside spectra from the failed primer sample as well as a carefully prepared sample (control primer) known to have been mixed and applied as per the manufacturer's instructions. The similarities in the C-O band between the unreacted Poly(Bisphenol-A-CO-Epichlorohydrin) and the failed sample spectra suggest a primer layer wherein the cross-linking reactions have not undergone completion. Comparison between the Poly(Bisphenol-A-CO-

Epichlorohydrin) and control spectra show a large alteration and subsequent dissimilarity between the two signatures, indicative of a properly cross-linked primer and further supporting the failure hypothesis.

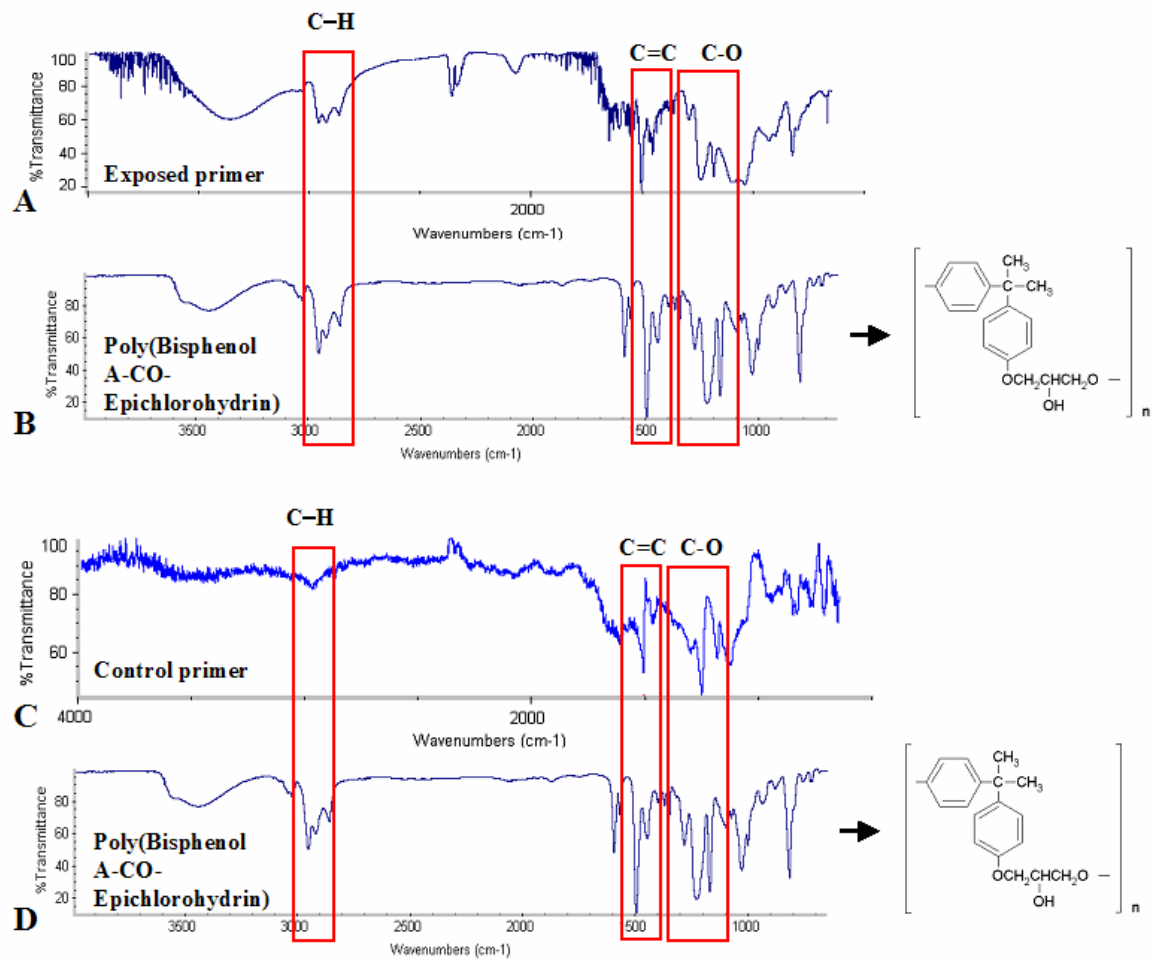

Figure 25. FTIR spectra showing comparison of CO, CH and C=C bands (highlighted) for A) Exposed (failed) primer, B&D) Poly(Bisphenol-A-CO-Epichlorohydrin), C) Control Primer. Similarities in the CO band between Poly(Bisphenol-A-CO-Epichlorohydrin) and the exposed primer indicate lack of proper cross-linking.

Analysis of the underlying pretreated substrate show the formation of a large pit in the region directly underlying the blistered area of the coating system. Figure 26 shows an optical micrograph of the substrate directly beneath the large osmotic blister zone while *figure 27 shows the results of the confocal scanning of the pit feature.*

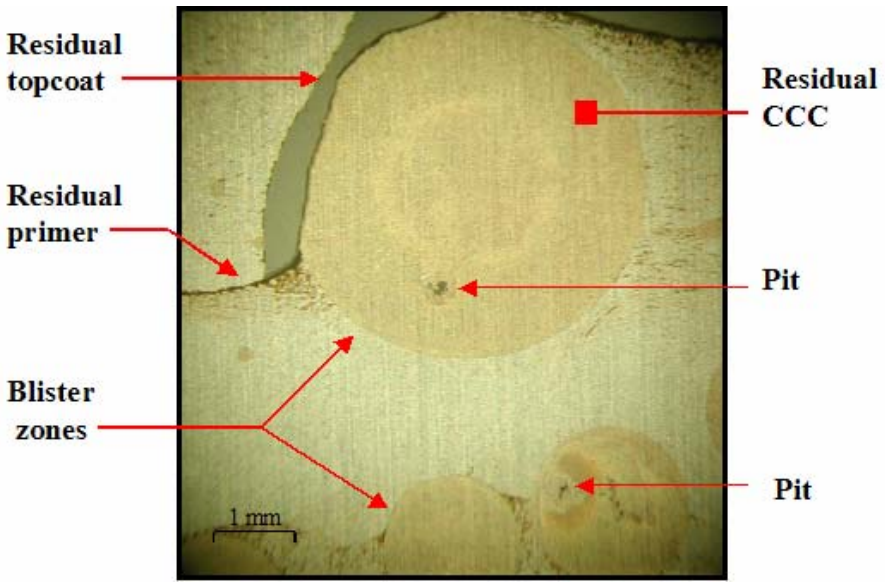

Figure 26. Optical micrograph showing underlying substrate regions of osmotic blister zones and pits.

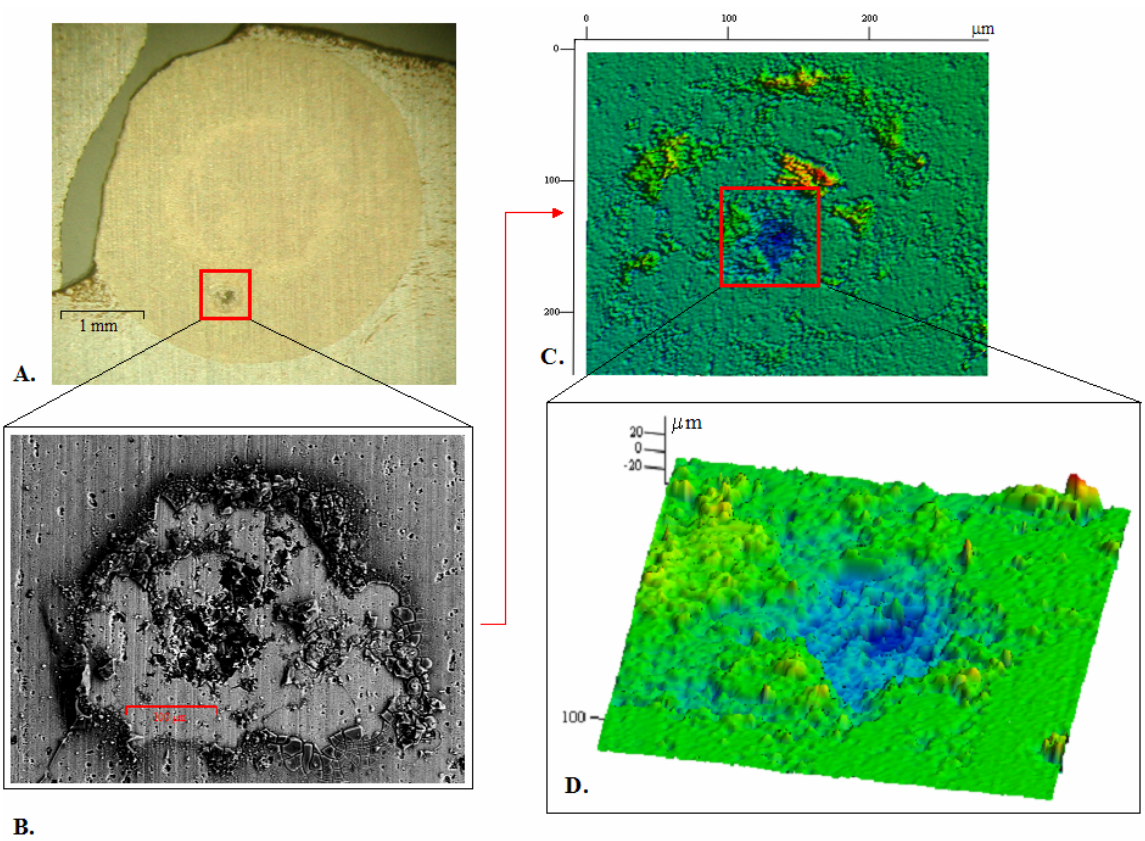

Figure 27. A) Optical micrograph of underlying substrate blister zone. B) SEM image showing pit feature in blister zone. C) Scanning confocal profilometry map of blister zone (region shown in B). D) Scanning confocal profilometry map showing pit detail and depth of approx. 20 µm.

Spot EDAX analysis was performed on the interior region of the pit as well as the adjacent area outside the pit. Figure 28 shows the results of this analysis. The large CU signal at the base of the pit compared to the adjacent exterior zone (bulk matrix composition) indicates the presence of a copper-rich intermetallic at the nucleating site of the pit. This is most likely due to the thin CCC film known to exist over intermetallic particles present in the bulk matrix of the Al alloy[1,2].

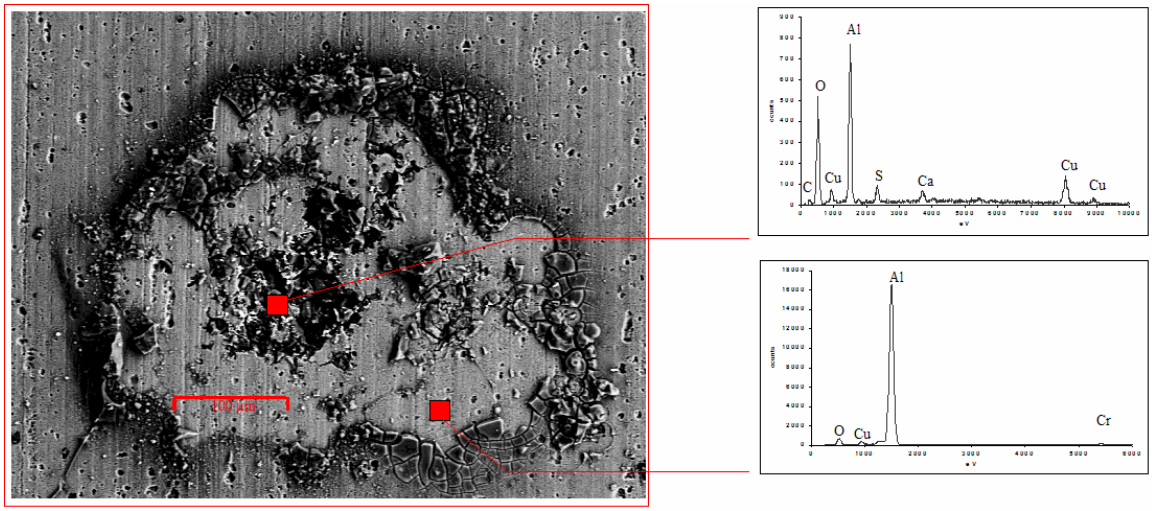

Figure 28. Spot EDAX analysis of pit feature showing possible presence of intermetallic at pit nucleation site (upper spectrum).

To verify the paucity of CCC film above the indicated intermetallic pit nucleation site small-spot XPS was performed. Figure 29 shows the results of this analysis showing a lack of elemental Cr at the site of the pit, confirming the failure hypothesis for the combined AL substrate / coating system D sample set.

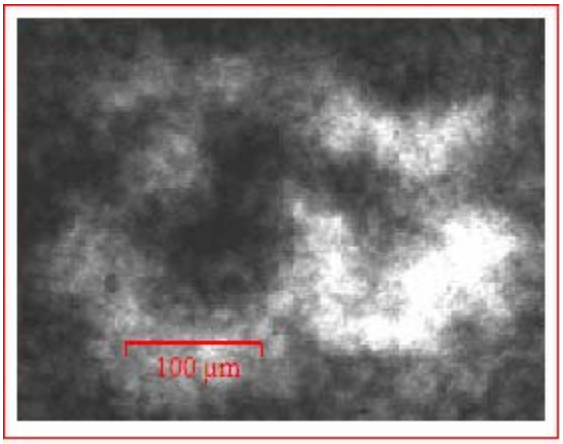

Figure 29. Small spot XPS image showing the spatial distribution of elemental chromium around pit feature in substrate of coating system D.

3. Femtosecond Laser Ablation-Assisted Depth Profiling

As mentioned previously, due to its high PVC coating system A exhibits mechanical properties that are unsuitable for microtome cross-sectioning. A novel technique involving the ultra fast optical phenomenon of laser ablation has been investigated for use as a tool to facilitate FTIR depth profiling on materials that cannot be depth profiled by other means. A pilot project was initiated to study the feasibility of this approach on the current set of military coatings with initial experiments performed on coating system B (Low VOC Army Future System). System B consists of a water dispersible CARC Polyurethane (Polymeric Bead Ext.) Aliphatic Polyurethane dispersion and modified isocyanate. The primer consists of a MIL-P-53030 water-based epoxy. It is meant to be applied to steel substrates pretreated with zinc phosphate.

Femtosecond Laser Ablation-Assisted Depth Profiling involves ablating regions of the coating to expose the underlying material. 1mm^2 "windows" are ablated into the topcoat at various depths, from which the IR spectrum can be gathered by some technique (usually Attenuated Total Reflectance or ATR). Since the laser is pulsed and not continuous wave, the depth of the windows is discreet with the minimum depth fixed by the removal rate per pulse. Figure 30 shows a schematic representation of how this technique is used.

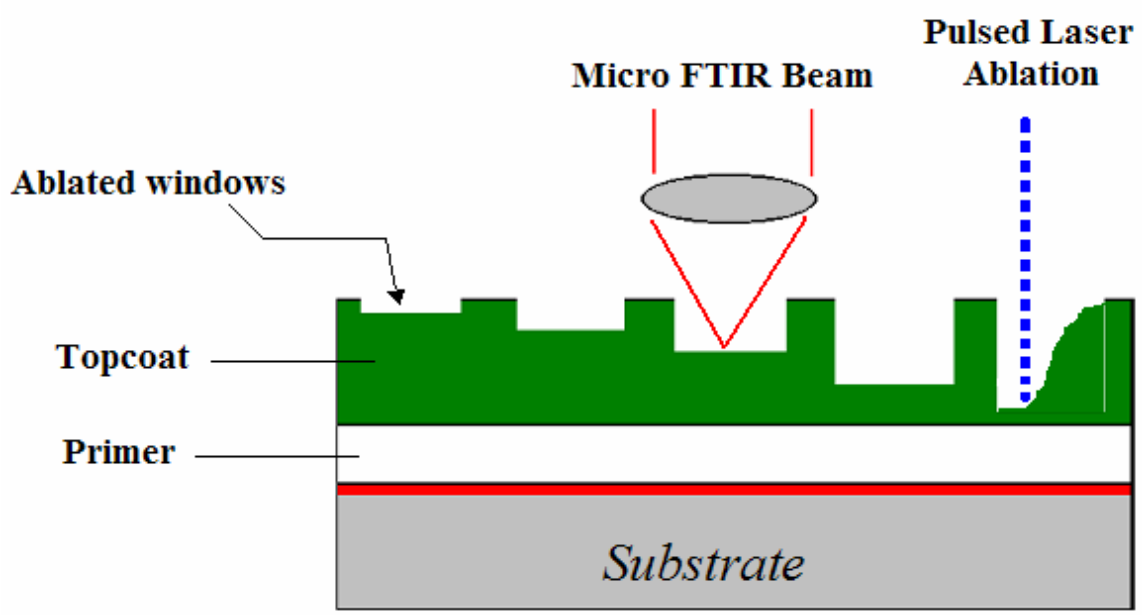

Figure 30. Experimental geometry of femtosecond laser ablation-assisted depth profiling. FTIR analysis can either be conducted by micro diffuse-reflectance or micro-ATR.

The removal rate is a function of the laser output power (which can vary) and the material type. Removal rates per pulse must be determined experimentally. For coating system B the average removal rate was found to be 5 μm / pulse. To create the windowed regions necessary for analysis the sample was mounted on a set of stepper-motor driven X-Y stages. Figure 31 shows the results of a 4-pulse per spot ablated region that resulted in a "window" approximately 20 μm deep.

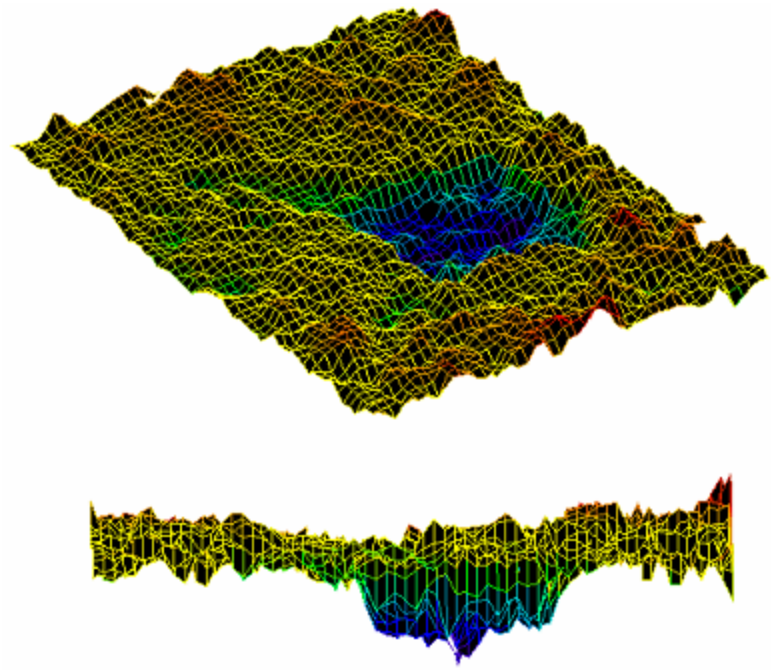

Figure 31. Zygometric scan of ablated window in coating system B approximately 20 microns deep.

The necessity of using an ultra-fast laser for material removal as opposed to lasers that emit pulses at comparatively larger time-scales (nanosecond pulses, for example) is that the intensity of the femtosecond-class laser has the ability to ablate material without inducing thermal effects to adjoining regions of material. This is the crucial factor that enables the use of femtosecond lasers for this particular application. Due to the complex and diverse nature of these coatings, however, it must be confirmed that the ablation process does not induce chemical bond alterations to either the inorganic additives and pigments or the organic binder matrix. ATR FTIR analysis was performed on a sample that had been subjected to a 4 pulse-per-spot ablation procedure on the topcoat of coating system B baseline. Spectra were collected both in the ablated region as well as outside the region. Results are shown in figure 32. It can be seen that no apparent structural changes are evident within between the two spectra. From this it can be concluded that the ablation process, when conducted on the femtosecond time scale, does not induced any visible or significant structural changes to coating system B's infrared spectrum. It is

therefore suitable for application as a depth profile enabler for this coating system. Experiments are to be conducted in the near future to assess the effect on coating system A. Due to the similarities between the polymeric binders of these two systems and the fact that system A contains even less polymeric material by volume (polymers being inherently more susceptible to bond manipulation due to thermal input) then coating system B, it is felt that this is a novel, highly useful technique and a viable and more suitable alternative to traditional ion beam techniques where composite coating materials are concerned.

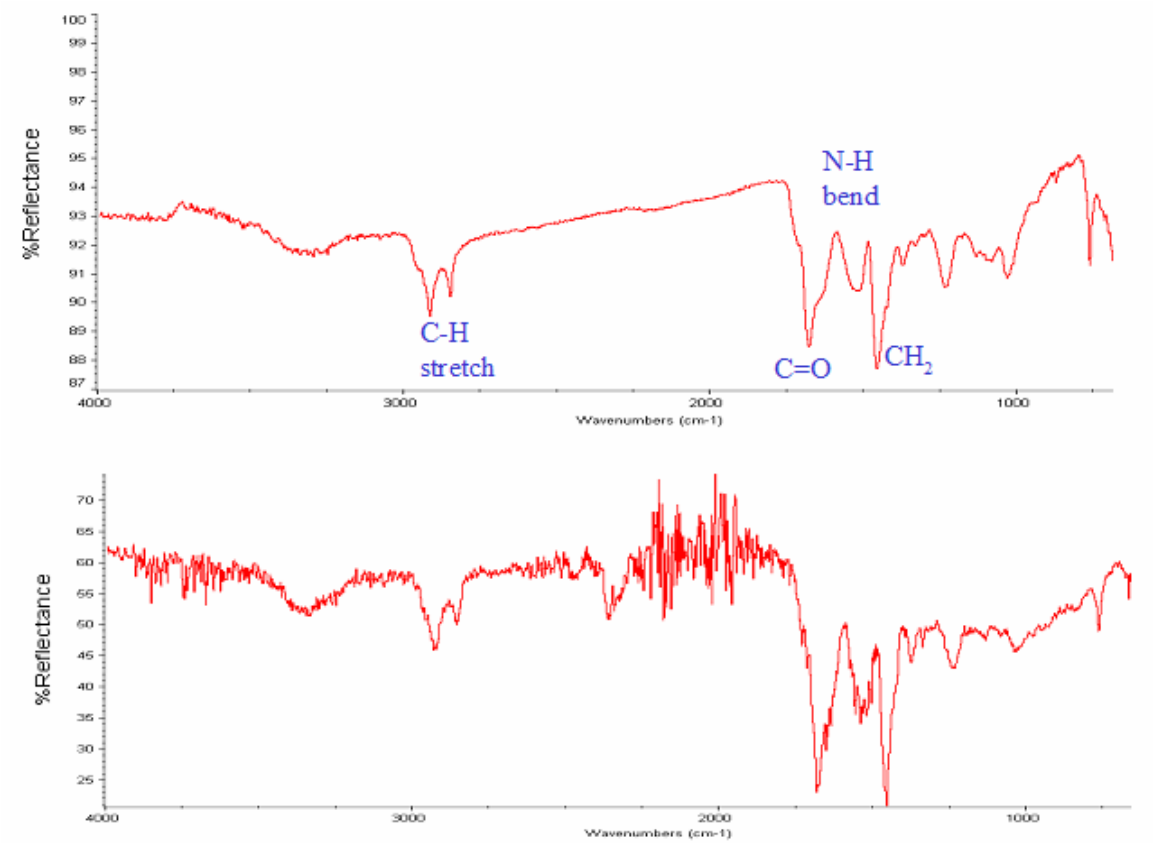

Figure 32. FTIR spectra comparing ablated (lower spectrum) vs. non-ablated (upper spectrum) topcoat signature for coating system B.

Conclusions

A vast FTIR database comprising over 30 samples, including baseline as well as accelerated aging specimens, has been assembled. This database represents the most complete and comprehensive infrared characterization of military coating systems currently available. Data contained in this collection consist of spatially resolved transmission-mode micro-FTIR analysis of topcoat/primer cross-sectioned samples. Analysis to date has indicated a UV-induced chain scission effect in the Amide II band of the spectrum for coating system C. This damage extends approximately 25 microns into the topcoat layer and supports the hypothesis proposed by Kovaleski et. al. (NAVAIR) that an increase in capacitance of their equivalent circuit model observed after UV exposure may be due to increase chain segment alignment within the topcoat layer. No evidence of C=O photooxidative product has been found at any depth in coating system C. This indicates the product is most likely created on the surface and is ablated environmentally, leaving loosely bound pigment and additive particles that cause color loss and chalking.

Analysis of coating system D has revealed incomplete cross-linking (and hence poor coating densification) due to improper formulation or improper application/mixing of the coating system primer. Poor densification of the film facilitates the movement of corrosive ions that ultimately collect at the primer/substrate interface. Data collected was shown to support the hypothesis that pitting of the substrate occurs at the intermetallic sites known to exist in Al alloy. These observations allowed for a reformulation of the equivalent circuit model proposed for coating system C by NAVAIR (based on their EIS data). Current coating samples do not exhibit incomplete cross-linking. These results indicate that substrates containing significant amounts of copper will compromise the effectiveness of the chromate conversion coating, allowing for the nucleation and growth of pitting. This speaks not only to the importance of proper coating formulation and application but proper substrate preparation as well. Both must be present in order to realize effective corrosion protection.

A novel technique for FTIR depth profiling materials that cannot be profiled by current methods has been proposed and its suitability to military coatings in particular has been verified experimentally. The technique will be used to depth profile coating system A.

References

1. *Jaime Vasquez M., Halada G. P., Clayton C. R., Longtin J. P.* Surf. Interface. Anal. *2002;* ***33****: 607.*
2. *Jaime Vasquez M., Kearns J. R., Halada G. P., Clayton C. R.* Surf. Interface. Anal. *2002;* ***33****: 796.*
3. *Wilhelm, C., Gardette, J-L.* Polymer. *1997;* ***38****(16): 4019.*
4. *Miyazawa, T., Shimanouchi, T., Mizushima, S-I.* J. Chem. Phys. *1956;* ***24****(2): 408.*

5. *Lin-Vien, D., Colthup, N. B., Fateley, W. G., Grasselli, J. G.* The Handbook of Infrared and Raman Characteristic Frequencies of Organic Molecules. *Academic Press, Inc. 1991.*
6. *Pavia, D. L., Lampman, G. M., Kriz, G. S.,* Introduction To Spectroscopy, 2nd ed. *Saunders College Publishing. 1996.*
7. *McMurry, J.* Organic Chemistry, 4th ed. *Brooks/Cole Publishing Company. 1996.*
8. *Shao, L., Zhang, L., Chen, M., Lu, H., Zhou, M.* Chem. Phys. Letters. *2001;* ***343****: 178.*

Mechanisms of Military Coatings Degradation: Surface Characterization via X-ray Photoelectron Spectroscopy

Wendy E. Kosik
Army Research Laboratory
Weapons and Materials Research Directorate

Polyurethane is known to possess excellent properties such as chemical, abrasion and mar resistance as well as good flexibility. Historically poly (ester-urethane) coatings prove to be exceptionally durable in both high temperature and humid environment. However, with extended exposure to sunlight polyurethane coatings undergo appearance failures; change in gloss and/or color, due to UV degradation. The photolytic stability is a function of environment and chemical formulation. Studies of model poly (ester-urethane) polymer systems have provided valuable insight into urethane linkage degradation and its reactivity in the absence of other reactive sites or polyester bi-product influence. This work will be utilized in interpreting the observations made in our non-ideal, fully pigmented military coating systems.

This report continues the degradation research by using XPS to support and give further insight into the previous FTIR work regarding the UV induced urethane degradation. Reactivity of the urethane function is as follows: 1) Radical induced oxidation of C (methylene group, CH2) in alpha position to NH of urethane groups 2) the oxidation of the methylene groups result in primary hydro peroxides which undergo a cage reaction and the formation of acetylurethane function 3) this readily reacts with water formed in-situ to give a carboxylic acid and urethane group. (Wilhelm and Gardette, *Polymer* Vol 38 No. 16, pp. 4019-4031, 1997)

It is the unique binding energies of each element that allows us to use XPS to identify the elements present at the surface of the coatings. The relative intensity, peak width/shape and binding energy allow us to determine the concentration of the elements relative to one another. In that same fashion, variations of the elemental binding energies (chemical shifts or deltas) of the carbon in the coating allows the chemical state (bonding scenario) to be determined. Quantifying these chemical states is achieved through simulating the C1s core spectra with a series component peaks and adjusting their position / shape parameters to achieve the best fit. It is our intent to then correlate the peak shifts with functional groups present in our degradation model.

The near surface (sampling depth: 10-80 Angstroms) chemistry was studied using x-ray photoelectron spectroscopy (XPS) for Coating systems A, B and C.

Coating System A

The atomic compositions measured by XPS for sample A, after exposure to accelerated QUV, static AZ and static FL weathering is shown in Table 1 and the trends that evolve are illustrated in Figure 1. The initial composition of the surface is very high in carbon and oxygen content, with a small amount of inorganic elements arising from the extenders and pigments in the coating. After aging, the atomic surface composition of sample A changes dramatically. The reduction in carbon content and simultaneous increase in silicon, aluminum, and oxygen indicates the loss of polymer (high carbon content), and the emergence of siliceous extenders (high Si, Al, and O content) at the surface. This is consistent with photo-degradation studies on aliphatic and aromatic urethane neat polymer films. In those studies, it has been shown that photo-degradation leads to chain scission ultimately resulting in mass loss in the polymer .

Table 1: Atomic Composition of Coating A (atomic %)

			Atomic Composition of Coating A (atomic %)							
Exposure	Weeks	Irradiance (MJ/m^2)	Chromium (Cr)	Oxygen (O)	Nitrogen (N)	Carbon (C)	Sulfur (S)	Silicon (Si)	Sodium (Na)	Aluminum (Al)
BL	0	0	0.00	15.66	1.30	79.84	0.22	2.30	0.28	0.40
QUV	3	74.57	0.54	34.06	4.34	52.85	0.28	6.30	0.49	1.14
QUV	6	149.14	0.50	38.37	6.56	45.97	0.00	6.91	0.52	1.17
QUV	12	298.28	1.09	44.47	5.47	37.03	0.00	9.95	0.47	1.47
QUV	18	447.42	0.75	36.53	6.48	44.43	0.00	10.11	0.42	1.27
QUV	48	1193.12	1.87	49.47	5.40	24.05	0.10	15.79	0.52	2.80
Az	7	65.29	0.68	28.44	4.37	58.68	0.31	5.98	0.20	1.53
Az	13	120.08	0.23	35.84	4.37	49.11	0.03	8.99	0.22	1.22
Az	25	203.4	0.93	43.55	3.86	38.97	0.00	10.18	0.02	2.49
Az	49	305.37	0.57	39.57	3.25	45.53	0.17	8.42	0.20	2.30
Az	97	603.52	1.45	54.43	2.48	24.56	0.04	13.67	0.11	3.25
Fl	7	57.03	0.59	41.26	3.94	44.12	0.18	7.58	0.13	2.21
Fl	13	91.15	0.47	39.39	4.06	44.78	0.12	8.18	0.18	2.82
Fl	25	151.41	0.59	45.26	3.88	36.59	0.22	9.51	0.64	3.30
Fl	49	270.65	0.68	41.90	3.94	40.04	0.04	9.58	0.16	3.66
Fl	97	501.37	0.81	50.02	2.64	34.15	0.00	9.56	0.04	2.78

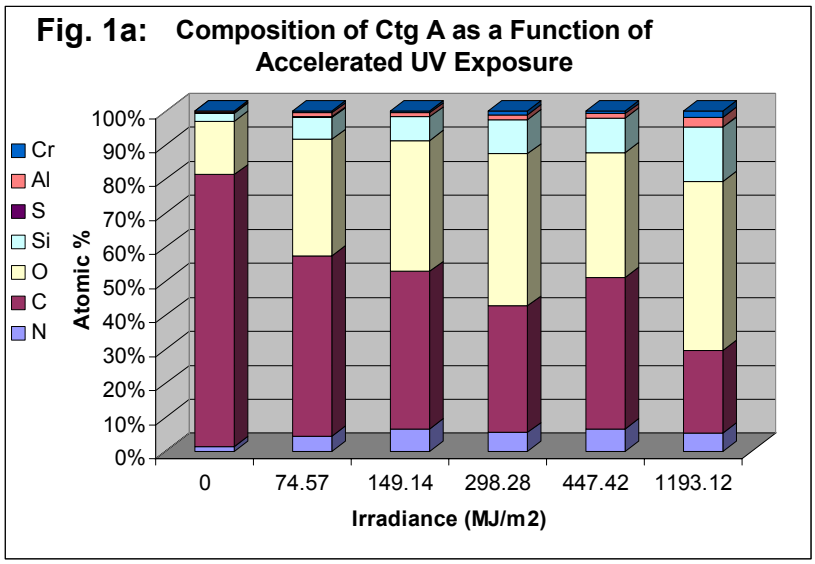
Fig. 1a: Composition of Ctg A as a Function of Accelerated UV Exposure
Cr
Al
S
Si
O
C
N
Atomic %
100%
90%
80%
70%
60%
50%
40%
30%
20%
10%
0%
0
74.57
149.14
298.28
447.42
1193.12
Irradiance (MJ/m2)

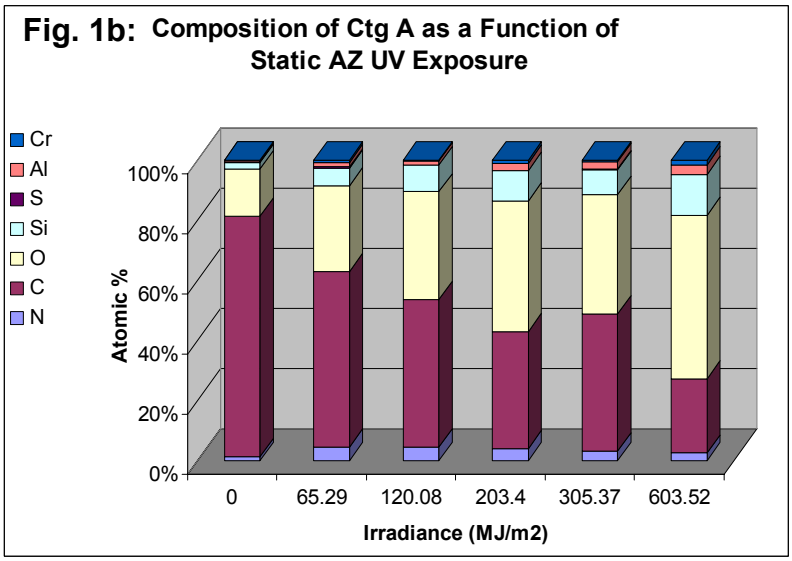
Fig. 1b: Composition of Ctg A as a Function of Static AZ UV Exposure
Cr
Al
S
Si
O
C
N
Atomic %
100%
80%
60%
40%
20%
0%
0
65.29
120.08
203.4
305.37
603.52
Irradiance (MJ/m2)

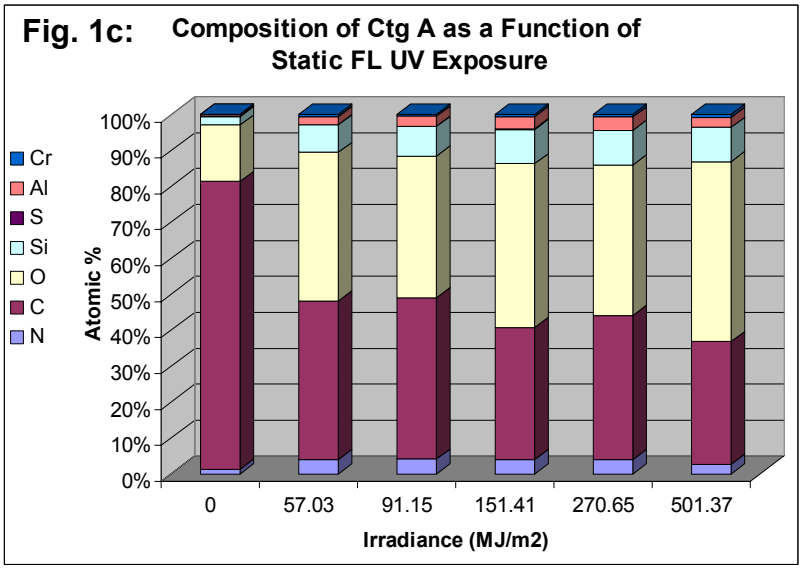
Fig. 1c: Composition of Ctg A as a Function of Static FL UV Exposure
Cr
Al
S
Si
O
C
N
Atomic %
100%
90%
80%
70%
60%
50%
40%
30%
20%
10%
0%
0
57.03
91.15
151.41
270.65
501.37
Irradiance (MJ/m2)

The C1s core electron spectra for coating A was fit with 5 peaks which can be correlated with proposed changes in the Carbon bond state as a function of UV induced degradation. The change in concentration for the various bond states (peaks) is illustrated in Figure 2 with the range of binding energy shifts in Table 2.

Fig 2a

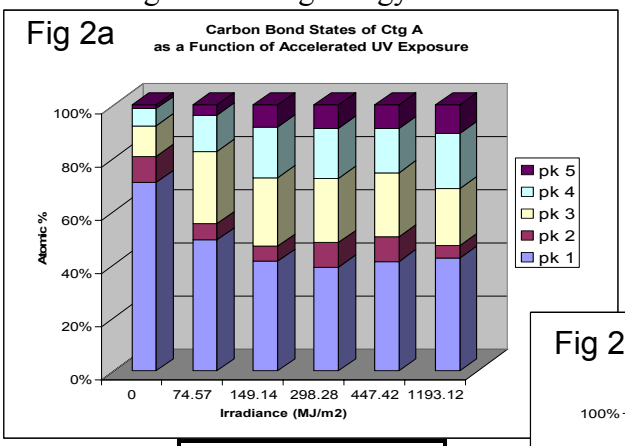

Fig 2b

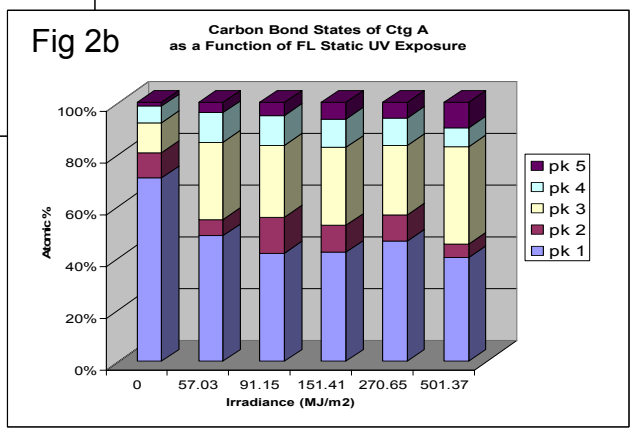

Table 2

C 1s Peak	Delta (eV)
1	0
2	0.5 – 0.8
3	1.5-1.8
4	4.2-4.6
5	2.8-3.3

Fig 2c

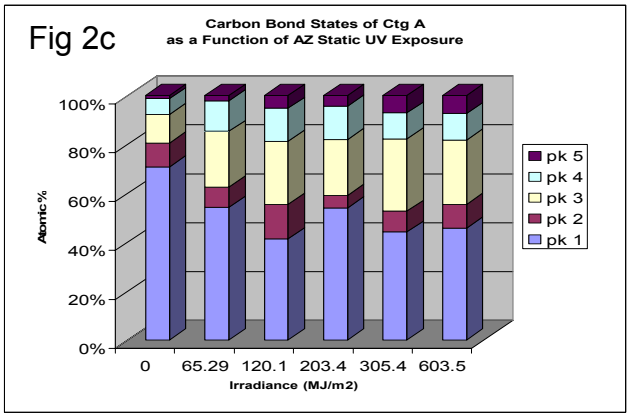

In this system peak 1 corresponds to C-C bonds that are found in the backbone of most polymers. Peak 2 was used to incorporate some charging effects of the XPS technique on polymers and for this analysis can also be attributed to C-C bonds. Peak 3, which has a binding energy shift of 1.5 – 1.8eV in coating A, is attributed to the oxidation of the carbon in either a hydroxyl or methoxide arrangement. Peak 4 demonstrates a binding energy shift of the C from 4.2 – 4.6 eV. This can be attributed to the influence of the N on the C 1s when in a urethane functional end group as well as when C is part of a carboxylic acid. Peak 5 has a delta of 2.8-3.3eV and correlates to increase number of carbonyl groups in the system.

Coating System B

The atomic compositions measured by XPS for samples B after exposure to accelerated QUV, static AZ and static FL weathering is shown in Table 3 and the trends that evolve are illustrated in Figure 3. The initial composition of the surface is very high in carbon and oxygen content, with a small amount of inorganic elements arising from the pigments in the coating. The QUV data shows little change in the surface composition of coating B. The FL and AZ exposures do show an increase in O with aging, but they do not have the emergence of in organic elements that coating A had, and which some are also constituents in the formula for coating B. This would indicate that there is no loss of binder. FTIR data presented previously also supported that there was not a significant amount of urethane linkage degradation. Closer examination of the carbon bond states for coating B may provide further insight.

Table 3: Atomic Composition of Coating B (atomic %)

		Atomic Composition of Coating B (atomic %)				
Exposure	Irradiance (MJ/m^2)	Oxygen (O)	Nitrogen (N)	Carbon (C)	Sulfur (S)	Silicon (Si)
BL	0	20.68	7.82	68.77	0.38	2.36
QUV	74.57	22.97	8.46	67.53	0.28	0.76
QUV	149.14	20.45	8.94	68.43	0.18	2.00
QUV	298.28	23.68	8.95	65.96	0.29	1.12
QUV	447.42	24.54	6.89	67.56	0.40	0.60
QUV	1193.12	27.74	10.35	58.94	0.51	2.47
Az	65.29	23.43	7.61	68.34	0.19	0.42
Az	120.08	24.71	8.06	65.25	0.18	1.80
Az	203.4	24.23	6.39	64.00	0.24	5.13
Az	305.37	32.31	4.58	57.81	0.15	5.15
Az	603.52	45.64	3.95	42.48	0.00	7.94
Fl	57.03	33.56	5.23	58.25	0.23	2.74
Fl	91.15	37.86	4.40	54.15	0.22	3.37
Fl	151.41	34.10	4.00	54.67	0.24	7.00
Fl	270.65	45.35	2.93	44.51	0.21	6.99
Fl	501.37	48.01	3.69	43.09	0.13	5.08

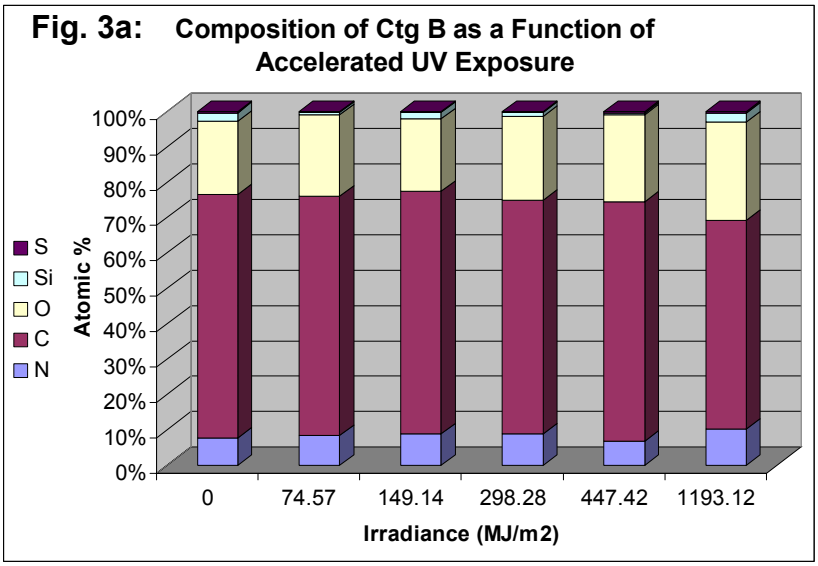
Fig. 3a: Composition of Ctg B as a Function of Accelerated UV Exposure
100%
90%
80%
70%
60%
50%
40%
30%
20%
10%
0%
Atomic %
S
Si
O
C
N
0
74.57
149.14
298.28
447.42
1193.12
Irradiance (MJ/m2)

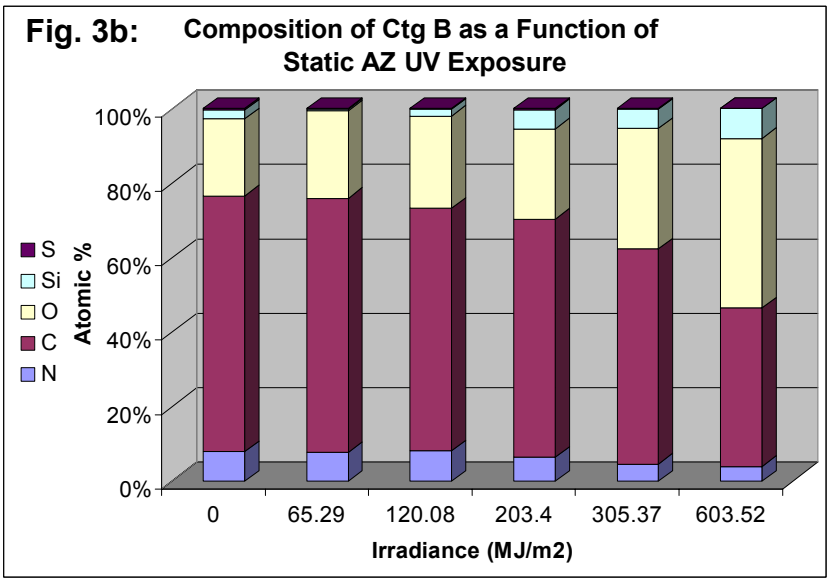
Fig. 3b: Composition of Ctg B as a Function of Static AZ UV Exposure
100%
80%
60%
40%
20%
0%
Atomic %
S
Si
O
C
N
0
65.29
120.08
203.4
305.37
603.52
Irradiance (MJ/m2)

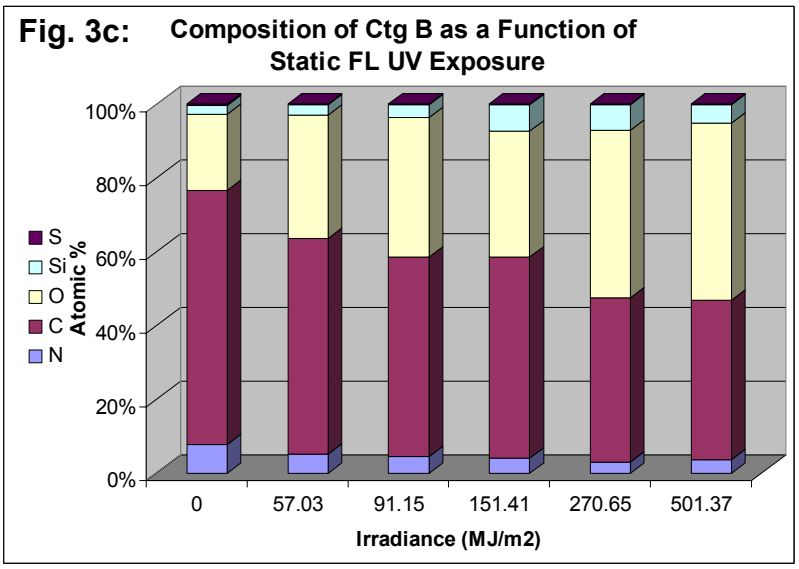
Fig. 3c: Composition of Ctg B as a Function of Static FL UV Exposure
100%
80%
60%
40%
20%
0%
Atomic %
S
Si
O
C
N
0
57.03
91.15
151.41
270.65
501.37
Irradiance (MJ/m2)

The C1s core electron spectra for coating B was fit with 5 peaks, which can be correlated with proposed changes in the Carbon bond state. The change in concentration for the various bond states (peaks) is illustrated in Figure 4 with the range of binding energy shifts in Table 4.

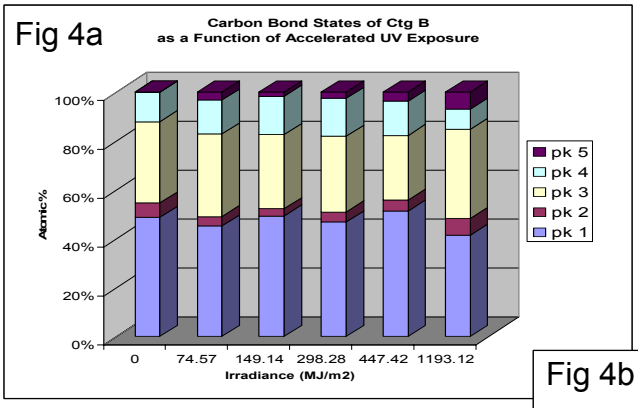

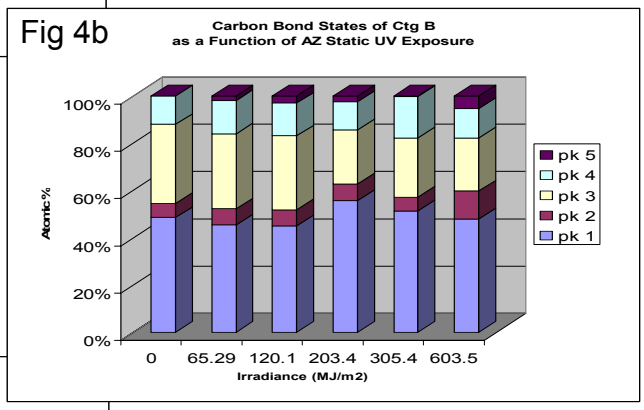

Table 4

C 1s peak	Delta (eV)
1	0
2	0.5 - 1
3	1.5 - 1.8
4	4.2 - 4.7
5	3 - 3.3

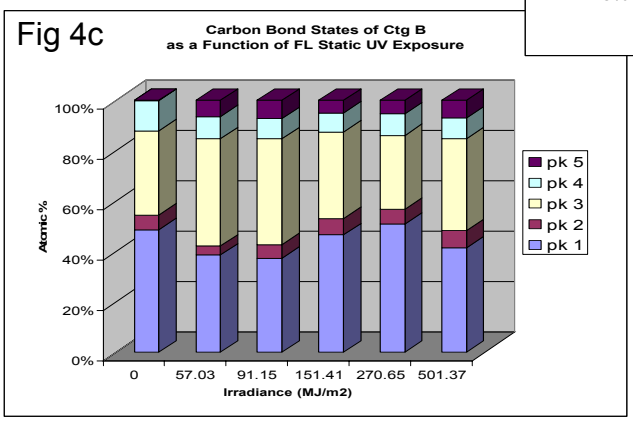

Here again, peak 1 corresponds to C-C bonds that are found in the backbone of most polymers. And peak 2 incorporates charging effects but may also be attributed to C-C bonding. Peak 3, which has a binding energy shift of 1.5 – 1.8eV in coating B, is attributed to the oxidation of the carbon in either a hydroxyl or methoxide arrangement. Peak 4 demonstrates a binding energy shift of the C from 4.2 – 4.7 eV. This can be attributed to the influence of the N on the C 1s when in a urethane functional end group as well as when C is part of a carboxylic acid. Peak 5 has a delta of 3-3.3eV and would correlate to carbonyl groups in the system.

Coating System C

The atomic compositions measured by XPS for samples C after exposure to Accelerated QUV, Static AZ and Static FL weathering is shown in Table 5 and the trends that evolve are illustrated in Figure 5. The initial composition of the surface is very high in carbon, oxygen and fluorine, with a small amount of inorganics attributed to coating extenders and pigments. The data shows an increase in O and Si with aging, a slight emergence of the remaining inorganic elements and a rapid decrease in the Fl content with age. The loss of Carbon and rapid emergence of Si pigment/extender elements in coating C is characteristic of binder degradation.

Table 5: Atomic Composition of Coating C (atomic %)

		Atomic Composition of Coating C (atomic %)							
Exposure	Irradiance (MJ/m^2)	Fluorine (FL)	Oxygen (O)	Nitrogen (N)	Carbon (C)	Sulfur (S)	Silicon (Si)	Calcium (Ca)	Aluminum (Al)
BL	0	11.98	18.41	3.78	63.37	0.51	1.94	0	0
QUV	74.57	10.59	24.78	4.20	53.75	0.40	4.86	0.76	0.65
QUV	149.14	9.92	25.41	4.28	52.62	0.59	5.62	1.03	0.54
QUV	298.28	3.59	34.52	3.67	47.20	1.03	7.29	1.82	0.89
QUV	447.42	0.45	32.24	4.30	50.74	0.23	9.74	1.19	1.10
QUV	1193.12	0.34	38.76	3.63	41.58	1.64	9.91	3.08	1.07
Az	65.29	1.51	29.80	3.78	56.32	0.18	3.07	0.00	0.68
Az	120.08	0.63	33.49	3.24	54.56	0.16	6.75	0.34	0.78
Az	203.4	0.33	37.00	3.79	48.70	0.06	10.66	0.53	1.41
Az	305.37	0.11	43.41	3.10	38.55	0.08	15.28	0.41	1.78
Az	603.52	0.08	47.43	2.77	29.21	0.07	18.57	0.67	2.81
Fl	57.03	1.57	29.80	3.78	58.01	0.00	5.38	0.43	1.10
Fl	91.15	0.63	33.49	3.24	53.99	0.04	6.55	0.77	1.29
Fl	151.41	0.33	37.00	3.79	46.10	0.03	10.49	0.66	1.59
Fl	270.65	0.11	43.41	3.20	37.01	0.05	12.93	0.67	2.27
Fl	501.37	0.08	47.43	2.77	31.70	0.00	15.76	0.60	1.65

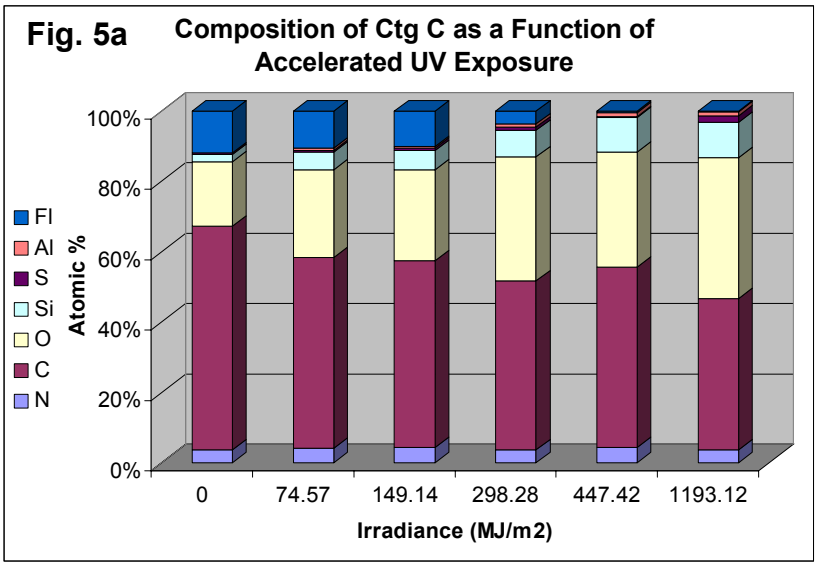
Fig. 5a
Composition of Ctg C as a Function of Accelerated UV Exposure
100%
80%
60%
40%
20%
0%
Atomic %
Fl
Al
S
Si
O
C
N
0
74.57
149.14
298.28
447.42
1193.12
Irradiance (MJ/m2)

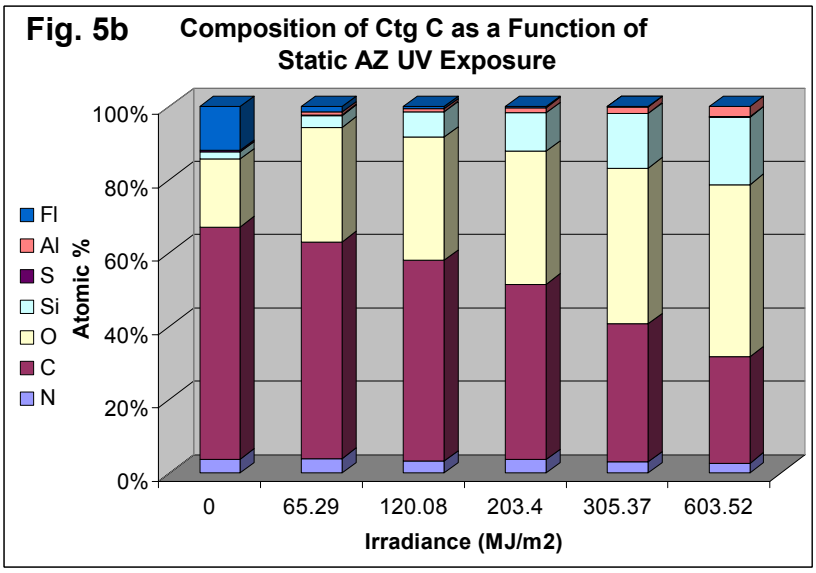
Fig. 5b
Composition of Ctg C as a Function of Static AZ UV Exposure
100%
80%
60%
40%
20%
0%
Atomic %
Fl
Al
S
Si
O
C
N
0
65.29
120.08
203.4
305.37
603.52
Irradiance (MJ/m2)

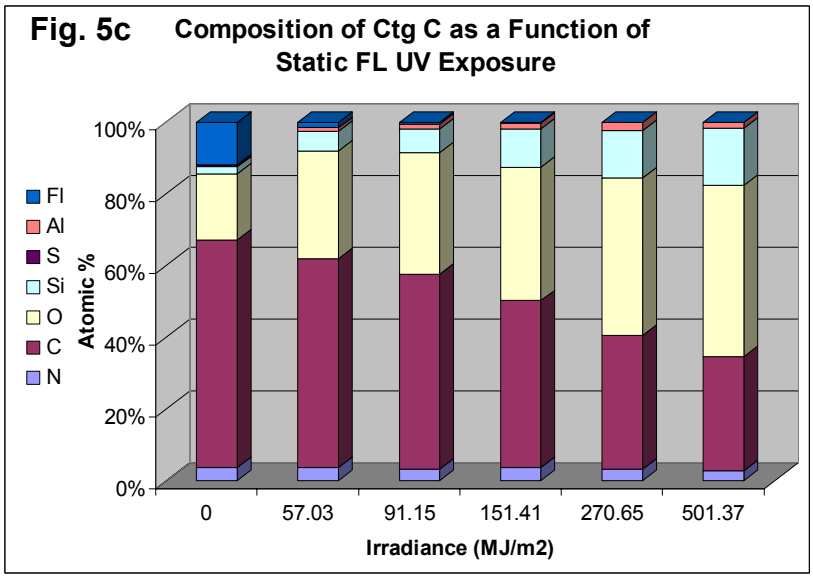
Fig. 5c
Composition of Ctg C as a Function of Static FL UV Exposure
100%
80%
60%
40%
20%
0%
Atomic %
Fl
Al
S
Si
O
C
N
0
57.03
91.15
151.41
270.65
501.37
Irradiance (MJ/m2)

The C1s core electron spectra for coating C was fit with 5 or 6 peaks, which can be correlated with proposed changes in the Carbon bond state. The change in concentration for the various bond states (peaks) is illustrated in Figure 6 with the range of binding energy shifts in Table 6.

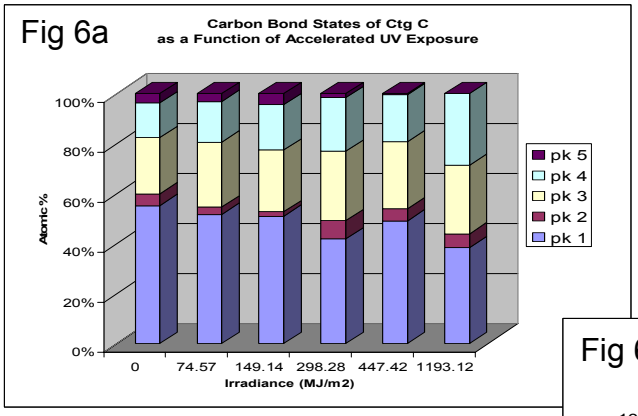

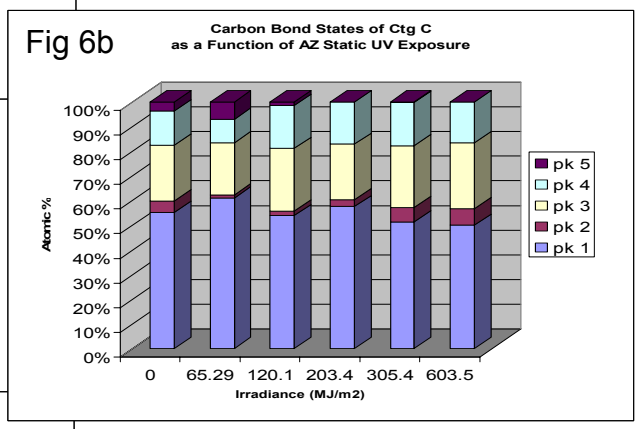

Table 6

C 1s peak	Delta (eV)
1	0
2	0.4 - 0.9
3	1.4 - 1.6
4	4 - 4.3
5	3 - 4.5*
6	1.8 - 3.1

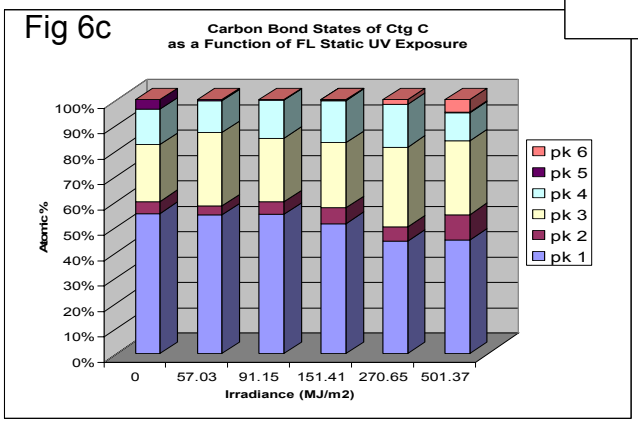

Here again, peak 1 and peak 2 corresponds to C-C bonds. Peak 3, which has a binding energy shift of 1.4 – 1.6eV in coating C, is attributed to the oxidation of the carbon in either a hydroxyl or methoxide arrangement. Peak 4 demonstrates a binding energy shift of the C from 4. – 4.3 eV. attributed to the N functional end group as well as carboxylic acid. Peak 5 has a delta of 3-4.3eV and would correlate to carbonyl groups in the system. One would note that the Fl exposure of coating C required a 6th peak to get a good C 1s core fit. This peak is relatively low in intensity but wide in shape. This would imply that it may have been an artifact from charge compensation and can be considered to be a "smearing" of peaks 2-5 and not attributed to any one C bond state.

Analysis

Background Theory:

Aliphatic urethanes:
Aliphatic diisocyanates such as hexamethylene diisocyanate (HDI) do undergo UV degradation but do not have the rapid discoloration/yellowing that is present when one uses an aromatic diisocyanate. All four topcoats incorporate some form of the aliphatic HDI as a building block. The topcoat in system B incorporates the modified HDI trimer closed ring isocyanurate structure. This structure provides a type of ring stabilization effect over linear HDI systems. While the topcoat of coating A is initiated with the HDI trimer in the more open branched biuret form. The resulting Poly(ester-urethane) cross-linked structures look like those shown in figures 7a and 7b.

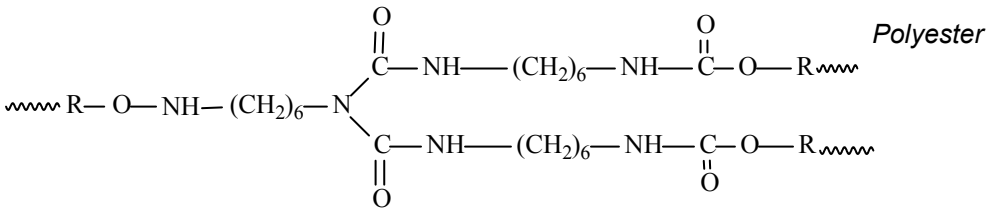

Fig 7a: **Poly(ester-urethane) cross-link with biuret HDI structure**

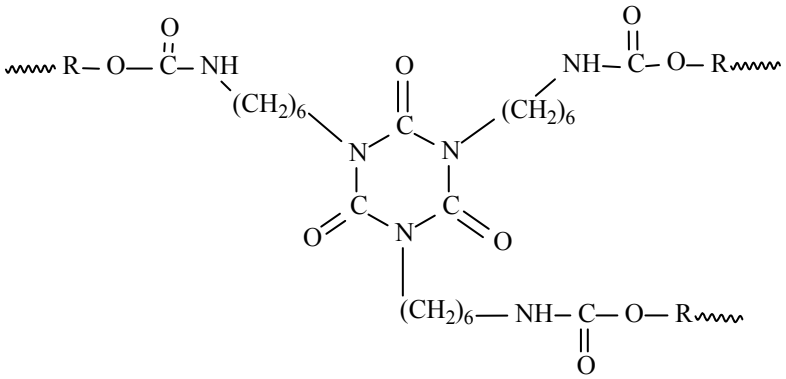

Fig 7b: **Poly(ester-urethane) cross-link with ring-stabilized HDI structure**

Two-component water based polyurethane coatings (topcoats B & D) are based upon an acrylic polyol emulsion (aliphatic polyisocyanate) and a water dispersible polisocyanate (hydrophillically modified diisocyanate polyisocayanurate). During the polyurethane film formation the following chemical functional groups can be formed: urethanes, ureas, amines, carbon dioxide.

Formation of urea can affect structure-property relationships of waterborne polyurethane. The influence of urea during film formation can alter the glass transition temperature, storage modulus, film hardness and cross-link density. Urethane linkages are formed when a hydroxyl-functional compound and a polyisocyanate cross linker undergo an addition reaction. However, isocyanates will also react with water to form short-lived carbonic acid then becoming carbon dioxide and amine. Isocyanate can further react with the amine bi-product producing polyurea. The goal is to have urethane cross-linking to dominate over urea formation. This is often why there is over indexing of isocyanate at a given stochiometry to accelerate the cross linking reaction of a polyurethane network formation and minimize the influence of the water driven urea formation.

The chemical species progression during film formation is important since some of these bi-products are also present after topcoat degradation. The degradation of polyurethane can result in amides, amines, urea, carboxylic acids, in-situ water for both solvent and water dispersible-based systems. The potential presence of these species during both film formation and degradation, make the chemical characterization of the non-ideal system less than trivial. This study identifies these functional groups and their growth or decay as a function of increased weathering

In a previous study of 3 HDI based non-pigmented ideal polymeric systems, loss of urethane structure in the presence of UV irradiation and oxygen. FTIR spectra indicated hydroxyl formation, loss of urethane structure, but did not indicate influence of the polyester segments on the photochemical behavior of the model aliphatic poly (ester-urethane) system. Long wavelength (>300nm) irradiation with no oxygen showed no noticeable change of spectra. It has been proposed that oxidation of the C atom in alpha position to the NH urethane linkage leads to the formulation of hydro peroxides, which through a series of reactions and short-lived photoproducts results in a carboxylic acid and urethane group. Figures 8a and 8b are illustrative of a probable outcome if systems A and B were ideal.

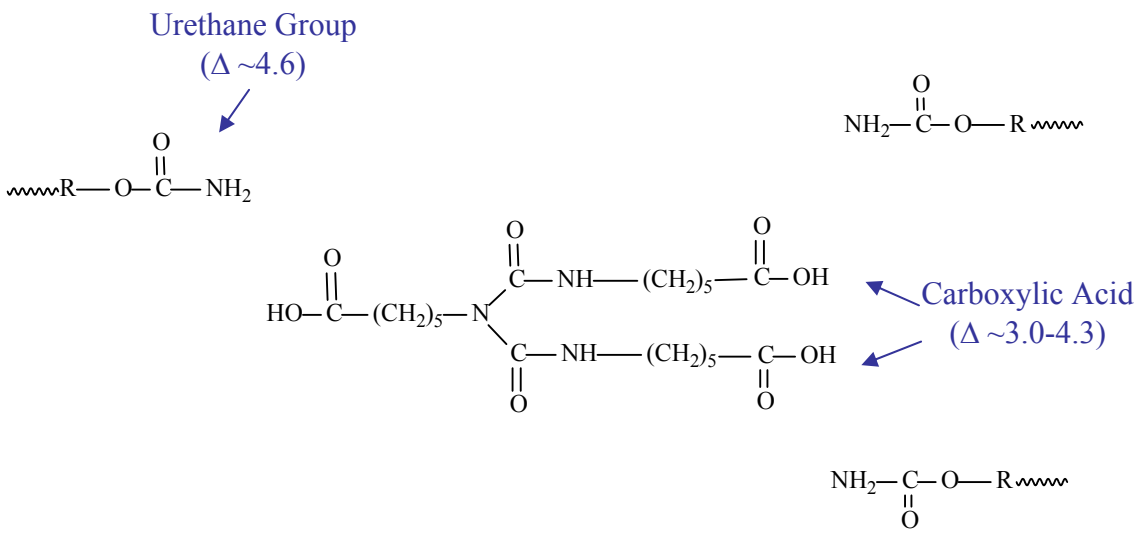

Illustration of biuret structure degradation

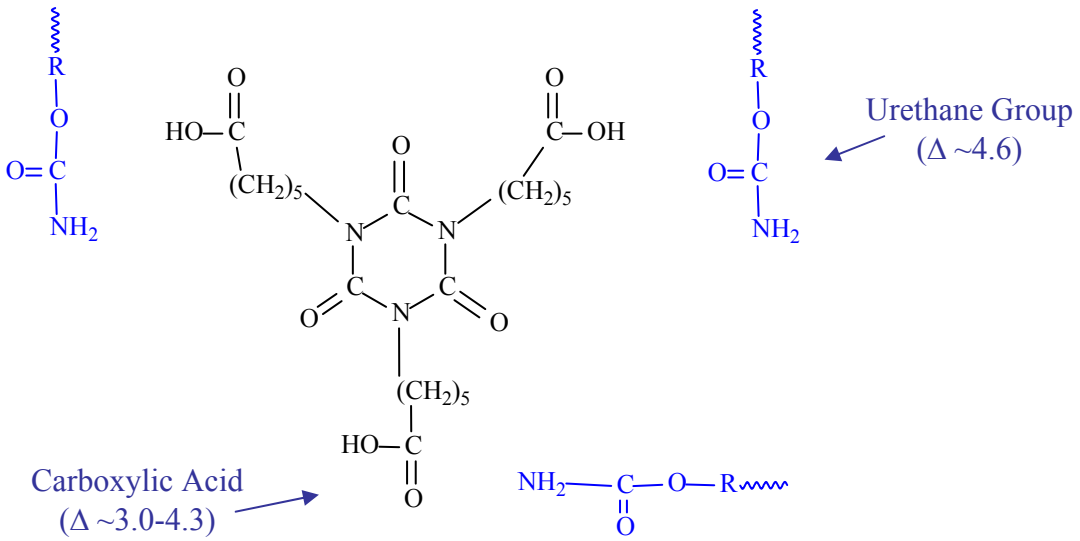

Fig 8b2 Illustration of ring-stabilized HDI structure degradation

Coating A

In examining Figures 2a-2c, all three exposure conditions show a sharp decrease in the C-C bonds (pks 1&2). Peaks 3 and 5 show increased oxidation states of the carbon. This coincides with the increased Oxygen content with exposure, illustrated in figures 3a-3c. Peak 4, which is attributed to carboxylic acid and urethane end groups, increases in all 3 exposures. These are the degradation by-products from our photo oxidation model. This XPS result compliments the previously reported FTIR analysis hence, supporting our UV induced photo oxidation model. The oxidation results in a loss of polymer (C) and

extenders (Si) and pigments are being exposed at surface. The increased scatter from inorganic particles may be correlated with the color and gloss change observed for coating A.

Coating B

Examination of figure 4a-c shows almost no change in the C-C bond concentration (pk 1&2) with aging. Peak 4, which is associated with the UV photo oxidation by-product shows little activity. The primary activity is associated with the carbonyl, hydroxyl or methoxide bonding states (peaks 5 & 3 respectively) of carbon. The increased oxygen with exposure in figures 3a- 3c supports this type of bonding. In the QUV exposure, the elemental ratios are almost constant- no significant degradation of the polymer. In AZ exposure, there is a significant increase in the Oxygen concentration (3b) and an increase in the carbonyl (C=O)functional groups (4b). The FL exposure has a sharper increase of oxygen with exposure (3c). this combined with the peaks 3&5 (4c) would lead to a connection between the increased humidity and the carbon oxidation. It should be noted that there is no evidence of the inorganic pigment particles showing through the surface,. FTIR data does not show significant urethane linkage degradation, and color durability is maintained in coating B. This evidence would support that the ring HDI structure of coating B, provides a type of stabilization of the urethane linkage in the polymer binder.

Coating C

Figures 5a-c show an almost immediate loss of all Fluorine of coating C with increased UV exposure. Silicon extenders and other inorganic do appear at the surface with increased aging. Peak 5 in figures 6a-c disappears rapidly with aging. It is plausible that the carbonyl bonding of peak 5 is associated with the Fl in coating C and burns off under UV exposure. Again peak 4 shows increase of carboxylic acid (hence urethane linkage degradation) but not at the drastic rate of coating A. Competing with peak 4 is the methoxide or hydroxyl arrangement of peak 3. This seams to increase with increased moisture content of the exposure environment. Since this is a NavAir coating, this is significant to its performance. Coating C did not show good color retention performance. The FTIR of this system supports the photo oxidation model proposed, but it is quite intricate and further examination may prove valuable.

Summary

Through the investigation of surface atomic concentrations, it has been verified that for coating A and C, there is a loss of polymer (C) and extenders (Si) and pigments are becoming more prevalent at surface. The increased scatter from such inorganic particles may be correlated with the color and gloss changes. This is consistent with photo-degradation studies on aliphatic and aromatic urethane neat polymer films. In those studies, it has been shown that photo-degradation leads to chain scission ultimately resulting in mass loss in the polymer. Coating B does not show evidence of significant urethane chain scission, and shows improved color retention. There does appear to be a surface oxidation under humid environment, but this does not appear to correlate with any performance requirement of coating B.

Carderock Division
Naval Surface Warfare Center
Philadelphia, PA 19112-1403

NSWCCD-62-TR-2003/01 **December 2002**

Survivability, Structures, and Materials Directorate
Technical Report

Mechanisms of Military Coatings Degradation – End of Fiscal Year 2002 Report

by

Anthony Eng
Laura McGrath
Forrest Pilgrim

Mechanisms of Military Coatings Degradation –End of Fiscal Year 2002 Report

NSWCCD-62-TR-2003/01

Approved for public release;
distribution is unlimited.

APPENDIX A

EIS Correlation Data

Coating A

NaCl immersion

Time (wk)	C_{pf} (F/cm^2)	n_{pf}	R_{pf} (ohm/cm^2)	C_{dl}(F/cm^2)	n_{dl}	R_{ct} (ohm/cm^2)
0	3.47E-09	0.88	1.49E+08	4.85E-09	0.55	3.70E+08
1	2.70E-09	0.92	8.31E+07	3.62E-09	0.59	4.32E+08
2	2.13E-09	0.95	6.02E+07	2.88E-09	0.59	7.22E+08
4	1.83E-09	0.96	5.75E+07	2.96E-09	0.62	8.13E+08
8	1.77E-09	0.97	3.55E+07	2.97E-09	0.57	1.08E+09
16	4.75E-09	0.9	2.51E+07	1.16E-08	0.76	6.67E+08

Arizona Exposure

UV (MJ/m^2)	C_{pf} (F/cm^2)	n_{pf}	R_{pf} (ohm/cm^2)	C_{dl}(F/cm^2)	n_{dl}	R_{ct} (ohm/cm^2)	adhesion	blistering	dE
0	3.47E-09	0.88	1.49E+08	4.85E-09	0.55	3.70E+08	5	5	0
65.29	2.5E-09	0.91	1.28E+07	6.58E-09	0.58	2.40E+08	5	5	0.32
120.08	1.55E-09	0.91	2.21E+09	1.07E-09	0.69	3.52E+09	4.5	5	0.54
203.4	1.21E-09	0.93	4.18E+09	1.43E-09	1	5.00E+09	5	5	3.46
305.37	6.98E-10	0.96	8.75E+08	3.84E-10	0.56	9.00E+09	5	5	4.6
604	1.92E-09	0.91	5.13E+07	2.34E-09	0.52	7.63E+08	4	5	7.95

ASTM B117

Time (wk)	C_{pf} (F/cm^2)	n_{pf}	R_{pf} (ohm/cm^2)	C_{dl}(F/cm^2)	n_{dl}	R_{ct} (ohm/cm^2)	adhesion	blistering
0	3.47E-09	0.88	1.49E+08	4.85E-09	0.55	3.70E+08	5	5
3	1.67E-09	0.96	4.07E+07	3.52E-09	0.66	9.77E+08		
6	1.99E-09	0.96	2.57E+07	5.70E-09	0.57	3.19E+08		
12	1.98E-09	0.96	5.44E+07	5.71E-09	0.61	1.52E+08	5	5
18	2.15E-09	0.96	9.83E+05	5.66E-09	0.47	9.39E+07	3	5
48	4.04E-09	0.96	2.05E+05	6.85E-09	0.49	1.26E+08	0	3

Florida Exposure

UV (MJ/m^2)	C_{pf} (F/cm^2)	n_{pf}	R_{pf} (ohm/cm^2)	C_{dl}(F/cm^2)	n_{dl}	R_{ct} (ohm/cm^2)	adhesion	blistering	dE
0	3.47E-09	0.88	1.49E+08	4.85E-09	0.55	3.70E+08	5	5	0
57.03	4.90E-10	0.96	1.12E+08	2.55E-10	0.66	1.29E+10	4	5	0.13
91.15	5.93E-12	0.92	1.92E+09	2.26E-10	0.31	1.50E+10	5	5	0.41
151.41	4.87E-10	0.99	1.10E+06	1.68E-10	0.86	5.90E+10	4.5	5	2.31
270.65	3.94E-10	1	1.24E+05	1.81E-10	0.78	3.42E+10	5	5	4.67
501	1.71E-09	0.93	3.68E+08	2.12E-09	0.84	8.50E+08	4.5	5	6.95

Coating A

GM9540P

Time (wk)	C_{pf} (F/cm^2)	n_{pf}	R_{pf} (ohm/cm^2)	C_{dl}(F/cm^2)	n_{dl}	R_{ct} (ohm/cm^2)	adhesion	blistering
0	3.47E-09	0.88	1.49E+08	4.85E-09	0.55	3.70E+08	5	5
3	6.84E-10	0.96	4.71E+05	4.8E-10	0.68	7.00E+09	4	5
6	1.88E-09	0.95	2.13E+07	5.15E-09	0.6	6.26E+08	4	5
12	4.45E-10	1	9.80E+03	8.48E-10	0.89	9.08E+09	4	5
18	3.75E-10	1	2.00E+04	6.45E-10	0.86	6.21E+10	5	5
48	8.84E-10	0.7	7.69E+04	1.30E-09	0.92	2.17E+08		

GM9540P Immersion

Time (wk)	C_{pf} (F/cm^2)	n_{pf}	R_{pf} (ohm/cm^2)	C_{dl}(F/cm^2)	n_{dl}	R_{ct} (ohm/cm^2)
0	4.88E-09	0.87	3.59E+06	9.87E-09	0.61	9.48E+07
1	3.53E-09	0.89	3.33E+06	8.75E-09	0.62	1.02E+08
2	4.67E-09	0.89	1.98E+06	8.49E-09	0.63	1.27E+08
4	3.4E-09	0.92	1.47E+06	6.94E-09	0.68	2.91E+08
8	3.79E-09	0.92	7.25E+05	6.19E-09	0.7	3.77E+08
16	3.68E-09	0.92	5.77E+05	5.74E-09	0.71	5.53E+08

Pennsylvania Exposure

UV (MJ/m^2)	C_{pf} (F/cm^2)	n_{pf}	R_{pf} (ohm/cm^2)	C_{dl}(F/cm^2)	n_{dl}	R_{ct} (ohm/cm^2)	adhesion	blistering
0	3.47E-09	0.88	1.49E+08	4.85E-09	0.55	3.70E+08	5	5
36	8.7E-10	0.94	5.06E+09	9.82E-10	1	8.00E+09	5	5
69	2.16E-09	0.9	2.72E+08	3.91E-09	0.85	4.93E+08	4.5	5
116	5.24E-10	0.97	3.41E+09	3.15E-10	1	7.76E+10	5	5
170	4.59E-12	1	5.04E+08	6.86E-12	0.72	1.53E+11	5	5
375	3.94E-09	0.9	1.16E+07	1.03E-09	0.51	1.96E+08	5	5

QUV Exposure

UV (MJ/m^2)	C_{pf} (F/cm^2)	n_{pf}	R_{pf} (ohm/cm^2)	C_{dl}(F/cm^2)	n_{dl}	R_{ct} (ohm/cm^2)	adhesion	blistering	dE
0	3.47E-09	0.88	1.49E+08	4.85E-09	0.55	3.70E+08	5	5	0
74.57	1.066E-09	0.92	8.33E+08	1.67E-10	0.63	5.71E+10	4.5	5	0.47
149.14	8.49E-10	0.94	8.51E+08	1.01E-09	1	1.61E+10	4	5	3.2
298.28	9.6E-10	0.93	4.35E+09	1.17E-09	1	3.16E+10	4.5	5	5.8
447.42	4.49E-10	0.98	5.81E+09	9.94E-10	1	1.00E+10	4.5	5	8.1
1193	4.37E-11	0.85	1.43E+05	3.88E-08	0.51	9.00E+08	5	5	13.3

Coating B

NaCl Immersion

Time (wk)	C_{pf} (F/cm^2)	n_{pf}	R_{pf} (ohm/cm^2)	C_{dl}(F/cm^2)	n_{dl}	R_{ct} (ohm/cm^2)
0	8.14E-09	0.91	1.51E+06	3.64E-08	0.45	2.72E+07
1	9.61E-09	0.89	5.22E+06	3.52E-08	0.54	2.58E+07
2	9.85E-09	0.89	1.00E+07	2.99E-08	0.61	2.67E+07
4	1.12E-08	0.89	1.41E+07	2.64E-08	0.62	4.77E+07
8	1.18E-08	0.87	1.08E+07	5.76E-08	0.48	6.28E+07
16	4.24E-08	0.77	1.27E+03	2.85E-08	0.71	1.90E+07

Arizona Exposure

UV (MJ/m^2)	C_{pf} (F/cm^2)	n_{pf}	R_{pf} (ohm/cm^2)	C_{dl}(F/cm^2)	n_{dl}	R_{ct} (ohm/cm^2)	adhesion	blistering	dE
0	8.14E-09	0.91	1.51E+06	3.64E-08	0.45	2.72E+07	5	5	0
65.29	3.37E-09	0.89	5.29E+05	3.01E-09	0.79	1.39E+09	4.5	5	0.76
120.08	1.40E-09	0.91	2.62E+07	3.04E-09	0.69	1.93E+09	4	5	0.91
203.4	2.68E-09	0.89	1.57E+05	6.36E-09	0.74	4.51E+08	5	5	1.24
305.37	6.78E-10	0.96	8.22E+07	1.23E-09	0.56	3.22E+09	5	5	1.27
604	1.05E-08	0.87	5.48E+06	4.68E-08	0.52	3.28E+06	4.5	5	1.7

ASTM B117

Time (wk)	C_{pf} (F/cm^2)	n_{pf}	R_{pf} (ohm/cm^2)	C_{dl}(F/cm^2)	n_{dl}	R_{ct} (ohm/cm^2)	adhesion	blistering
0	8.14E-09	0.91	1.51E+06	3.64E-08	0.45	2.72E+07	5	5
3	1.29E-08	0.88	6.48E+06	1.07E-07	0.66	3.74E+06		
6	1.96E-08	0.83	5.47E+05	6.47E-06	0.54	1.00E+06		
12	8.37E-09	0.80	2.07E+05	3.74E-08	0.47	7.94E+06	1	1
18	4.02E-07	0.57	4.79E+04	8.83E-05	0.48	2.16E+05	0	4
48	2.23E-10	0.97	2.71E+05	7.61E-09	0.48	5.16E+07	0	5

Florida Exposure

UV (MJ/m^2)	C_{pf} (F/cm^2)	n_{pf}	R_{pf} (ohm/cm^2)	C_{dl}(F/cm^2)	n_{dl}	R_{ct} (ohm/cm^2)	adhesion	blistering	dE
0	8.14E-09	0.91	1.51E+06	3.64E-08	0.45	2.72E+07	5	5	0
57.03	2.00E-09	0.9	1.32E+06	3.88E-09	0.72	1.20E+09	4	5	0.94
91.15	1.18E-09	0.94	1.42E+08	1.51E-09	0.54	1.70E+10	4	5	1.1
151.41	1.05E-09	0.96	1.32E+05	2.88E-09	0.59	1.16E+10	4	5	1.22
270.65	6.62E-10	0.98	1.59E+09	4.31E-10	0.61	3.87E+09	5	5	1.32
501	4.73E-09	0.86	8.70E+04	1.49E-08	0.63	1.01E+06	4	5	1.65

Coating B

GM9540P

Time (wk)	C_{pf} (F/cm^2)	n_{pf}	R_{pf} (ohm/cm^2)	C_{dl}(F/cm^2)	n_{dl}	R_{ct} (ohm/cm^2)	adhesion	blistering
0	8.14E-09	0.91	1.51E+06	3.64E-08	0.45	2.72E+07	5	5
3	2.02E-09	0.9	4.73E+06	2.23E-09	0.74	2.30E+09	4	5
6	1.85E-09	0.91	2.71E+06	4.30E-09	0.67	4.57E+09	4	5
12	1.81E-09	0.92	3.77E+05	4.25E-09	0.7	6.90E+08	4	5
18	1.29E-09	0.93	1.12E+06	4.25E-09	0.63	1.06E+09	4	5
48	9.00E-09	0.96	4.90E+08	7.71E-10	0.56	3.87E+09		

GM9540P Immersion

Time (wk)	C_{pf} (F/cm^2)	n_{pf}	R_{pf} (ohm/cm^2)	C_{dl}(F/cm^2)	n_{dl}	R_{ct} (ohm/cm^2)
0	3.19E-08	0.82	1.15E+06	4.41E-07	0.37	4.26E+06
1	2.79E-08	0.83	1.53E+06	3.18E-07	0.4	4.77E+06
2	2.56E-08	0.83	1.68E+06	2.58E-07	0.42	5.08E+06
4	1.94E-08	0.85	2.35E+06	1.38E-07	0.46	5.54E+06
8	2.54E-08	0.84	1.66E+06	2.43E-07	0.43	5.00E+06
16	2.81E-08	0.83	1.18E+06	3.32E-07	0.42	4.30E+06

Pennsylvania Exposure

UV (MJ/m^2)	C_{pf} (F/cm^2)	n_{pf}	R_{pf} (ohm/cm^2)	C_{dl}(F/cm^2)	n_{dl}	R_{ct} (ohm/cm^2)	adhesion	blistering
0	8.14E-09	0.91	1.51E+06	3.64E-08	0.45	2.72E+07	5	5
36	1.86E-09	0.91	1.46E+05	3.77E-09	0.8	1.14E+09	4.5	5
69	7.75E-10	0.96	3.37E+08	1.04E-09	0.49	1.93E+09	4.5	5
116	8.37E-10	0.95	4.23E+08	9.69E-09	0.57	3.10E+09	4.5	5
170	7.49E-10	0.97	5.79E+08	5.54E-10	0.6	5.80E+09	4	5
375	1.30E-09	0.97	1.05E+04	1.09E-08	0.76	8.94E+07	4	5

QUV Exposure

UV (MJ/m^2)	C_{pf} (F/cm^2)	n_{pf}	R_{pf} (ohm/cm^2)	C_{dl}(F/cm^2)	n_{dl}	R_{ct} (ohm/cm^2)	adhesion	blistering	dE
0	8.14E-09	0.91	1.51E+06	3.64E-08	0.45	2.72E+07	5	5	0
74.57	5.21E-09	0.85	4.72E+06	4.09E-10	0.97	2.24E+09	5	5	0.55
149.14	5.47E-09	0.88	6.76E+08	5.59E-08	1	1.00E+09	4	4.9	0.57
298.28	4.47E-09	0.9	6.28E+08	2.46E-08	1	1.00E+09	4	5	0.75
447.42	8.23E-09	0.88	5.50E+07	1.20E-08	0.73	4.03E+08	5	5	0.87
1193	9.77E-08	0.72	1.19E+04	1.95E-06	0.37	1.00E+07	4	5	1.3

Coating C

NaCl Immersion

Time (wk)	C_{pf} (F/cm^2)	n_{pf}	R_{pf} (ohm/cm^2)	C_{dl}(F/cm^2)	n_{dl}	R_{ct} (ohm/cm^2)
0	1.39E-09	0.95	8.99E+05	1.3E-08	0.5	9.56E+07
1	1.53E-09	0.94	1.07E+06	1.38E-08	0.52	1.07E+08
2	1.78E-09	0.93	1.07E+06	1.53E-08	0.54	9.21E+07
4	1.99E-09	0.93	1.13E+06	1.6E-08	0.56	7.16E+07
8	8.45E-09	0.81	2.85E+05	3.30E-07	0.68	2.66E+07
16	2.15E-09	0.93	1.29E+06	1.5E-08	0.58	4.84E+07

Arizona Exposure

UV (MJ/m^2)	C_{pf} (F/cm^2)	n_{pf}	R_{pf} (ohm/cm^2)	C_{dl}(F/cm^2)	n_{dl}	R_{ct} (ohm/cm^2)	adhesion	blistering	dE
0	1.39E-09	0.95	8.99E+05	1.3E-08	0.5	9.56E+07	0	5	0
65.29	9E-10	0.95	1.79E+08	9.97E-10	0.5	1.55E+10	0	4	0.17
120.08	1.08E-09	0.95	2.67E+08	9.7E-10	0.47	5.25E+09	0	5	0.18
203.4	1.05E-09	0.95	3.29E+08	7.38E-10	0.61	7.85E+09	0	3	0.52
305.37	7.25E-10	0.97	9.57E+08	3.26E-10	0.86	1.00E+10	0	3	1.28
604	2.37E-09	0.93	2.20E+05	1.75E-08	0.52	4.50E+07	0	4	2.55

ASTM B117

Time (wk)	C_{pf} (F/cm^2)	n_{pf}	R_{pf} (ohm/cm^2)	C_{dl}(F/cm^2)	n_{dl}	R_{ct} (ohm/cm^2)	adhesion	blistering
0	1.39E-09	0.95	8.99E+05	1.3E-08	0.5	9.56E+07	0	5
3	2.12E-09	0.94	4.76E+05	9.91E-09	0.6	2.18E+08		
6	2.78E-09	0.92	1.30E+05	1.32E-08	0.67	1.44E+08		
12	2.48E-09	0.93	1.87E+06	7.13E-09	0.49	4.86E+08	3	5
18	2.55E-09	0.94	3.95E+05	1.16E-08	0.53	1.35E+08	3.5	4.9
48	1.32E-09	0.95	1.62E+08	1.04E-09	0.67	4.68E+09	3	5

Florida Exposure

UV (MJ/m^2)	C_{pf} (F/cm^2)	n_{pf}	R_{pf} (ohm/cm^2)	C_{dl}(F/cm^2)	n_{dl}	R_{ct} (ohm/cm^2)	adhesion	blistering	dE
0	1.39E-09	0.95	8.99E+05	1.3E-08	0.5	9.56E+07	0	5	0
57.03	9.99E-10	0.96	3.97E+04	8.98E-09	0.55	3.68E+07	0.1	3	0.35
91.15	1.18E-09	0.95	2.33E+05	3.17E-09	0.53	4.60E+08	0	3	0.44
151.41	8.35E-10	0.98	5.11E+08	7.81E-10	0.5	4.00E+09	0	1	0.43
270.65	9.28E-10	0.98	1.23E+09	3.58E-09	0.94	2.50E+09	0	2	0.88
501	3.53E-09	0.9	1.46E+06	2.95E-08	0.56	2.68E+07	0	2	2.4

Coating C

GM9540P

Time (wk)	C_{pf} (F/cm^2)	n_{pf}	R_{pf} (ohm/cm^2)	C_{dl}(F/cm^2)	n_{dl}	R_{ct} (ohm/cm^2)	adhesion	blistering
0	1.39E-09	0.95	8.99E+05	1.3E-08	0.5	9.56E+07	0	5
3	9.46E-10	0.94	4.97E+08	1.35E-09	0.7	5.81E+09	0.5	5
6	2.78E-09	0.89	1.00E+08	4.23E-09	0.62	6.50E+08	2	5
12	1.37E-09	0.93	1.15E+08	1.5E-09	0.56	3.05E+09	0	5
18	2.27E-09	0.91	3.77E+05	4.8E-09	0.48	2.66E+08	0	1
48	1.20E-09	0.96	2.24E+08	6.86E-10	0.44	2.58E+09	0	1

GM9540P Immersion

Time (wk)	C_{pf} (F/cm^2)	n_{pf}	R_{pf} (ohm/cm^2)	C_{dl}(F/cm^2)	n_{dl}	R_{ct} (ohm/cm^2)
0	1.24E-09	0.95	8.25E+05	1.24E-08	0.5	1.12E+08
1	1.3E-09	0.95	5.74E+05	1.45E-08	0.5	1.11E+08
2	1.58E-09	0.94	7.61E+05	1.66E-08	0.53	8.31E+07
4	4.42E-09	0.88	6.57E+06	1.55E-08	0.56	1.00E+08
8	4.13E-09	0.9	2.77E+06	1.50E-08	0.56	8.80E+07
16	2.00E-09	0.93	1.06E+06	1.46E-08	0.56	1.03E+08
32	2.81E-09	0.93	4.65E+06	1.02E-08	0.59	1.74E+08

Pennsylvania Exposure

UV (MJ/m^2)	C_{pf} (F/cm^2)	n_{pf}	R_{pf} (ohm/cm^2)	C_{dl}(F/cm^2)	n_{dl}	R_{ct} (ohm/cm^2)	adhesion	blistering
0	1.39E-09	0.95	8.99E+05	1.3E-08	0.5	9.56E+07	0	5
36	1.21E-09	0.95	4.55E+05	2.84E-09	0.52	3.93E+08	1	4
69	2.08E-09	0.9	7.48E+08	1.67E-09	0.86	2.30E+09	0	3
116	1.31E-09	0.94	1.43E+08	3.03E-09	0.5	4.23E+09	0	2
170	7.33E-10	0.97	3.79E+06	4.93E-10	0.57	7.30E+09	0	4
375	7.14E-10	0.88	6.85E+06	4.48E-09	0.6	8.65E+07	0	1

QUV Exposure

UV (MJ/m^2)	C_{pf} (F/cm^2)	n_{pf}	R_{pf} (ohm/cm^2)	C_{dl}(F/cm^2)	n_{dl}	R_{ct} (ohm/cm^2)	adhesion	blistering	dE
0	1.39E-09	0.95	8.99E+05	1.3E-08	0.5	9.56E+07	0	5	0
74.57	1.04E-09	0.95	1.80E+08	7.83E-10	0.6	3.22E+09	0	5	0.27
149.14	1.1E-09	0.94	1.82E+08	1.66E-09	0.6	3.91E+09	0	4	0.28
298.28	1.12E-09	0.94	1.60E+08	1.56E-09	0.6	1.93E+09	0.65	1	0.47
447.42	1.04E-09	0.96	1.11E+09	2E-10	0.9	1.91E+10	0	1	1.4
1193	5.71E-09	0.89	1.09E+06	3.00E-08	0.55	1.78E+07	1	3	6.1

Coating D

NaCl Immersion

Time (wk)	C_{pf} (F/cm^2)	n_{pf}	R_{pf} (ohm/cm^2)	C_{dl}(F/cm^2)	n_{dl}	R_{ct} (ohm/cm^2)
0	2.15E-06	0.67	5.57E+03	1.73E-05	0.92	1.02E+07
1	1.45E-06	0.71	4.57E+03	1.94E-05	0.91	3.92E+06
2	8.36E-07	0.76	4.40E+03	2.09E-05	0.89	8.49E+05
4	5.37E-07	0.8	4.05E+03	2.27E-05	0.86	8.33E+05
8	4.87E-07	0.81	3.46E+03	2.25E-05	0.88	5.75E+05

Arizona exposure

UV (MJ/m^2)	C_{pf} (F/cm^2)	n_{pf}	R_{pf} (ohm/cm^2)	C_{dl}(F/cm^2)	n_{dl}	R_{ct} (ohm/cm^2)	adhesion	blistering	dE
0	2.15E-06	0.67	5.57E+03	1.73E-05	0.92	1.02E+07	3	3	0
65.29	2.18E-09	0.9	3.12E+05	9.33E-09	0.55	1.74E+08	3	2	0.21
120.08	5.25E-09	0.86	1.90E+03	1.75E-07	0.51	5.66E+06	3	1	0.64
203.4	7.82E-10	0.96	2.38E+05	2.84E-09	0.59	6.00E+08	2	1	0.95
305.37	7.79E-10	0.96	5.45E+05	3.78E-09	0.48	4.00E+08	3	1	0.51
604	1.12E-07	0.69	2.75E+03	5.98E-07	0.68	1.11E+05	3	1	2.5

ASTM B117

Time (wk)	C_{pf} (F/cm^2)	n_{pf}	R_{pf} (ohm/cm^2)	C_{dl}(F/cm^2)	n_{dl}	R_{ct} (ohm/cm^2)	adhesion	blistering
0	2.15E-06	0.67	5.57E+03	1.73E-05	0.92	1.02E+07	4	4
3	4.94E-07	0.81	3.21E+03	2.21E-05	0.92	4.44E+06		
6	3.80E-07	0.82	3.11E+03	2.61E-05	0.89	4.84E+06		
12	3.88E-07	0.82	2.49E+03	2.31E-05	0.95	6.45E+06	4	3
18	5.96E-07	0.8	8.47E+02	3.10E-05	0.91	1.62E+06	4	5
48	3.68E-10	1.06	6.83E+03	3.06E-08	0.64	8.32E+06	3.5	5

Florida Exposure

UV (MJ/m^2)	C_{pf} (F/cm^2)	n_{pf}	R_{pf} (ohm/cm^2)	C_{dl}(F/cm^2)	n_{dl}	R_{ct} (ohm/cm^2)	adhesion	blistering	dE
0	2.15E-06	0.67	5.57E+03	1.73E-05	0.92	1.02E+07	4	4	0
57.03	3.88E-05	0.78	1.50E+04	3.44E-07	0.42	1.06E+06	3	3	0.99
91.15	1.77E-08	0.79	5.67E+04	8.06E-08	0.43	2.50E+07	4	3	1.31
151.41	3.85E-12	0.99	5.30E+08	3.68E-11	0.5	8.48E+09	3	3	1.43
270.65	2.55E-09	0.91	2.30E+07	6.38E-09	0.73	2.65E+08	3	3	2.73
501	6.90E-08	0.76	1.39E+05	1.63E-05	0.78	4.00E+06	3	1	4.1

Coating D

GM9540P

Time (wk)	C_{pf} (F/cm^2)	n_{pf}	R_{pf} (ohm/cm^2)	C_{dl}(F/cm^2)	n_{dl}	R_{ct} (ohm/cm^2)	adhesion	blistering
0	2.15E-06	0.67	5.57E+03	1.73E-05	0.92	1.02E+07	4	4
3	4.16E-08	0.69	2.06E+05	6.32E-07	0.5	8.14E+05	3	1
6	1.87E-07	0.68	8.97E+04	4.31E-07	0.66	3.83E+05		
12	2.31E-07	0.65	2.94E+04	1.87E-07	0.67	4.18E+05	4	3
18	1.45E-07	0.69	5.49E+04	2.42E-07	0.65	3.04E+05	3	3
48	4.26E-08	0.79	3.01E+04	4.71E-07	0.54	3.27E+05	3	1

GM9540P Immersion

Time (wk)	C_{pf} (F/cm^2)	n_{pf}	R_{pf} (ohm/cm^2)	C_{dl}(F/cm^2)	n_{dl}	R_{ct} (ohm/cm^2)
0	4.40E-07		1.02E+02	1.64E-05		700000
1	9.11E-07		1.09E+02	1.71E-05		650000
2						
4						
8	2.92E-06		4.65E+01	1.83E-05		2390000

Pennsylvania Exposure

UV (MJ/m^2)	C_{pf} (F/cm^2)	n_{pf}	R_{pf} (ohm/cm^2)	C_{dl}(F/cm^2)	n_{dl}	R_{ct} (ohm/cm^2)	adhesion	blistering
0	2.15E-06	0.67	5.57E+03	1.73E-05	0.92	1.02E+07	4	4
36	1.12E-08	0.81	4.04E+04	5.30E-07	0.5	1.55E+06	3.5	1
69	5.53E-09	0.85	4.30E+04	2.98E-07	0.42	2.70E+06	3	2
116	1.43E-09	0.94	1.22E+05	1.82E-08	0.51	4.35E+07	2	2
170	9.07E-10	0.97	4.51E+05	3.32E-09	0.56	8.06E+08	3.5	2
375	4.85E-08	0.75	5.90E+03	1.40E-06	0.52	2.37E+05	2	2

QUV Exposure

UV (MJ/m^2)	C_{pf} (F/cm^2)	n_{pf}	R_{pf} (ohm/cm^2)	C_{dl}(F/cm^2)	n_{dl}	R_{ct} (ohm/cm^2)	adhesion	blistering	dE
0	2.15E-06	0.67	5.57E+03	1.73E-05	0.92	1.02E+07	4	4	0
74.57	3.35E-09	0.88	1.10E+05	1.32E-08	0.5	1.50E+08	4	2	0.45
149.14	3.24E-08	0.76	3.85E+04	7.85E-07	0.4	1.18E+06	3	2	0.54
298.28	4.13E-07	0.59	6.46E+04	9.74E-06	0.4	6.00E+06	3	3	0.71
447.42	6.71E-08	0.67	1.68E+05	1.91E-07	0.63	9.43E+05	2	2	0.77
1193	4.90E-06	0.44	1.31E+04	1.22E-05	0.99	4.00E+06	2.5	1	0.98

Coating A
Arizona
Color change (dE)

UV expos. (MJ/m^2)	AAdE	AQC_{pf}	AQR_{pf}	AQC_{dl}
0.00	0.00E+00	3.43E-09	1.64E+08	4.80E-09
65.29	0.32	1.07E-09	8.33E+08	1.67E-10
120.08	0.54	8.49E-10	8.51E+08	1.01E-09
203.4	3.46	9.6E-10	4.35E+09	1.17E-09
305.37	4.6	4.49E-10	5.81E+09	9.94E-10
604	7.95	4.37E-11	1.43E+05	3.88E-08

Regression Statistics	
Multiple R	0.9999
R Square	0.9997
Adjusted R Square	0.9994
Standard Error	0.0792
Observations	6

ANOVA

	df	*SS*	*MS*	*F*	*Significance F*
Regression	3	49.283	16.428	2619.852	0.000
Residual	2	0.013	0.006		
Total	5	49.295			

	Coefficients	*Standard Error*	*t Stat*	*P-value*	*Lower 95%*	*Upper 95%*
Constant	-7.25E-02	0.097295	-0.74	0.5341	-4.91E-01	3.46E-01
AQC_{pf}	-3.03E+08	38693612	-7.83	0.0159	-4.69E+08	-1.36E+08
AQR_{pf}	8.03E-10	1.94E-11	41.38	0.0006	7.20E-10	8.87E-10
AQC_{dl}	2.07E+08	3166287	65.40	0.0002	1.93E+08	2.21E+08

RESIDUAL OUTPUT

Observation	*Predicted AAde*	*Residuals*	*Standard Residuals*
0.00	0.014	-0.014	-0.283
0.32	0.308	0.012	0.236
0.54	0.563	-0.023	-0.458
3.46	3.373	0.087	1.746
4.6	4.663	-0.063	-1.266
7.95	7.949	0.001	0.026

Coating C
Arizona
Color change (dE)

CAdE	CQR_{pf}	CQC_{pf}
0.00	8.99E+05	1.39E-09
0.17	1.80E+08	1.04E-09
0.18	1.82E+08	1.1E-09
0.52	1.60E+08	1.12E-09
1.28	1.11E+09	1.04E-09
2.55	1.09E+06	5.71E-09

Regression Statistics	
Multiple R	0.9867
R Square	0.9736
Adjusted R Square	0.9560
Standard Error	0.2053
Observations	6

ANOVA

	df	*SS*	*MS*	*F*	*Significance F*
Regression	2	4.6645	2.3322	55.3268	0.0043
Residual	3	0.1265	0.0422		
Total	5	4.7909			

	Coefficients	*Standard Error*	*t Stat*	*P-value*	*Lower 95%*	*Upper 95%*
Constant	-0.5761	0.1595	-3.6109	0.0365	-1.0838	-0.0684
CQR_{pf}	1.1853E-09	2.33969E-10	5.066066703	0.0148	4.40708E-10	1.9299E-09
CQC_{pf}	545595867.3	52408103.42	10.41052493	0.0019	378809735.7	712381998.9

RESIDUAL OUTPUT

Observation	*Predicted CAdE*	*Residuals*	*Standard Residuals*
0.00	0.183	-0.183	-1.153
0.17	0.205	-0.035	-0.218
0.18	0.240	-0.060	-0.376
0.52	0.225	0.295	1.857
1.28	1.307	-0.027	-0.170
2.55	2.541	0.009	0.059

Coating A
Florida
Color change (dE)

AFdE	ABC_{pf}	AQC_{pf}	AQR_{pf}
0	3.43E-09	3.43E-09	1.64E+08
0.13	1.67E-09	1.07E-09	8.33E+08
0.41	1.99E-09	8.49E-10	8.51E+08
2.31	1.98E-09	9.6E-10	4.35E+09
4.67	2.15E-09	4.49E-10	5.81E+09
6.95	4.04E-09	4.37E-11	1.43E+05

Regression Statistics	
Multiple R	0.9944
R Square	0.9888
Adjusted R Square	0.9720
Standard Error	0.4774
Observations	6

ANOVA

	df	*SS*	*MS*	*F*	*Significance F*
Regression	3	40.2798	13.4266	58.9042	0.0167
Residual	2	0.4559	0.2279		
Total	5	40.7357			

	Coefficients	*Standard Error*	*t Stat*	*P-value*	*Lower 95%*	*Upper 95%*
Constant	-3.259	0.837	-3.892	0.0601	-6.862	0.344
ABCpf	2532204658	2.57E+08	9.855	0.0101	1426603682	3637805634
AQCpf	-1609979545	1.9E+08	-8.481	0.0136	-2426748133	-793210956.8
AQRpf	5.26935E-10	1.04E-10	5.066	0.0368	7.93945E-11	9.74475E-10

RESIDUAL OUTPUT

Observation	*Predicted AFdE*	*Residuals*	*Standard Residuals*
0	-0.009	0.009	0.031
0.13	-0.308	0.438	1.449
0.41	0.862	-0.452	-1.495
2.31	2.501	-0.191	-0.633
4.67	4.524	0.146	0.484
6.95	6.901	0.049	0.163

Coating C
Florida
Color change (dE)

CFdE	CQR_{pf}	CQC_{pf}	CBC_{pf}
0.00	899000	1.39E-09	1.39E-09
0.35	1.8E+08	1.04E-09	2.12E-09
0.44	1.82E+08	1.1E-09	2.78E-09
0.43	1.6E+08	1.12E-09	2.48E-09
0.88	1.11E+09	1.04E-09	2.55E-09
2.4	1.09E+06	5.71E-09	1.32E-09

Regression Statistics	
Multiple R	0.9968
R Square	0.9937
Adjusted R Square	0.9842
Standard Error	0.1076
Observations	6

ANOVA

	df	*SS*	*MS*	*F*	*Significance F*
Regression	3	3.6372	1.2124	104.6327	0.0095
Residual	2	0.0232	0.0116		
Total	5	3.6604			

	Coefficients	*Standard Err*	*t Stat*	*P-value*	*Lower 95%*	*Upper 95%*
Intercept	-1.2056	0.2773	-4.3479	0.0490	-2.3987	-0.0125
CQR_{pf}	5.33E-10	1.34E-10	3.9669	0.0581	-4.5145E-11	1.11191E-09
CQC_{pf}	5.46E+08	34432230	15.8432	0.0040	397368181	693668245.3
CBC_{pf}	3.67E+08	1.14E+08	3.2253	0.0842	-122702824	857390960.8

RESIDUAL OUTPUT

Observation	*Predicted CFdE*	*Residuals*	*Standard Residuals*
0.00	0.0637	-0.0637	-0.9363
0.35	0.2365	0.1135	1.6671
0.44	0.5127	-0.0727	-1.0686
0.43	0.4017	0.0283	0.4154
0.88	0.8905	-0.0105	-0.1543
2.4	2.3948	0.0052	0.0768

Coating B
Arizona
Color change (dE)

BAdE	BQC_{pf}	BGC_{pf}
0.00E+00	8.14E-09	8.14E-09
0.76	5.21E-09	2.02E-09
0.91	5.47E-09	1.85E-09
1.24	4.47E-09	1.81E-09
1.27	8.23E-09	1.29E-09
1.7	9.77E-08	9.00E-09

Regression Statistics	
Multiple R	0.9616
R Square	0.9247
Adjusted R Square	0.8745
Standard Error	0.2056
Observations	6

ANOVA

	df	*SS*	*MS*	*F*	*Significance F*
Regression	2	1.5570	0.7785	18.4222	0.0207
Residual	3	0.1268	0.0423		
Total	5	1.6838			

	Coefficients	*Standard Error*	*t Stat*	*P-value*	*Lower 95%*	*Upper 95%*
Constant	1.2306	0.1368	8.9935	0.0029	0.7951	1.6660
BQC_{pf}	20864655.78	3464100.837	6.0231	0.0092	9840331	31888981
BGC_{pf}	-174182606.8	36497259.12	-4.7725	0.0175	-290333283	-58031930

RESIDUAL OUTPUT

Observation	*Predicted BAdE*	*Residuals*	*Standard Residuals*
0.00	-0.0174	0.0174	0.1095
0.76	0.9874	-0.2274	-1.4282
0.91	1.0225	-0.1125	-0.7063
1.24	1.0086	0.2314	1.4534
1.27	1.1776	0.0924	0.5803
1.7	1.7014	-0.0014	-0.0088

Coating D
Arizona
Color change (dE)

DAdE	DQC_{pf}	DGC_{pf}
0.00E+00	2.15E-06	2.15E-06
0.21	3.35E-09	4.16E-08
0.64	3.24E-08	1.87E-07
0.95	4.13E-07	2.31E-07
0.51	6.71E-08	1.45E-07
2.5	4.90E-06	4.26E-08

Regression Statistics	
Multiple R	0.9657
R Square	0.9325
Adjusted R Square	0.8875
Standard Error	0.3004
Observations	6

ANOVA

	df	*SS*	*MS*	*F*	*Significance F*
Regression	2	3.7395	1.8698	20.7169	0.0175
Residual	3	0.2708	0.0903		
Total	5	4.0103			

	Coefficients	*Standard Error*	*t Stat*	*P-value*	*Lower 95%*	*Upper 95%*
Constant	0.6147	0.1621	3.7925	0.0322	0.0989	1.1306
DQC_{pf}	392826.8158	69500.83057	5.6521	0.0110	171643.9469	614009.6848
DGC_{pf}	-661577.7156	164694.572	-4.0170	0.0277	-1185709.839	-137445.5917

RESIDUAL OUTPUT

Observation	*Predicted DAdE*	*Residuals*	*Standard Residuals*
0.00	0.037	-0.037	-0.159
0.21	0.589	-0.379	-1.627
0.64	0.504	0.136	0.585
0.95	0.624	0.326	1.400
0.51	0.545	-0.035	-0.151
2.5	2.511	-0.011	-0.049

Coating B
Florida
Color change (dE)

BFdE	BQC_{pf}	BGC_{pf}
0	8.14E-09	8.14E-09
0.94	5.21E-09	2.02E-09
1.1	5.47E-09	1.85E-09
1.22	4.47E-09	1.81E-09
1.32	8.23E-09	1.29E-09
1.65	9.77E-08	9.00E-09

Regression Statistics	
Multiple R	0.9888
R Square	0.9778
Adjusted R Square	0.9630
Standard Error	0.1081
Observations	6

ANOVA

	df	*SS*	*MS*	*F*	*Significance F*
Regression	2	1.5430	0.7715	66.0140	0.0033
Residual	3	0.0351	0.0117		
Total	5	1.5781			

	Coefficients	*Standard Error*	*t Stat*	*P-value*	*Lower 95%*	*Upper 95%*
Constant	1.3557	0.0720	18.8408	0.0003	1.1267	1.5847
BQC_{pf}	20332702.09	1821721.32	11.1613	0.0015	14535166.4	26130237.82
BGC_{pf}	-187956831.8	19193389.1	-9.7928	0.0023	-249038819	-126874844.3

RESIDUAL OUTPUT

Observation	*Predicted BFdE*	*Residuals*	*Standard Residuals*
0.00	-0.009	0.009	0.105
0.94	1.082	-0.142	-1.695
1.1	1.119	-0.019	-0.229
1.22	1.106	0.114	1.357
1.32	1.281	0.039	0.471
1.65	1.651	-0.001	-0.007

Coating D
Florida
Color change (dE)

DFdE	DQC_{pf}	DGC_{pf}
0.00E+00	2.15E-06	2.15E-06
0.99	3.35E-09	4.16E-08
1.31	3.24E-08	1.87E-07
1.43	4.13E-07	2.31E-07
2.73	6.71E-08	1.45E-07
4.1	4.90E-06	4.26E-08

Regression Statistics	
Multiple R	0.9050
R Square	0.8191
Adjusted R Square	0.6985
Standard Error	0.7926
Observations	6

ANOVA

	df	*SS*	*MS*	*F*	*Significance F*
Regression	2	8.5338	4.2669	6.7921	0.0769
Residual	3	1.8846	0.6282		
Total	5	10.4184			

	Coefficients	*Standard Error*	*t Stat*	*P-value*	*Lower 95%*	*Upper 95%*
Intercept	1.7451	0.4277	4.0807	0.0266	0.3841	3.1061
DQC_{pf}	488893.0024	183363.3	2.6663	0.0759	-94651.4	1072437.407
DGC_{pf}	-1290468.4	434511.9	-2.9699	0.0591	-2673280.6	92343.79317

RESIDUAL OUTPUT

Observation	*Predicted DFdE*	*Residuals*	*Standard Residuals*
0.00	0.022	-0.022	-0.035
0.99	1.693	-0.703	-1.145
1.31	1.520	-0.210	-0.341
1.43	1.649	-0.219	-0.357
2.73	1.591	1.139	1.856
4.1	4.086	0.014	0.023

Coating A
Arizona
Adhesion

AAadhes	AQC_{dl}
5	4.80E-09
5	1.67E-10
4.5	1.01E-09
5	1.17E-09
5	9.94E-10
4	3.88E-08

Regression Statistics	
Multiple R	0.8636
R Square	0.7459
Adjusted R Square	0.6823
Standard Error	0.2358
Observations	6

ANOVA

	df	*SS*	*MS*	*F*	*Significance F*
Regression	1	0.6526	0.6526	11.7402	0.0266
Residual	4	0.2224	0.0556		
Total	5	0.8750			

	Coefficients	*tandard Err*	*t Stat*	*P-value*	*Lower 95%*	*Upper 95%*
Constant	4.935200205	0.110393	44.70587	1.5E-06	4.628700361	5.241700049
AQC_{dl}	-23672295.63	6908803	-3.426396	0.026623	-42854248.17	-4490343.089

RESIDUAL OUTPUT

Observation	*Predicted AAad*	*Residuals*	*Standard Residuals*
5	4.822	0.178	0.846
5	4.931	0.069	0.326
4.5	4.911	-0.411	-1.950
5	4.908	0.092	0.439
5	4.912	0.088	0.419
4	4.017	-0.017	-0.079

Coating A
Florida
Adhesion

AFadhes	AQRct	ABCpf
5	2.57E+08	3.43E-09
4	5.71E+10	1.67E-09
5	1.61E+10	1.99E-09
4.5	3.16E+10	1.98E-09
5	1.00E+10	2.15E-09
4.5	9.00E+08	4.04E-09

Regression Statistics	
Multiple R	0.9745
R Square	0.9497
Adjusted R Square	0.9161
Standard Error	0.1182
Observations	6

ANOVA

	df	*SS*	*MS*	*F*	*Significance F*
Regression	2	0.7914	0.3957	28.3016	0.0113
Residual	3	0.0419	0.0140		
Total	5	0.8333			

	Coefficients	*Standard Error*	*t Stat*	*P-value*	*Lower 95%*	*Upper 95%*
Constant	6.1674	0.2781	22.1734	0.0002	5.2822	7.0526
AQRct	-2.72933E-11	3.71E-12	-7.3494	0.0052	-3.91119E-11	-1.54746E-11
ABCpf	-382679450	84741031	-4.5159	0.0203	-652363484.9	-112995415

RESIDUAL OUTPUT

Observation	*Predicted AFad*	*Residuals*	*Standard Residuals*
5	4.848	0.152	1.662
4	3.970	0.030	0.329
5	4.966	0.034	0.366
4.5	4.547	-0.047	-0.516
5	5.072	-0.072	-0.783
4.5	4.597	-0.097	-1.057

Coating B
Arizona
Adhesion

BAad	BGRct
5	2.72E+07
4.5	2.30E+09
4	4.57E+09
5	6.90E+08
5	1.06E+09
4.5	3.87E+09

Regression Statistics	
Multiple R	0.9353
R Square	0.8747
Adjusted R Square	0.8434
Standard Error	0.1616
Observations	6

ANOVA

	df	*SS*	*MS*	*F*	*Significance F*
Regression	1	0.7289	0.7289	27.9264	0.0062
Residual	4	0.1044	0.0261		
Total	5	0.8333			

	Coefficients	*Standard Error*	*t Stat*	*P-value*	*Lower 95%*	*Upper 95%*
Constant	5.1033	0.1057	48.2699	1.1E-06	4.8098	5.3969
BGRct	-2.0931E-10	3.96071E-11	-5.2845	0.0062	-3.19272E-10	-9.93381E-11

RESIDUAL OUTPUT

Observation	*Predicted BAad*	*Residuals*	*Standard Residuals*
5	5.098	-0.098	-0.676
4.5	4.622	-0.122	-0.844
4	4.147	-0.147	-1.016
5	4.959	0.041	0.284
5	4.881	0.119	0.820
4.5	4.293	0.207	1.430

Coating D
Arizona
Adhesion

DAad	DBRpf	DBRct	DBCpf
3	5570	1.02E+07	2.15E-06
3	3206	4.44E+06	4.94E-07
3	3105	4.84E+06	3.80E-07
2	2492	6.45E+06	3.88E-07
3	847	1.62E+06	5.96E-07
3	6827	8.32E+06	3.68E-10

Regression Statistics	
Multiple R	0.9757
R Square	0.9519
Adjusted R Square	0.8798
Standard Error	0.1415
Observations	6

ANOVA

	df	*SS*	*MS*	*F*	*Significance F*
Regression	3	0.7933	0.2644	13.1991	0.0712
Residual	2	0.0401	0.0200		
Total	5	0.8333			

	Coefficients	*Standard Error*	*t Stat*	*P-value*	*Lower 95%*	*Upper 95%*
Constant	2.9197	0.1372	21.2780	0.0022	2.3293	3.5101
DBRpf	0.0004	0.0001	6.0654	0.0261	0.0001	0.0007
DBRct	-3.28996E-07	5.49E-08	-5.9881	0.0268	-5.65392E-07	-9.26E-08
DBCpf	517459	112975.8	4.5803	0.0445	31362.59491	1003555

RESIDUAL OUTPUT

Observation	*Predicted DAad*	*Residuals*	*Standard Residuals*
3	2.998	0.002	0.022
3	3.055	-0.055	-0.610
3	2.822	0.178	1.990
2	2.040	-0.040	-0.448
3	3.049	-0.049	-0.549
3	3.036	-0.036	-0.405

Coating B
Florida
Adhesion

BFad	BGCdl	BBCdl
5	3.64E-08	3.64E-08
4	2.23E-09	1.07E-07
4	4.30E-09	6.47E-06
4	4.25E-09	3.74E-08
5	4.25E-09	8.83E-05
4	7.71E-10	7.61E-09

Regression Statistics	
Multiple R	0.9933
R Square	0.9867
Adjusted R Square	0.9778
Standard Error	0.0769
Observations	6

ANOVA

	df	*SS*	*MS*	*F*	*Significance F*
Regression	2	1.3156	0.6578	111.2292	0.0015
Residual	3	0.0177	0.0059		
Total	5	1.3333			

	Coefficients	*Standard Error*	*t Stat*	*P-value*	*Lower 95%*	*Upper 95%*
Constant	3.8999	0.0429	90.8589	2.94E-06	3.7633	4.0365
BGC_{dl}	29922516	2559177	11.6922	0.0013	21778065.91	38066965.88
BBC_{dl}	10936.2	980.9953	11.1481	0.0015	7814.232699	14058.16818

RESIDUAL OUTPUT

Observation	*Predicted Y*	*Residuals*	*Standard Residuals*
5	4.989	0.011	0.176
4	3.968	0.032	0.540
4	4.099	-0.099	-1.668
4	4.028	-0.028	-0.462
5	4.993	0.007	0.122
4	3.923	0.077	1.291